SYSTEMS-LEVEL CHARACTERIZATION OF OVARIAN CANCER METABOLISM

A Thesis
Presented to
The Academic Faculty

by

Kathleen A. Vermeersch

In Partial Fulfillment
of the Requirements for the Degree
Doctorate of Philosophy in the
School of Chemical & Biomolecular Engineering

Georgia Institute of Technology
December 2014

SYSTEMS-LEVEL CHARACTERIZATION OF OVARIAN CANCER METABOLISM

Approved by:

Dr. Mark P Styczynski, Advisor
School of Chemical & Biomedical Engineering
Georgia Institute of Technology

Dr. Andreas S. Bommarius
School of Chemical & Biomedical Engineering
Georgia Institute of Technology

Dr. Rachel Chen
School of Chemical & Biomedical Engineering
Georgia Institute of Technology

Dr. Michelle R. Dawson
School of Chemical & Biomedical Engineering
Georgia Institute of Technology

Dr. John F. McDonald
School of Biology
Georgia Institute of Technology

Date Approved: August 20, 2014

I dedicate this work to my family.

ACKNOWLEDGEMENTS

There are many people I would like to thank for supporting me during my time here at Georgia Institute of Technology:

Dr. Mark Styczynski for pushing me to become a better researcher and for all your support and guidance over the past five years.

My committee members, Dr. Andreas Bommarius, Dr. Rachel Chen, Dr. Michelle Dawson, and Dr. John McDonald for your suggestions and help on my research.

The entire Styczynski group for your continuous help and for always making me laugh when I most needed it.

The McDonald research group, especially Lijuan Wang and Roman Mezencev, for your suggestions and critiques on my project and for help with cell culture.

My friends both here at Georgia Tech and from the Ohio State University, especially Ismael Gomez, Brian Setzler, Erin Redmond, Aubrey Tiernan and Steph Didas, for keeping me somewhat sane and for all our fun times.

My family for their love and faith in me and for always supporting me through the years.

TABLE OF CONTENTS

LIST OF TABLES

LIST OF FIGURES

ABBREVIATIONS

α-KG: α-ketoglutarate

2HG: 2-hydroxyglutarate

2PG: 2-phosphoglycerate

3PG: 3-phosphoglycerate

ABC: ATP (adenosine triphosphate)-binding cassette

AKT1: kinase downstream of PI3K

ALDH: aldehyde dehydrogenase

ANOVA: analysis of variance

ATP: adenosine-5'-triphosphate

bFGF: basic fibroblast growth factor

BPG: 1,3-bisphosphoglycerate

BSA: bovine serum albumin

CCs: cancer cells

CE: capillary electrophoresis

CGSCs: cultured GSCs

CO_2: carbon dioxide

CoA: Coenzyme A

CRC: colorectal cancer

CSCs: cancer stem cells

DART: direct analysis in real time

DHAP: dihydroxyacetone phosphate

DIMS: direct infusion mass spectrometry

DMEM/F12: Dulbecco's modified eagle medium/nutrient mixture F-12

DMSO: dimethylsulfoxide

DNA: deoxyribonucleic acid

EGF: epidermal growth factor

EMT: epithelial-mesenchymal transition

ETS: E26 transformation-specific gene family

F6P: fructose-6-phosphate

FAMEs: fatty acid methyl esters

FBP: fructose-1,6-bisphosphate

FDR: false discovery rate

FH: fumarate hydratase

G3P: glyceraldehyde-3-phospate

G6P: glucose-6-phosphate

G6PD: glucose-6-phosphate dehydrogenase

GABA: gamma-aminobutyric acid

GC: gas chromatography

GLS: glutaminase

GSEA: gene set enrichment analysis

GSCs: glioma stem cells

HCC: hepatocarcinoma or hepatocellular cancer

HER-2: human epidermal growth factor receptor 2

HIF: hypoxic inducing factor

HK: hexokinase

HMDB: Human Metabolite Database

HR-MAS-NMR: high resolution magic angle spinning nuclear magnetic resonance

HR-NMR: high resolution nuclear magnetic resonance

IC_{50}: half maximal inhibitory concentration

IDH1/IDH2: isocitrate dehydrogenase 1/2

iPSCs: induced pluripotent stem cells

KEGG: Kyoto Encyclopedia of Genes and Genomes

KNN: k-nearest neighbors

LC: liquid chromatography

LDHA: lactate dehydrogenase A

mESCs: mouse embryonic stem cells

MET: mesenchymal- epithelial transition

mRNAs: messenger RNA

MS: mass spectrometry

MSEA: metabolite set enrichment analysis

MPEA: metabolite pathway enrichment analysis

MSTFA: *N*-methyl-*N*-(trimethylsilyl) trifluoroacetamide

Myc: (c-Myc) transcription factor encoded by oncogene MYC

NADP+: nicotinamide adenine dinucleotide phosphate

NADPH: nicotinamide adenine dinucleotide phosphate, reduced

NCI: national cancer institute

NMR: nuclear magnetic resonance

OAA: oxaloacetate

OCCs: ovarian cancer cells

OCSCs: ovarian cancer stem cells

p53: tumor suppressor protein encoded by TP53

P5CS: delta 1-pyrroline-5-carboxylate synthase

PBS: phosphate buffered saline

PC: principal component

PCA: principal components analysis

PEP: phosphoenolpyruvate

PFK: phosofructosekinase

PGAM1: phosphoglycerate mutase 1

PHD: prolyl hydroxylases

PI3K: phosphatidylinositide 3-kinases

PK: pyruvate kinase

PKM1: pyruvate kinase isozyme M1

PKM2: pyruvate kinase isozyme M2

PLS-DA: partial least squares discriminant analysis

POX/PRODH: proline dehydrogenase

PPP: pentose phosphate pathway

PYCR: pyrroline-5-carboxylate reductase

QC: quality control

QTOF: quadrupole time-of-flight

RNA: ribonucleic acids

ROS: reactive oxygen species

RPMI: Roswell Park Memorial Institute medium 1640

SDH: succinate dehydrogenase

S/N: signal-to-noise

SOG: serine synthesis, one-carbon metabolism, and glycine cleavage system pathway

TCA: tricarboxylic acid

tCho: total choline containing compounds

TGF-beta: transforming growth factor beta

TMCS: trimethylchlorosilane

TOF: time-of-flight

TIGAR: TP53-induced glycolysis and apoptosis regulator

SUMMARY

While it has been known for almost a century that energy metabolism in cancer cells is dysfunctional, only recently has the importance of metabolism in cancer come to be more generally recognized. Dysfunctional metabolism is now acknowledged as a hallmark of cancer, and recently, further examples of altered metabolism in cancer cells have been demonstrated. Despite some targeted study of metabolism in cancer, its systems-level dynamics remain relatively unexplored, and a deeper understanding of these metabolic behaviors could profoundly affect the way that cancer is understood or even treated. Cancer stem cells are stem-like cancer cells that have been identified within tumors and are also poorly understood. Cancer stem cells are a major concern for effective cancer treatment: they have self-renewal capabilities, can differentiate into cancer cells, and exhibit chemo- and radioresistance; they are thus suspected as a primary cause of cancer recurrence. The purpose of this thesis was to characterize cancer metabolism *in vitro* using epithelial ovarian cancer as a model on an untargeted, systems-level, basis with particular attention paid to the difference between cancer stem cell metabolism and cancer cell metabolism.

Gene expression analysis of ovarian cancer stem cells and ovarian cancer cells previously identified several metabolic pathways that were significantly enriched in differentially expressed genes between cancer stem cells and their parental isogenic cell line. To determine if there were substantial metabolic changes corresponding with these transcriptional differences, two-dimensional gas chromatography coupled to mass spectrometry was used to measure the metabolite profiles of the ovarian cancer and cancer stem cell lines (Chapter 2). These two cell lines exhibited significant metabolic differences in both intracellular and extracellular metabolite measurements. Pathway analysis of intracellular metabolomics data revealed close overlap with

metabolic pathways identified from gene expression data, with four out of six pathways found to be enriched in gene-level analysis also enriched in metabolite-level analysis. One of the most significantly enriched pathways, arginine and proline metabolism, contains multiple metabolites that are each statistically significantly different between the two cells. Two of those metabolites, proline and putrescine, have been previously implicated in cancer, but the changes displayed between normal and cancer cells are discordant with the changes they display between cancer cells and cancer stem cells. This behavior can be explained in the context of current research in stem cell metabolism, suggesting that ovarian cancer stem cells may exist in a metabolic balance between potency and proliferation. Overall, metabolism in this ovarian cancer stem cell line is distinct from that of more differentiated isogenic cancer cells, showing similarities to stem cell metabolism that suggest the potential importance of metabolism for the cancer stem cell phenotype.

The *in vitro* cell culture conditions for this initial work, though, differ drastically from *in vivo* tumor conditions. To capture the metabolic profiles that would be more likely in a tumor *in vivo*, biologically-based perturbations were applied to the ovarian cancer cell and cancer stem cell grown *in vitro* (Chapter 3). Glucose deprivation, hypoxia, and ischemia are all conditions that occur naturally in tumors; they all perturbed ovarian cancer and cancer stem cell metabolism, but not in the same ways between the cell types. Hypoxia had a much larger effect on ovarian cancer cell metabolism, while glucose deprivation had a greater effect on ovarian cancer stem cell metabolism. Chemotherapeutics treatment with docetaxel caused metabolic changes mostly in amino acid and carbohydrate metabolism in ovarian cancer cells, though the most significantly altered metabolite was uracil. Ovarian cancer stem cell metabolism was not affected by

docetaxel. These differences will deepen our understanding of the metabolic changes occurring within the *in vivo* tumor.

To expand the model system of cancer metabolism to be even more representative of *in vivo* conditions, metabolic profiles were taken of an *in vitro* model of the epithelial-mesenchymal transition (EMT), a well-known process in embryonic development now believed to take part in tumor metastasis and the origin of cancer stem cells (Chapter 4). Metabolic samples were taken over a mesenchymal to epithelial transition (MET) and a subsequent EMT. During the two phenotypic changes, no corresponding metabolomic changes were detected, suggesting that EMT/MET does not perturb cellular metabolism.

This work explores the metabolic differences between an ovarian cancer cell line and its isogenic cancer stem cell line under various conditions, providing the first-ever characterization of ovarian cancer stem cell metabolism. This systems-level characterization of cancer metabolism may ultimately be key in the development of chemotherapeutics that target metabolic pathways; related future work and the broader relevance of the findings of this thesis are presented in Chapter 5.

Chapter 1 Background and introduction

Portions of this chapter are reproduced under license from our published review, *Applications of metabolomics in cancer research,* in the Journal of Carcinogenesis.[1]

1.1. Cancer & cancer stem cells

Cancer is the second leading cause of death in the United States, accounting for 25% of total deaths.[2] In recent years, it has even overtaken heart disease related deaths in those younger than 80.[2] Ovarian cancer was the fifth leading cause of cancer-related deaths in American women in 2010.[3] Worldwide, ovarian cancer was newly diagnosed in 226,000 females and was responsible for 140,000 deaths in 2008.[4] Ovarian cancer targets mostly women over 50 and is the most fatal gynecological cancer, mainly because 70% of the cases detected are at an advanced stage, when five-year survival rates are 30%.[2, 5] Epithelial ovarian cancer is the most prevalent form of ovarian cancer, accounting for around 90% of cases.[6]

Cancer cells (CCs) differ from normal cells by a number of distinguishable hallmarks that were enumerated by Hanahan and Weinberg in 2000.[7] The most well-known of these six hallmarks are CCs' ability to proliferate uncontrollably and invade nearby tissues or distant tissues through metastasis.[8] Others include inactivation or evasion of growth suppressors, mutation into immortal cells that can replicate indefinitely, inducement of angiogenesis, and evasion of apoptotic as well as autophagic signaling pathways.[7] Continuing research has prompted the addition of four new hallmarks of cancer: genomic instability, an ability to harness the immune system's tumor-promoting potential and inactivate its destructive abilities, and an altered metabolism in order to enhance growth rate and evade destruction.[9] It is the altered metabolism

of cancer that is the focus of this thesis; further details on cancer metabolism will be discussed in section 1.2.

CCs within tumors display differing levels of differentiation and proliferation capabilities.[10, 11] A number of theories exist to explain the heterogeneity of CCs within a tumor, including the stochastic model and cancer stem cell model. The stochastic model, illustrated in Figure 1.1*b*, postulates that any cancerous cell has the potential to form a tumor. A mutation (which has an equal chance of happening in any cancerous cell) is required to give normal cancerous cells the potential to populate the heterogeneous cells within a tumor To become a tumor-forming cell, a cancerous cell undergoes a mutation that has an equal chance of happening in any cancerous cell. The cancer stem cell model, shown in Figure 1.1*c*, is arranged in a hierarchy with the top tier formed by cancer stem cells (CSCs). CSCs have the potential for self-renewal and differentiation into the heterogeneous cells that form the tumor.[10, 12] CSCs may arise from mutations of different cells: normal stem cells, progenitor cells, or differentiated cells with the ability to self-renew.[10, 12] After the CSCs, varying degrees of differentiated cells fill the next level and fully differentiated CCs lie at the bottom of the hierarchy.[12] The main difference between these two models is that in the stochastic model, every cell has the potential to form a tumor through a mutation, while in the cancer stem cell model, only the CSCs have the potential to form a tumor.

When these models were initially created, most people believed that only one model could be correct. Now, researchers believe that tumor heterogeneity actually occurs through a mixture of these two models.[10, 11, 13, 14] In this combined model, shown in Figure 1.1*d*, CSCs are the only cancerous cells with the potential of forming a tumor, but the CSC state is not static. Instead, CSCs can transition to a differentiated state and other cancerous cells can transition to CSC state forming a new CSC (CSC2 in Figure 1.1*d*).

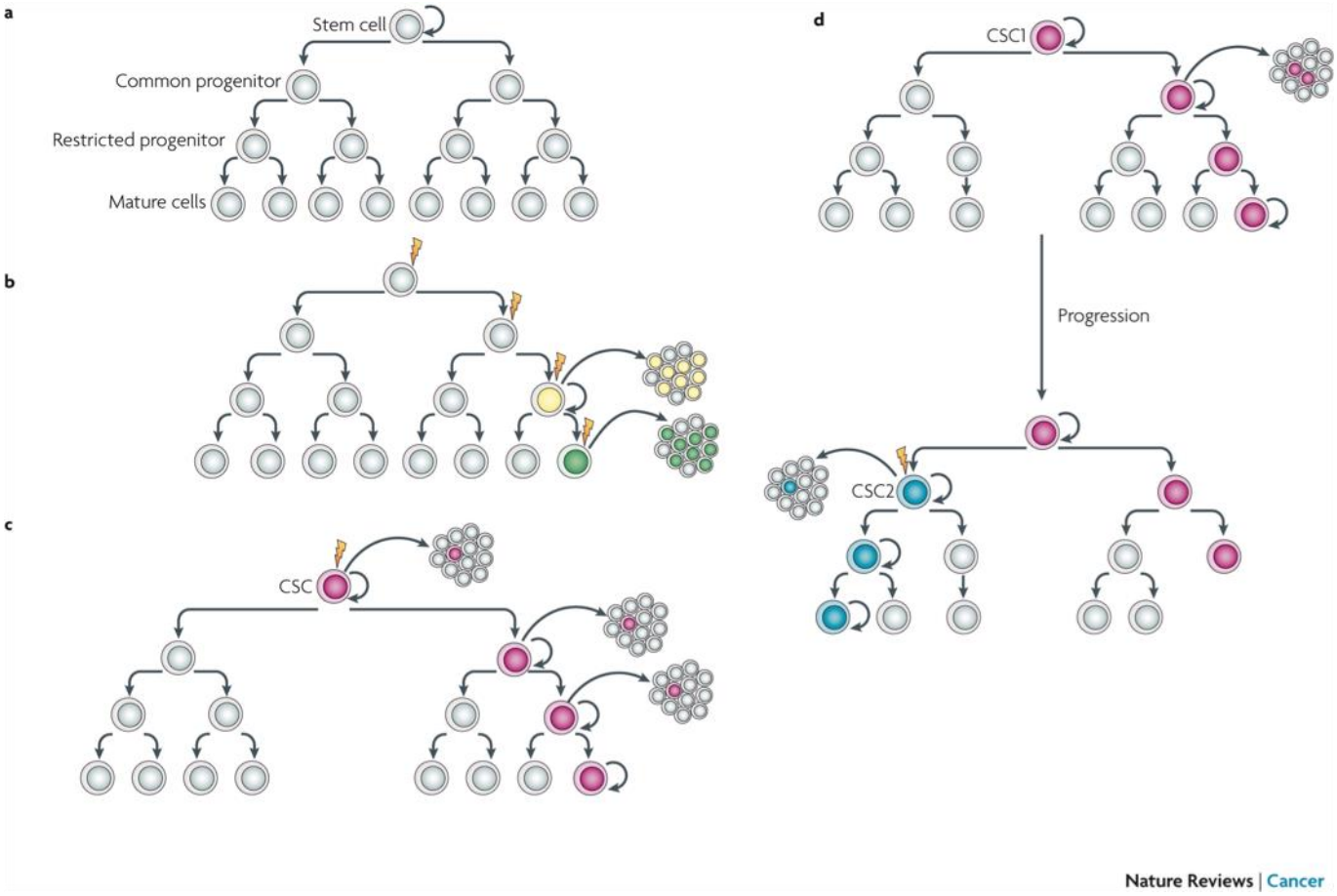

Figure 1.1: Tumor heterogeneity is more plastic than originally modeled. a) Typical stem cell hierarchy with stem cells at the top, followed by progenitor cells, and finally, fully differentiated, mature cells. b) Stochastic model (or clonal modal) where every cell has an equal chance of forming a tumor. Mutations (lightning bolts) can give cancerous cells the ability to form a tumor, as shown in the yellow and green transformed cells. c) The cancer stem cell follows closely the normal stem cell hierarchy, where only the CSCs have the ability to form a tumor. Each CSC (pink cells) has the potential for asymmetric and symmetric replication as well as the potential to form a tumor. d) The combined model of tumor heterogeneity has aspects of both the stochastic and cancer stem cell modal. Here, only CSCs (CSC1; pink) have the ability to form a tumor, but mutations can generate new CSCs (CSC2; blue), which also have tumor forming potential. Reprinted by permission from Macmillan Publishers Ltd: [Nat. Rev. Cancer] Visvader, J.E. & Lindeman, G.J, 2008[10], copyright (2008).

Original evidence for CSCs came from isolation of cells from hematological malignancies and transplantation into animal models.[12, 15, 16] The first evidence for solid tumor CSCs was found in breast cancer.[10, 17] Tumor cells were isolated from human breast cancer tumors and pleural effusions and sorted based on cell surface markers. Only one group of CCs (a small fraction of the total number of cells) was able to completely reconstitute the original tumor upon

transplantation. These cells were labeled as CSCs. CCs that did not have the CSC markers were not able to reconstitute the original tumor, even when using 100 times the amount of CSCs used to form the tumor. Currently, CSCs are isolated and identified by their cell surface markers, but the lack of unique surface markers solely marking CSCs is proving problematic for complete isolation.[18] Nonetheless, CSCs have been isolated from numerous cancers,[19] including ovarian cancer.[6, 20-23]

Recently, a link has been found between CSCs and epithelial-mesenchymal transition (EMT).[24, 25] EMT is a normal event during embryonic development, where epithelial cells are induced into a mesenchymal phenotype in order to develop more advanced structures and functions.[26] Epithelial cells have strong cell-cell adhesion through multiple types of junctions, which makes them tightly packed and immobile. Mesenchymal cells do not form junctions; instead, they have migratory and invasive properties. CCs have hijacked the EMT, albeit incompletely, resulting in further tumor progression and induction of metastasis. Normal CCs undergoing EMT have been shown to acquire CSC-like behavior,[24, 25] as shown in Figure 1.2. During EMT, normal CCs obtain some stem cell-like properties, including self-renewal capabilities. By acquiring CSC-like behavior, these newly metastatic cells become perfectly situated to form a new tumor as CSCs inherently have the properties needed for a cell to form a metastatic lesion.[27]

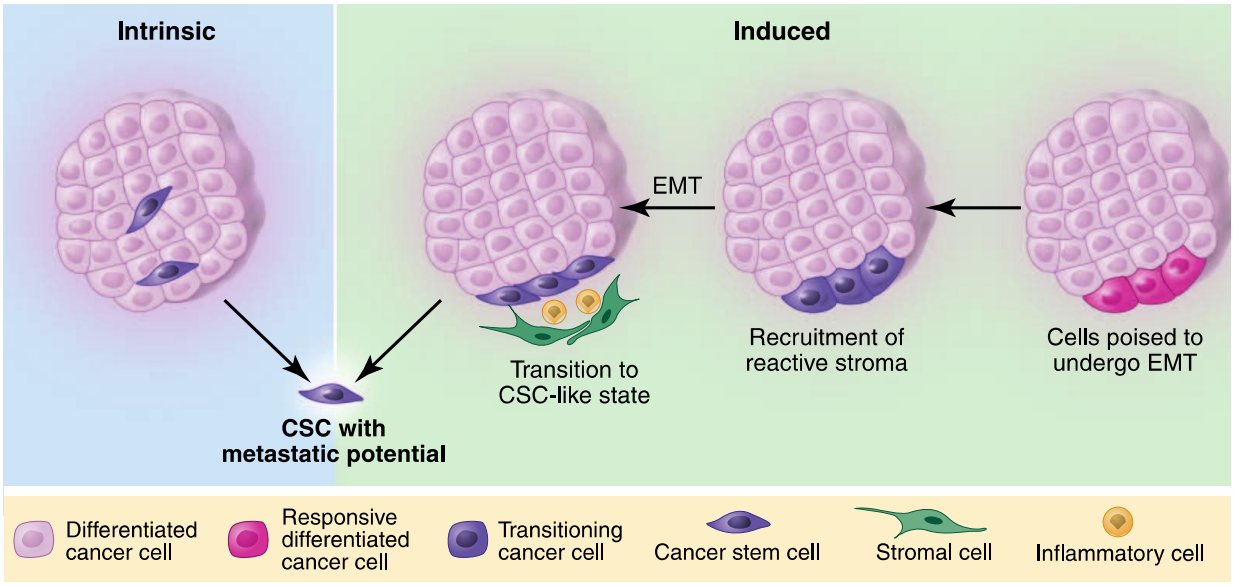

Figure 1.2: Tumor CSCs can be induced by EMT. Intrinsic CSCs are formed from mutations in stem cells, progenitor cells, or differentiated cells that have gained self-renewal powers. EMT-induced CSCs are caused by signals from the reactive stroma that induce the CCs to undergo EMT. The EMT forms mesenchymal cells with CSC properties. From Chaffer *et al*, 2011[27]. Reprinted with permission from AAAS.

CSCs pose a major problem for cancer treatments, as they exhibit resistance to traditional chemotherapeutics.[10, 19, 28] CSCs are believed to be able to resist chemotherapy through several approaches, including ATP (adenosine triphosphate)-binding cassette (ABC) drug pumps that expel chemotherapeutics from the cell,[29] entrance into quiescence which grants resistance to toxins targeting fast replicating cells, and resistance to apoptosis.[19, 28] Since CSCs are chemotherapeutic resistant and have the ability to recapitulate a new tumor, CSCs are believed to be a major cause of cancer recurrence. A significant challenge in ovarian cancer treatment is the fact that most patients die of its recurrence, after initial treatment.[5] Ovarian cancer stem cells (OCSCs) have not only been shown to be resistant to traditional chemotherapeutics, but have proliferated in the presence of chemotherapy, leading to the necessity of OCSC-targeted therapeutics.[30, 31] One area of research that could lead to therapeutic targets is the study of CSC metabolism and how it differs from CC metabolism.

1.2. Cancer metabolism

Broadly defined, metabolism is the set of processes catalyzing the production of energy and cellular building blocks (amino acids, nucleotides, lipids, etc.) from the nutrients a cell takes up from the environment. These building blocks, and the biochemical intermediates generated during their production and utilization, are collectively referred to as metabolites. Metabolite levels integrate the effects of gene regulation, post-transcriptional regulation, pathway interactions, and environmental perturbations; this downstream synthesis of diverse signals ultimately makes metabolites direct molecular readouts of cell status that reflect a meaningful physiological phenotype.[32-35] Therefore, it is not surprising that metabolism is altered in cancer since there are many other alterations in cancer cells that would be reflected in metabolism. One major question stems from this, though; does the altered metabolism merely reflect the cancer state or does the altered metabolism additionally contribute to and sustain the cancer state?

1.2.1. Warburg effect and supporting mutations

Though reprogramming of energy metabolism was only recently recognized as an emerging hallmark of cancer,[9] altered cancer metabolism was first identified almost a century ago when Warburg discovered that cancer cells primarily use anaerobic glycolysis to produce their energy instead of oxidative phosphorylation, even in the presence of oxygen – a phenomenon known as the Warburg effect or aerobic glycolysis.[36, 37]

Over the years, many common cancer mutations have been shown to support the Warburg effect.[38] AKT1, HIF, and p53 together cause increased flux of glucose through glycolysis and down-regulation of flux through the tricarboxylic acid (TCA) cycle (Figure 1.3), thereby supporting the Warburg effect and carcinogenesis.[39-47] AKT1 is a downstream effector in the PI3K pathway, which is up-regulated in cancer. AKT1 administers growth and survival signaling and has a strong effect on metabolism[27]: it stimulates glycolysis through phosphorylation of

glycolytic enzymes and transcriptional up-regulation of glucose transporters.[39] Hypoxia-inducible factor 1 (HIF1), whose induction is caused by the highly hypoxic conditions present in tumors, induces the Warburg effect by increasing glycolytic transport and expression of enzymatic genes while down-regulating the TCA cycle, a critical pathway that feeds electrons to oxidative phosphorylation.[40] HIF1 decreases TCA cycle flux via pyruvate dehydrogenase[41-43], the enzyme linking glycolysis and the TCA cycle. p53, a commonly down-regulated gene in cancer, has several regulatory functions that control metabolism[38]. Although p53 promotes expression of hexokinase (the first enzyme in glycolysis),[44] it also stimulates oxidative phosphorylation,[45] induces the expression of TP53-induced glycolysis and apoptosis regulator (TIGAR) (an enzyme that down-regulates glycolysis),[46] and down-regulates phosphoglycerate mutase (PGAM1) (a glycolytic enzyme)[47]. Therefore, even though p53 normally promotes hexokinase, overall, the down-regulation of p53 in cancer still supports the Warburg effect.

Loss-of-function mutations of mitochondrial enzymes succinate dehydrogenase (SDH) and fumarate hydratase (FH) also support the Warburg effect.[48] The mutations of these two tumor suppressors allow for build-up of succinate and fumarate in the mitochondria, leading to their eventual escape. These metabolites have been shown to inhibit prolyl hydroxylases (PHDs) – a family of enzymes that participate in multiple pathways, one of which is to tag HIF for degradation.[48-51] Therefore, accumulation of succinate and fumarate support HIF accumulation, which leads to increased glucose transfer into the cell and suppression of the TCA cycle, as discussed above.

Pyruvate kinase (PK) is another commonly altered enzyme in cancer with metabolic implications (Figure 1.3). PK converts phosphoenolpyruvate (PEP) into pyruvate and is a rate-limiting step in glycolysis. There are four human isoforms of PK: L, R, M1 and M2. L and R are limited to a few

specific cell types. M1 is expressed in most adult cells, and M2 is expressed in self-renewing cells, like embryonic stem cells.[52] PKM2 is less active than PKM1, is activated allosterically by fructose-1,6-bisphosphate (FBP), and is negatively regulated through tyrosine kinase signaling in CCs. [53, 54] Expression of less-active, rate-limiting PKM2 leads to a smaller flux of its catalyzed reaction and an accumulation of upstream glycolytic intermediates.[38] Interestingly, most CCs express the isoform PKM2, switching over from PKM1 expression during carcinogenesis. Research into PKM2's effect on cancer has shown that CCs expressing PKM2 consume less oxygen and produce more lactate than the same CCs expressing PKM1, suggesting a significant role in the manifestation of the Warburg effect.[55] Lung CCs expressing PKM2 *in vivo* showed faster tumor development, a greater number of tumors, and larger tumors than the same cells expressing PKM1.[55]

Expression of PKM2 in most cancer cells causes the rate-limiting step of glycolysis to become even slower, which would normally result in accumulation of glycolytic intermediates and the natural down-regulation of glycolysis. However in cancer cells, glycolytic intermediates are rerouted down one of the many pathways that branch off from glycolysis. One of the most notable of these pathways is the pentose phosphate pathway (PPP), which produces NADPH (nicotinamide adenine dinucleotide phosphate, reduced) and ribose-5-phosphate, both important reagents for biosynthetic pathways required for proliferation. It has been discovered that p53, discussed above as a regulator of many metabolic pathways, also controls flux into the PPP via control of glucose-6-phosphate dehydrogenase (G6PD), which catalyzes the rate-limiting reaction between glycolysis and the PPP.[56] In normally functioning cells, cytoplasmic p53 inhibits G6PD and thus limits metabolic flux through the PPP.[56] Since p53 is inactivated in most tumors, cytosolic p53 is not present to inhibit G6PD in CCs, increasing the flux into the PPP and

increasing production of NADPH and ribose-5-phosphate.[56] These metabolites are then used by the highly proliferative cells.

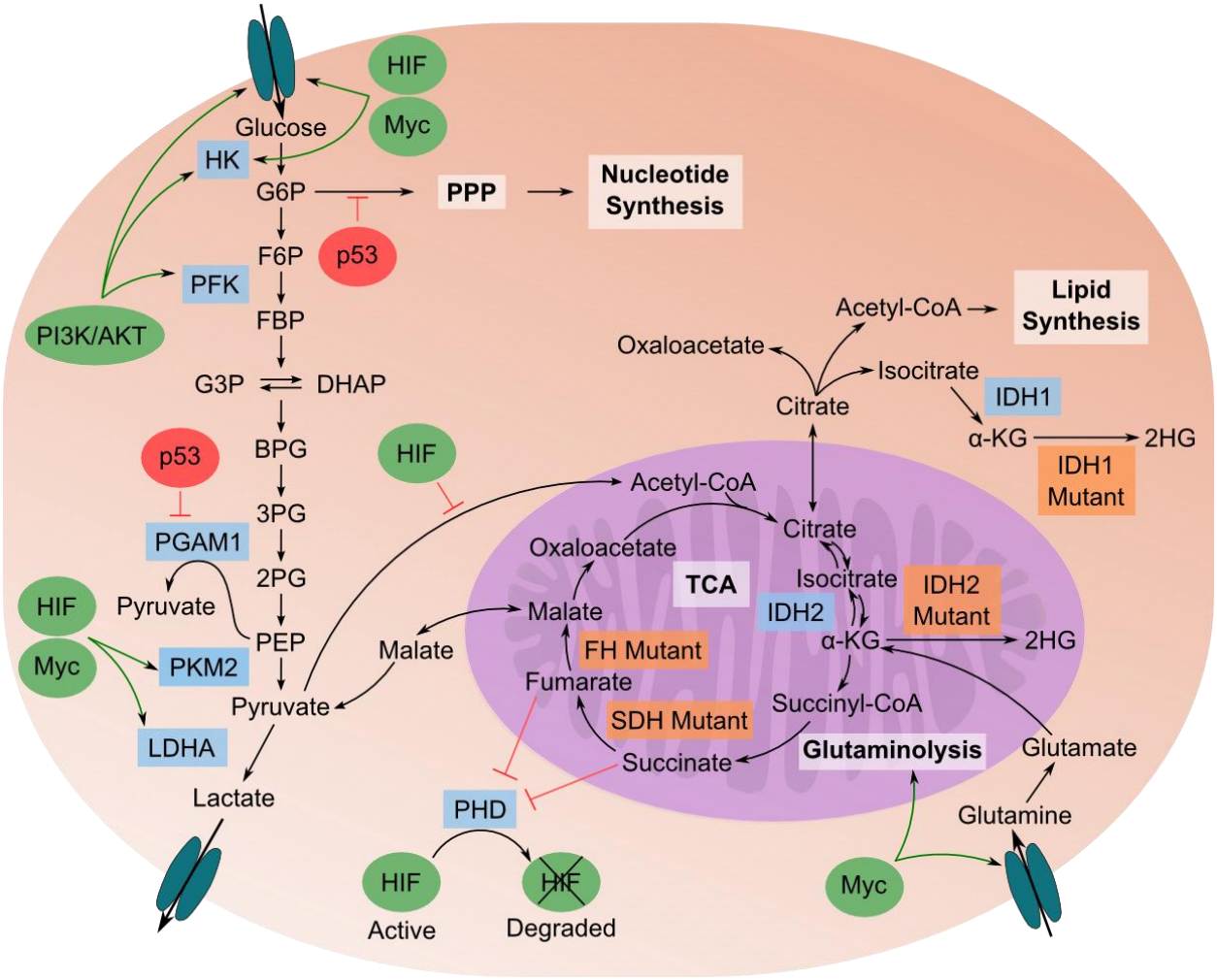

Figure 1.3. Illustration of important relationships between metabolome, proteome, and genome in cancerous cells. Glycolysis breaks down glucose into pyruvate, which is then fermented to lactate; pyruvate flux through the TCA cycle is down-regulated in cancer cells. Pathways branching off of glycolysis (such as the PPP) generate biochemical building blocks to sustain the high proliferative rate of cancer cells. Specific genetic and enzyme-level behaviors are described in the main text. Blue boxes are enzymes important in transitioning to a cancer metabolic phenotype; orange boxes are enzymes that are mutated in cancer cells. Green ovals are oncogenes that are up-regulated in cancer; red ovals are tumor suppressors that are down-regulated in cancer. Abbreviations are as defined in the abbreviations section. Figure from Vermeersch, *et al*, 2013.[1]

Even with most CCs expressing less-active PKM2 over PKM1, they still produce abnormally high levels of lactic acid. This increase in lactic acid production suggests the possible existence

of another path from PEP to pyruvate, as pyruvate fermentation produces lactic acid. An alternative pathway has been found, shown in Figure 1.3, that converts PEP to pyruvate through the phosphorylation of the glycolytic enzyme phosphoglycerate mutase 1 (PGAM1).[57] PEP has been shown to directly phosphorylate PGAM1 without requiring enolase conversion of PEP to 2-phosphoglycerate.[57] The phosphorylation reaction produces pyruvate without producing ATP, allowing pyruvate production to be decoupled from energy generation and the low activity of PKM2.[57] By decoupling energy generation from glycolysis, pyruvate production from PEP can continue, regardless of ATP regulation or dependence on PKM2. This continuous pyruvate production accounts for the high levels of lactic acid characteristic of CCs.

A consequence of the Warburg effect is an elevated amount of lactic acid production, which is expelled by the CCs into their environment.[37] The lactic acid and CO_2 (generated by the PPP) produced is enough to lower the extracellular pH from 7.4 (physiological pH) to below 6.5 in some tumor locations.[58] This acidic environment helps cancer cells to decrease sensitivity to hypoxia, stimulate metastasis, and increase drug resistance.[59, 60] Recent research indicates that lactate might help suppress immune response to the tumor, as well as induce chronic inflammation in the tumor site.[61] Overall, the acidic environment of the tumor helps maintain and further tumorigenic potential.

1.2.2. Glutaminolysis

Along with aerobic glycolysis, another pathway discovered to have increased flux in cancer cells is glutaminolysis.[62] Glutaminolysis is a catabolic pathway that converts glutamine to lactate, producing NADPH. By increasing the flux through glutaminolysis, cancer cells are able to produce an abundance of NADPH, completely covering the needs of fatty acid biosynthesis.[62]

Glutamine has also been shown to play an important role in cancer metabolism by serving as an anaplerotic precursor to oxaloacetate (OAA), a TCA intermediate.[62]

c-Myc, a protein produced by the oncogene MYC, interacts with HIF to regulate several enzymes involved in glucose metabolism, shown in Figure 1.3, but has also recently been shown to play a role in glutaminolysis.[63, 64] Mitochondrial glutaminase (GLS) expression correlated with Myc expression in several different cell lines, including a human prostate cancer cell line.[64] GLS is a mitochondrial enzyme that converts glutamine to glutamate, the first step in the anaplerotic conversion of glutamine to OAA. Through characterization of the relationship between GLS and Myc expression, it was discovered that Myc indirectly regulates GLS through two microRNAs, miR-23a and miR-23b.[64] miR-23a/b target the 3' UTR of GLS and inhibit GLS expression. Myc alleviates miR-23a/b inhibition by transcriptionally repressing these two microRNAs, which in turn allows for increased GLS expression. The effect of Myc upon the conversion of glutamine to proline has also been studied. It was shown that Myc stimulates proline production by suppressing proline oxidase, also known as proline dehydrogenase (POX/PRODH), through miR-23b*[64, 65] (miR-23b & miR-23b* are processed from the same transcript). POX/PRODH is an enzyme involved in the first step of proline catabolism. This enzyme has been shown to act like a tumor suppressor[66-69] - when proline is metabolized to glutamine, electrons are produced and in turn produce ROS, which eventually leads to apoptosis. It is not yet known why proline production is stimulated through conversion of glutamine.

The effect of GLS suppression on glutamine-dependent tumor cells has also been studied. Tumor cells are able to use glucose sources to compensate for the lack of glutamine using the enzyme pyruvate carboxylase.[70] In some glutamine-independent cancer cell lines in which GLS suppression had no effect, pyruvate carboxylase was also found to be active. During

gluconeogenesis, pyruvate carboxylase is responsible for producing oxaloacetate. The mechanism of pyruvate carboxylase induction is not yet known, but it is believed to be complex.[70] Pyruvate carboxylase may allow glutamine-dependent cancer cells a pathway for resistance against glutamine-targeted therapies.

1.2.3. Altered Metabolism: Byproduct or Condition of Cancer?

Cancer metabolism is clearly different from normal cellular metabolism, but it has still not been conclusively determined if this alteration is a byproduct or a necessary condition of cancer. Originally, Warburg postulated his effect as a condition of cancer, and not as a product of the cells being cancerous.[37] Recently, experimental evidence has been offered in favor of the metabolism shift being a determinant of cancer. As mentioned above, when CCs were forced to express PKM1 over PKM2 *in vivo*, decreased tumor growth and development rate were seen. PKM1 expression was shown to favor oxidative phosphorylation over glycolysis, showing that CCs not partaking in the Warburg effect were at a proliferative disadvantage to those that did. Further experimental support has been provided by a dicholoroacetate-activated shift from glycolysis to oxidative phosphorylation in CCs causing a decreased growth rate and apoptotic sensitivity in the CCs, two cancer hallmarks.[71] The fact that this metabolic alteration has the capability to cause CCs to lose defining hallmarks suggests that cancer metabolism is a necessary condition of cancer rather than just a byproduct.

Further evidence of metabolism assisting in the carcinogenic transition comes from the additional regulatory roles that metabolites play in controlling proliferation. For example, some metabolites can also serve as signaling molecules. Diacylglycerol, a lipid that plays a structural role in membranes, acts as a second messenger in mammalian cells; deregulation of diacylglycerol can lead to cancer progression through activation of protein kinase C, a family of

kinases that regulate cellular process such as proliferation and apoptosis.[72] Arginine, a metabolite involved in many anabolic pathways, plays a role as a signaling molecule in angiogenesis, tumor development, and apoptosis.[73] Along with having roles as signaling molecules, metabolites can also directly control gene expression in three different ways: they can bind to regulatory regions of mRNAs, activate transcription factors upon binding, and take part in epigenetic regulation such as post-transcriptional modification of histones.[73] Since metabolism assists in the transition to a cancerous state and affects many pathways through signaling and control of gene expression, it serves as a potential target for cancer therapeutics.[74, 75]

1.2.4. Cancer stem cell metabolism

Though study of CSC metabolism is an emerging field, there are suggestions that CSC metabolism would differ from CC metabolism. CSCs exist in a state of quiescence, and therefore their metabolic demands are probably quite different from the fast-growing state of CCs. Along with this, one of the assays used to separate CSCs from CCs is based on the enzymatic activity of aldehyde dehydrogenase (ALDH).[76]ALDH activity is higher in CSCs and is thought to be connected to their chemoresistance.[77] Intriguingly, ALDH activity is higher in quiescent CSCs, suggesting that this difference is not merely an artifact of a slower metabolic rate of CSCs compared to CCs, which indicates that both enzymes and metabolite levels in pathways associated with ALDH could also differ to some extent between these two cells.

As previously described, one of the most well-known metabolic alterations in cancer is the Warburg effect. In an effort to determine if CSCs utilize anaerobic glycolysis to the same extent CCs do, one group looked at glycolysis utilization in glioma and glioma stem cells (GSCs).[78] They discovered that GSCs have much lower glycolysis activity than glioma cells and mainly use oxidative phosphorylation for most of their ATP generation, although GSCs were still able to

switch freely between the two energy-generating pathways. They theorized that glioma cells switch to anaerobic glycolysis during differentiation from GSCs. Interestingly, another group has looked at CSCs in glioblastomas and has found the exact opposite holds true for these CSCs; they have high flux through glycolysis and use this pathway for most of their energy generation.[79] Based on these observations, it is possible that different CSC populations could have unique metabolic profiles that vary between different cell types.

Even though there has been some preliminary research done on CSC metabolism, most of it has been extremely focused on glycolysis and the Warburg effect. Only one study has been done that looks at system-wide metabolic differences between CCs and CSCs, and that study focused more on the metabolic differences between freshly derived CSCs and cultured CSCs and the tumors formed from these cells.[80] With a better understanding of systems-level metabolic differences between CSCs and CCs, we would better understand how CSCs function and therefore be better prepared to isolate and treat these cells.

1.3. Metabolomics and cancer

Metabolomics is the emerging field focused on comprehensive profiling of metabolites in a sample, whether intracellular or from circulating biofluids. The ability of metabolomics to measure high-throughput, system-wide phenotypes gives it great power in the field of oncology to further characterize what is happening in cancer cells.

1.3.1. Metabolomics analytical technology

Metabolites are very chemically diverse; they range from non-polar, long chain lipids to polar, small amino acids. Due to this vast chemical diversity, no single analytical method can measure at once all possible metabolites. Therefore, researches will either confine themselves to a smaller range of metabolites or combine multiple metabolomics technologies to cover a wider range. The

two dominant metabolomics technologies are nuclear magnetic resonance (NMR) spectroscopy and mass spectrometry (MS) coupled to a separation technique. Both of these technologies and the roles they play in metabolomics are extensively detailed elsewhere,[81-83] but a brief description will be given here.

1.3.1.1. Nuclear Magnetic Resonance

NMR spectroscopy provides quantitative and structural information and can measure a wide range of metabolites with little to no sample preparation. Techniques including high resolution NMR (HR-NMR) spectroscopy and high resolution magic angle spinning NMR (HR-MAS-NMR) spectroscopy have been used to profile cancer metabolism in biofluids as well as tissue samples, and are particularly valuable since they do not destroy samples, allowing for parallel analysis with other techniques.[84, 85] Another emerging technology, hyperpolarized NMR spectroscopy, has been used to characterize cancer metabolism by tracing metabolite levels *in vivo*[86], with potential applications in clinical diagnosis or treatment of cancer.[87] One limitation of NMR spectroscopy, though, is its low sensitivity and thus higher limits of detection for metabolites. Additionally, in complex mixtures the interpretability of NMR spectra and association with specific metabolite identities can be difficult.

1.3.1.2. Mass Spectrometry

MS provides semi-quantitative information with very high sensitivity, allowing the analysis of low-abundance metabolites. MS-based analyses can be broadly divided into direct injection techniques – including direct infusion mass spectrometry (DIMS)[88] and direct analysis in real time (DART-MS)[89] – and separation-coupled techniques, including gas chromatography (GC-MS), liquid chromatography (LC-MS), and capillary electrophoresis (CE-MS). Common types of mass spectrometers include time-of-flight (TOF), quadrupole time-of-flight (QTOF),

quadrupole, and orbitrap. Separation methods and MS can also be combined in series (GCxGC-MS or LC-MS/MS) to gain better separation or more structural information. However, many MS-based techniques require extensive sample preparation and usually can only measure specific subsets of metabolites.

1.3.1.3. Data Handling, Processing, and Analysis

The complex raw data captured by metabolomics instruments must first be converted into human-interpretable measurements; the resulting vast datasets then require significant analysis and interpretation. Numerous data processing techniques and packages have been created for all steps of this data-processing pipeline.[90] Packages vary depending on the technology used to generate the data set and the goal of the processing. For example, packages aimed at specific technologies (XCMS for LC-MS)[91] will have different metabolite identification methods than packages aimed at another technology (ChromaTOF for GC-TOF-MS). Even though packages differ, most processing pipelines follow a similar trend (but not necessarily in this order): quantification of analyte levels in some way, identification of analytes, and finally alignment of analytes across multiple samples. Analysis of these processed metabolomic data sets can involve several different techniques, many of which can be categorized as univariate or multivariate analysis.[92] Univariate analyses only assess one variable at a time; common examples include fold change calculations and statistical hypothesis testing (t-test, ANOVA) with false discovery rate correction. Multivariate analyses takes into account two or more variables and include correlations, principal components analysis (PCA), partial least squares discriminant analysis (PLS-DA), and set/pathway enrichment analysis. Both uni- and multivariate approaches are usually used for analysis of metabolomics data sets, in order to capture metabolite variation on both an individual and a systems-scale level.

1.3.2. Metabolomics-based discoveries of altered cancer metabolism

The system-wide analyses of metabolomics allow a unique opportunity for the study of cancer biology by enabling deep investigation of targeted aspects of cancer metabolism while also allowing discovery-based analysis of metabolism writ large.

For example, $NADP^+$-dependent isocitrate dehydrogenases 1 and 2 (IDH1 and IDH2) are commonly subject to gain-of-function point mutations in gliomas.[93] Using metabolomics, it was discovered that mutated IDH1 and IDH2 catalyze *(R)*-2-hydroxyglutarate (2HG), a rare metabolite, from α-ketoglutarate (α-KG) (Figure 1.3).[94] 2HG has been referred to as an oncometabolite, as its production helps to further the cancer phenotype.[94, 95] Metabolic profiling on glioma cells using LC-MS/MS and GC-MS showed that IDH1/2 mutations caused *N*-acetylated amino acid and TCA cycle intermediate levels to drop and biosynthetic molecules to accumulate, while not affecting glycolytic intermediates.[96] The effects of IDH1/2 mutations on the metabolome were very similar to the changes caused by treating normal cells with 2HG, showing that it is production of the oncometabolite 2HG and not the loss of IDH1/2's normal function that causes these changes.[96]

Another (though somewhat disputed[97]) example of mechanistic insight from metabolomics is in sarcosine's putative role in prostate cancer progression. Samples from patients with benign, localized and metastatic prostate cancer were profiled using both LC-MS and GC-MS. From this metabolic profiling, sarcosine levels were identified as increasing from benign to metastatic prostate cancer. *In vitro*, sarcosine levels were shown to directly correlate to a cell's level of invasiveness. Further investigation showed that sarcosine is regulated by an androgen receptor and ETS gene fusions through transcriptional control of its regulatory enzymes.[98]

A final example of metabolomics-based mechanistic insight is the recent study of extracellular metabolite profiles across the NCI-60 cancer cell lines.[99] Glycine consumption was found to be correlated with proliferation rate in cancerous cells, but not in proliferative non-cancerous cells, suggesting cancer-specific behavior. *De novo* purine nucleotide biosynthesis was one pathway involved in the increased glycine consumption. Follow-up analysis of breast cancer gene expression data revealed that glycine mitochondrial enzyme expression correlated with cancer mortality.

1.3.3. Biomarkers and diagnosis

A central focus in cancer metabolomics research is biomarker discovery. Metabolites are reasonable biomarkers and diagnostics, as they can be easily measured from noninvasive urine or blood samples. Many groups are attempting to use metabolic profiles as biomarkers or diagnostic tools since levels of multiple metabolites can provide better classification than a single entity. For example, the diagnostic capability of a set of 113 *cis*-diol structured urinary metabolites for liver cancer resulted in a lower false-positive rate than the traditional tumor marker alpha-fetoprotein when classifying liver cancer against hepatocirrhosis and chronic hepatitis samples.[100] Essentially every type of cancer is being investigated for metabolic biomarkers and diagnosis, including breast,[101-107] colon,[108-113] kidney,[114-117] liver,[100, 118-124] and ovarian.

A major focus in ovarian cancer metabolomics research has been in early detection, as the 5-year survival rate when caught in early stages is greater than 90%, but when diagnosed in later stages (as it is for most patients) is almost inverted.[125, 126] A number of studies have attempted to use metabolomics analysis of urine or serum as an early diagnosis tool.[89, 127, 128] One particularly promising model used DART-MS to profile the metabolome of 44 ovarian cancer patients and 50

healthy patients through serum samples, obtaining 99% separation accuracy using a customized algorithm.[89]

1.3.4. Emerging applications of metabolomics in cancer research

1.3.4.1. Metabolomics and Metastasis

Metabolomics research has shown promising results for detection of metastasis. Metabolic profiles of serum or urine samples suggest predictive capabilities for diagnosing metastases forming from gastric cancer[129], colorectal cancer [130], kidney[131, 132], and breast cancer[104, 105, 133]. Other studies have focused on specific metastatic sites such as leptomeningeal carcinomatosis[134] and bone metastases[135], the latter of which contain higher levels of cholesterol for prostate cancer metastases when compared to other cancerous bone metastases and normal bone.

1.3.4.2. Staging of Cancer

Beyond detection, metabolomics may also serve a role in distinguishing between different stages of cancer. In one study, GC-MS analysis of serum from pancreatic cancer patients was able to distinguish between Stage III, Stage IVa, and Stage IVb groups.[136] Another study used GC-TOF-MS to analyze ovarian cancer samples and showed metabolic distinction between ovarian carcinomas and borderline tumors.[137] In colorectal cancer, HR-MAS-NMR profiling not only distinguished between tumor and adjacent mucosa samples, but also between the mucosa samples themselves based on the stage of their adjacent tumor.[138]

1.3.4.3. Metabolomics and Treatment

An emerging field of study for metabolomics is pharmacometabolomics – the use of metabolomics to predict physiological responses for drug efficacy and/or toxicity. There are currently few pharmacometabolomics studies in oncology, but research in the area is expected to

grow[139], particularly since pharmacometabolomics is already achieving widespread attention in other fields[140-146]. In a pharmacometabolomic study of toxicity effects of capecitabine on colorectal cancer patients, lipoprotein-derived lipid levels were discovered to correlate with the intensity of toxicity, yielding predictive capabilities.[147] In another study, metabolic profiling of serum before and during chemotherapy from breast cancer patients with metastasis found that metabolite profiles from HER-2 positive patients treated with paclitaxel and lapatinib correlated with overall survival and time to progression (though the correlation did not hold across the entire population).[148]

1.4. Thesis overview

Metabolomics holds great promise for advancing the understanding, diagnosis, and treatment of cancer. The approach has already been used to uncover and verify mechanisms of carcinogenesis and proliferation, identify numerous candidate diagnostic biomarkers in biofluid and biopsy samples, and even contribute to the staging of cancers and the characterization of treatment efficacy. However, one area metabolomics research has not been applied to is the differences between CC and CSC metabolism. Applying proven metabolomics techniques to CC and CSC metabolism will allow further understanding in an area of cancer that has been largely unexplored until now.

The purpose of this thesis was to profile CC and CSC metabolism *in vitro* using epithelial ovarian cancer as a model through three different approaches: (a) studying their baseline metabolic differences, (b) profiling metabolic differences in response to biologically based perturbations, and (c) profiling metabolic changes during mesenchymal-epithelial transition (MET).

1.4.1. Baseline metabolic differences between OCCs and OCSCs

As discussed above, there are initial indications that CSC and CC metabolism differ. For instance, CSCs are known to proliferate at a lower rate than CCs and could have different metabolic requirements based purely on their proliferation rates. In order to fully understand the differences between these two cells, a comparison between OCCs and OCSCs during normal growth was made. This comparison provided baseline differences between the two cell types. Profiling the cells over a period of 48 hours determined how the cells change during their normal feeding cycle and if there are significant changes over time during normal growth. Baseline differences can be used to understand the different metabolic requirements of the OCSCs as compared to the OCCs.

1.4.2. Metabolomic differences between OCCs and OCSCs in response to biologically based perturbations

In vitro growth conditions differ drastically from growth conditions found within the tumor. *In vitro*, all cells are supplied with an overabundance of nutrients, plenty of oxygen, and their environment is cleaned out every two to four days to remove buildup of expelled molecules and to provide fresh supplies of nutrients. Tumor conditions are nowhere near as ideal or stable as *in vitro* conditions. Cells do not grown in a monolayer, therefore the cells in the middle of the tumor do not receive an adequate supply of nutrients or oxygen, even with angiogenesis. Overall, these cells are growing in conditions far from ideal, and therefore they must alter their metabolism to continue to proliferate and sustain the tumor.

To mimic the harsh conditions in the *in vivo* tumor environment, biologically based perturbations were applied to the *in vitro* grown OCCs and OCSCs. The perturbations chosen for these experiments were glucose deprivation, hypoxia, ischemia, and chemotherapeutic treatment, which were applied over a period of 48 hours with time points taken. Profiling and comparing

OCC and OCSC metabolism in response to these perturbations can further understanding on how the two cells handle the stresses encountered in the tumor microenvironment.

1.4.3. Metabolic changes during MET

As discussed above, the epithelial to mesenchymal transition (EMT) occurs normally during embryonic development. Research into tumor metastasis has led to the belief that CCs use EMT to gain metastatic potential. Cells undergoing EMT have also been shown to obtain stem-like properties. MET is the reversal of EMT, and would mimic CCs losing stem-like properties. This experiment profiled the metabolism of OCCs undergoing MET – induced through microRNA transfection - and then the reverse EMT as the microRNA levels drop. Metabolic changes during differentiation-like conditions might give insight into metabolic pathways that could be targeted to stop the plastic transition between CSCs and CCs.

1.5. References

1. Vermeersch, K.A. & Styczynski, M.P. Applications of metabolomics in cancer research. *J Carcinog* **12**, 9 (2013).
2. Siegel, R., Ma, J., Zou, Z. & Jemal, A. Cancer statistics, 2014. *CA: A Cancer Journal for Clinicians* **64**, 9-29 (2014).
3. Jemal, A., Siegel, R., Xu, J.Q. & Ward, E. Cancer Statistics, 2010. *Ca-a Cancer Journal for Clinicians* **60**, 277-300 (2010).
4. Jemal, A. et al. Global Cancer Statistics. *Ca-a Cancer Journal for Clinicians* **61**, 69-90 (2011).
5. Pignata, S. et al. Chemotherapy in epithelial ovarian cancer. *Cancer Letters* **303**, 73-83 (2011).
6. Bapat, S.A. Human ovarian cancer stem cells. *Reproduction* **140**, 33-41 (2010).
7. Hanahan, D. & Weinberg, R.A. The hallmarks of cancer. *Cell* **100**, 57-70 (2000).
8. Stratton, M.R., Campbell, P.J. & Futreal, P.A. The cancer genome. *Nature* **458**, 719-724 (2009).
9. Hanahan, D. & Weinberg, R.A. Hallmarks of Cancer: The Next Generation. *Cell* **144**, 646-674 (2011).
10. Visvader, J.E. & Lindeman, G.J. Cancer stem cells in solid tumours: accumulating evidence and unresolved questions. *Nat. Rev. Cancer* **8**, 755-768 (2008).
11. Sugihara, E. & Saya, H. Complexity of cancer stem cells. *International Journal of Cancer* **132**, 1249-1259 (2013).
12. Reya, T., Morrison, S.J., Clarke, M.F. & Weissman, I.L. Stem cells, cancer, and cancer stem cells. *Nature* **414**, 105-111 (2001).

13. Magee, J.A., Piskounova, E. & Morrison, S.J. Cancer stem cells: impact, heterogeneity, and uncertainty. *Cancer Cell* **21**, 283-296 (2012).
14. Shackleton, M. Normal stem cells and cancer stem cells: similar and different. *Seminars in Cancer Biology* **20**, 85-92 (2010).
15. Lapidot, T. et al. A cell initiating human acute myeloid leukaemia after transplantation into SCID mice. *Nature* **367**, 645-648 (1994).
16. Bonnet, D. & Dick, J.E. Human acute myeloid leukemia is organized as a hierarchy that originates from a primitive hematopoietic cell. *Nat Med* **3**, 730-737 (1997).
17. Al-Hajj, M., Wicha, M.S., Benito-Hernandez, A., Morrison, S.J. & Clarke, M.F. Prospective identification of tumorigenic breast cancer cells. *Proc Natl Acad Sci U S A* **100**, 3983-3988 (2003).
18. Medema, J.P. Cancer stem cells: The challenges ahead. *Nat Cell Biol* **15**, 338-344 (2013).
19. Garvalov, B.K. & Acker, T. Cancer stem cells: a new framework for the design of tumor therapies. *Journal of Molecular Medicine-Jmm* **89**, 95-107 (2011).
20. Bapat, S.A., Mali, A.M., Koppikar, C.B. & Kurrey, N.K. Stem and Progenitor-Like Cells Contribute to the Aggressive Behavior of Human Epithelial Ovarian Cancer. *Cancer Res.* **65**, 3025-3029 (2005).
21. Curley, M.D. et al. CD133 Expression Defines a Tumor Initiating Cell Population in Primary Human Ovarian Cancer. *Stem Cells* **27**, 2875-2883 (2009).
22. Zhang, S. et al. Identification and Characterization of Ovarian Cancer-Initiating Cells from Primary Human Tumors. *Cancer Res.* **68**, 4311-4320 (2008).
23. Gao, Q.L., Geng, L., Kvalheim, G., Gaudernack, G. & Suo, Z.H. Identification of Cancer Stem-like Side Population Cells in Ovarian Cancer Cell Line OVCAR-3. *Ultrastruct. Pathol.* **33**, 175-181 (2009).
24. Morel, A.-P. et al. Generation of Breast Cancer Stem Cells through Epithelial-Mesenchymal Transition. *PLoS ONE* **3**, e2888 (2008).
25. Mani, S.A. et al. The Epithelial-Mesenchymal Transition Generates Cells with Properties of Stem Cells. *Cell* **133**, 704-715 (2008).
26. Micalizzi, D.S., Farabaugh, S.M. & Ford, H.L. Epithelial-mesenchymal transition in cancer: parallels between normal development and tumor progression. *J Mammary Gland Biol Neoplasia* **15**, 117-134 (2010).
27. Chaffer, C.L. & Weinberg, R.A. A perspective on cancer cell metastasis. *Science* **331**, 1559-1564 (2011).
28. Gangemi, R. et al. Cancer Stem Cells: A New Paradigm for Understanding Tumor Growth and Progression and Drug Resistance. *Current Medicinal Chemistry* **16**, 1688-1703 (2009).
29. Sharom, F.J. ABC multidrug transporters: structure, function and role in chemoresistance. *Pharmacogenomics* **9**, 105-127 (2008).
30. Alvero, A.B. et al. Molecular phenotyping of human ovarian cancer stem cells unravel the mechanisms for repair and chemo-resistance. *Cell Cycle* **8**, 158-166 (2009).
31. Meirelles, K. et al. Human ovarian cancer stem/progenitor cells are stimulated by doxorubicin but inhibited by Mullerian inhibiting substance. *Proceedings of the National Academy of Sciences* (2012).
32. Assfalg, M. et al. Evidence of different metabolic phenotypes in humans. *Proc. Natl. Acad. Sci. U. S. A.* **105**, 1420-1424 (2008).

33. Bernini, P. et al. Individual Human Phenotypes in Metabolic Space and Time. *Journal of Proteome Research* **8**, 4264-4271 (2009).
34. Fiehn, O. Metabolomics - the link between genotypes and phenotypes. *Plant Mol. Biol.* **48**, 155-171 (2002).
35. O'Connell, T.M. Recent advances in metabolomics in oncology. *Bioanalysis* **4**, 431-451 (2012).
36. Warburg, O., Posener, K. & Negelein, E. On the metabolism of carcinoma cells. *Biochemische Zeitschrift* **152**, 309-344 (1924).
37. Warburg, O. Origin of Cancer Cells. *Science* **123**, 309-314 (1956).
38. Cairns, R.A., Harris, I.S. & Mak, T.W. Regulation of cancer cell metabolism. *Nat. Rev. Cancer* **11**, 85-95 (2011).
39. Elstrom, R.L. et al. Akt stimulates aerobic glycolysis in cancer cells. *Cancer Res.* **64**, 3892-3899 (2004).
40. Semenza, G.L. HIF-1: upstream and downstream of cancer metabolism. *Current Opinion in Genetics & Development* **20**, 51-56 (2010).
41. Papandreou, I., Cairns, R.A., Fontana, L., Lim, A.L. & Denko, N.C. HIF-1 mediates adaptation to hypoxia by actively downregulating mitochondrial oxygen consumption. *Cell Metabolism* **3**, 187-197 (2006).
42. Kim, J.W., Tchernyshyov, I., Semenza, G.L. & Dang, C.V. HIF-1-mediated expression of pyruvate dehydrogenase kinase: A metabolic switch required for cellular adaptation to hypoxia. *Cell Metabolism* **3**, 177-185 (2006).
43. Lu, C.W., Lin, S.C., Chen, K.F., Lai, Y.Y. & Tsai, S.J. Induction of pyruvate dehydrogenase kinase-3 by hypoxia-inducible factor-1 promotes metabolic switch and drug resistance. *Journal of Biological Chemistry* **283**, 28106-28114 (2008).
44. Mathupala, S.P., Heese, C. & Pedersen, P.L. Glucose catabolism in cancer cells - The type II hexokinase promoter contains functionally active response elements for the tumor suppressor p53. *Journal of Biological Chemistry* **272**, 22776-22780 (1997).
45. Matoba, S. et al. p53 regulates mitochondrial respiration. *Science* **312**, 1650-1653 (2006).
46. Bensaad, K. et al. TIGAR, a p53-inducible regulator of glycolysis and apoptosis. *Cell* **126**, 107-120 (2006).
47. Kondoh, H. et al. Glycolytic enzymes can modulate cellular life span. *Cancer Res.* **65**, 177-185 (2005).
48. King, A., Selak, M.A. & Gottlieb, E. Succinate dehydrogenase and fumarate hydratase: linking mitochondrial dysfunction and cancer. *Oncogene* **25**, 4675-4682 (2006).
49. Selak, M.A. et al. Succinate links TCA cycle dysfunction to oncogenesis by inhibiting HIF-α prolyl hydroxylase. *Cancer Cell* **7**, 77-85 (2005).
50. Isaacs, J.S. et al. HIF overexpression correlates with biallelic loss of fumarate hydratase in renal cancer: Novel role of fumarate in regulation of HIF stability. *Cancer Cell* **8**, 143-153 (2005).
51. Pollard, P.J. et al. Accumulation of Krebs cycle intermediates and over-expression of HIF1α in tumours which result from germline FH and SDH mutations. *Hum. Mol. Genet.* **14**, 2231-2239 (2005).
52. Mazurek, S., Boschek, C.B., Hugo, F. & Eigenbrodt, E. Pyruvate kinase type M2 and its role in tumor growth and spreading. *Seminars in Cancer Biology* **15**, 300-308 (2005).
53. Jurica, M.S. et al. The allosteric regulation of pyruvate kinase by fructose-1,6-bisphosphate. *Structure (London, England : 1993)* **6**, 195-210 (1998).

54. Vander Heiden, M.G. et al. Bcl-x(L) complements Saccharomyces cerevisiae genes that facilitate the switch from glycolytic to oxidative metabolism. *Journal of Biological Chemistry* **277**, 44870-44876 (2002).
55. Christofk, H.R. et al. The M2 splice isoform of pyruvate kinase is important for cancer metabolism and tumour growth. *Nature* **452**, 230-U274 (2008).
56. Jiang, P. et al. p53 regulates biosynthesis through direct inactivation of glucose-6-phosphate dehydrogenase. *Nature Cell Biology* **13**, 310-U278 (2011).
57. Heiden, M.G.V. et al. Evidence for an Alternative Glycolytic Pathway in Rapidly Proliferating Cells. *Science* **329**, 1492-1499 (2010).
58. Fukamachi, T. et al. Tumor specific low pH environments enhance the cytotoxicity of lovastatin and cantharidin. *Cancer Lett* **297**, 182-189 (2010).
59. Gillies, R.J., Robey, I. & Gatenby, R.A. Causes and consequences of increased glucose metabolism of cancers. *Journal of nuclear medicine : official publication, Society of Nuclear Medicine* **49 Suppl 2**, 24S-42S (2008).
60. Kato, Y. et al. Acidic extracellular microenvironment and cancer. *Cancer Cell Int* **13**, 89 (2013).
61. Choi, S.Y., Collins, C.C., Gout, P.W. & Wang, Y. Cancer-generated lactic acid: a regulatory, immunosuppressive metabolite? *J Pathol* **230**, 350-355 (2013).
62. DeBerardinis, R.J. et al. Beyond aerobic glycolysis: Transformed cells can engage in glutamine metabolism that exceeds the requirement for protein and nucleotide synthesis. *Proc. Natl. Acad. Sci. U. S. A.* **104**, 19345-19350 (2007).
63. Wise, D.R. et al. Myc regulates a transcriptional program that stimulates mitochondrial glutaminolysis and leads to glutamine addiction. *Proc. Natl. Acad. Sci. U. S. A.* **105**, 18782-18787 (2008).
64. Gao, P. et al. c-Myc suppression of miR-23a/b enhances mitochondrial glutaminase expression and glutamine metabolism. *Nature* **458**, 762-U100 (2009).
65. Liu, W. et al. miR-23b*targets proline oxidase, a novel tumor suppressor protein in renal cancer. *Oncogene* **29**, 4914-4924 (2010).
66. Donald, S.P. et al. Proline oxidase, encoded by p53-induced gene-6, catalyzes the generation of proline-dependent reactive oxygen species. *Cancer Res.* **61**, 1810-1815 (2001).
67. Liu, Y., Borchert, G.L., Surazynski, A., Hu, C.A. & Phang, J.M. Proline oxidase activates both intrinsic and extrinsic pathways for apoptosis: the role of ROS/superoxides, NFAT and MEK/ERK signaling. *Oncogene* **25**, 5640-5647 (2006).
68. Liu, Y., Borchert, G.L., Surazynski, A. & Phang, J.M. Proline oxidase, a p53-induced gene, targets COX-2/PGE(2) signaling to induce apoptosis and inhibit tumor growth in colorectal cancers. *Oncogene* **27**, 6729-6737 (2008).
69. Liu, Y.M. et al. Proline Oxidase Functions as a Mitochondrial Tumor Suppressor in Human Cancers. *Cancer Res.* **69**, 6414-6422 (2009).
70. Cheng, T.L. et al. Pyruvate carboxylase is required for glutamine-independent growth of tumor cells. *Proc. Natl. Acad. Sci. U. S. A.* **108**, 8674-8679 (2011).
71. Bonnet, S. et al. A Mitochondria-K+ Channel Axis Is Suppressed in Cancer and Its Normalization Promotes Apoptosis and Inhibits Cancer Growth. *Cancer cell* **11**, 37-51 (2007).
72. Griner, E.M. & Kazanietz, M.G. Protein kinase C and other diacylglycerol effectors in cancer. *Nat Rev Cancer* **7**, 281-294 (2007).

73. Arakaki, A.K. et al. Identification of metabolites with anticancer properties by computational metabolomics. *Molecular Cancer* **7** (2008).
74. Kurrey, N.K. et al. Snail and Slug mediate radioresistance and chemoresistance by antagonizing p53-mediated apoptosis and acquiring a stem-like phenotype in ovarian cancer cells. *Stem Cells (Durham, NC, U. S.)* **27**, 2059-2068 (2009).
75. Eastham, A.M. et al. Epithelial-Mesenchymal Transition Events during Human Embryonic Stem Cell Differentiation. *Cancer Res.* **67**, 11254-11262 (2007).
76. Ma, I. & Allan, A.L. The role of human aldehyde dehydrogenase in normal and cancer stem cells. *Stem cell reviews* **7**, 292-306 (2011).
77. Tanei, T. et al. Association of breast cancer stem cells identified by aldehyde dehydrogenase 1 expression with resistance to sequential Paclitaxel and epirubicin-based chemotherapy for breast cancers. *Clin Cancer Res* **15**, 4234-4241 (2009).
78. Vlashi, E. et al. Metabolic state of glioma stem cells and nontumorigenic cells. *Proceedings of the National Academy of Sciences* (2011).
79. Zhou, Y. et al. Metabolic alterations in highly tumorigenic glioblastoma cells: preference for hypoxia and high dependency on glycolysis. *J Biol Chem* **286**, 32843-32853 (2011).
80. Mlynarik, V. et al. In vivo metabolic profiling of glioma-initiating cells using proton magnetic resonance spectroscopy at 14.1 Tesla. *NMR in biomedicine* **25**, 506-513 (2012).
81. Dunn, W.B., Bailey, N.J.C. & Johnson, H.E. Measuring the metabolome: current analytical technologies. *Analyst* **130**, 606-625 (2005).
82. Zhang, A.H., Sun, H., Wang, P., Han, Y. & Wang, X.J. Modern analytical techniques in metabolomics analysis. *Analyst* **137**, 293-300 (2012).
83. Dunn, W.B., Broadhurst, D.I., Atherton, H.J., Goodacre, R. & Griffin, J.L. Systems level studies of mammalian metabolomes: the roles of mass spectrometry and nuclear magnetic resonance spectroscopy. *Chemical Society reviews* **40**, 387-426 (2011).
84. Duarte, I.F. & Gil, A.M. Metabolic signatures of cancer unveiled by NMR spectroscopy of human biofluids. *Progress in Nuclear Magnetic Resonance Spectroscopy* **62**, 51-74 (2012).
85. Beckonert, O. et al. High-resolution magic-angle-spinning NMR spectroscopy for metabolic profiling of intact tissues. *Nat. Protoc.* **5**, 1019-1032 (2010).
86. Marin-Valencia, I. et al. Analysis of tumor metabolism reveals mitochondrial glucose oxidation in genetically diverse human glioblastomas in the mouse brain in vivo. *Cell Metab* **15**, 827-837 (2012).
87. Kurhanewicz, J. et al. Analysis of cancer metabolism by imaging hyperpolarized nuclei: prospects for translation to clinical research. *Neoplasia (New York, N.Y.)* **13**, 81-97 (2011).
88. Lin, L. et al. Direct infusion mass spectrometry or liquid chromatography mass spectrometry for human metabonomics? A serum metabonomic study of kidney cancer. *Analyst* **135**, 2970-2978 (2010).
89. Zhou, M. et al. Rapid Mass Spectrometric Metabolic Profiling of Blood Sera Detects Ovarian Cancer with High Accuracy. *Cancer Epidemiology Biomarkers & Prevention* **19** (2010).
90. Blekherman, G. et al. Bioinformatics tools for cancer metabolomics. *Metabolomics* **7**, 329-343 (2011).
91. Tautenhahn, R., Patti, G.J., Rinehart, D. & Siuzdak, G. XCMS Online: a web-based platform to process untargeted metabolomic data. *Anal Chem* **84**, 5035-5039 (2012).

92. Saccenti, E., Hoefsloot, H.J., Smilde, A., Westerhuis, J. & Hendriks, M.W.B. Reflections on univariate and multivariate analysis of metabolomics data. *Metabolomics*, 1-14 (2013).
93. Yan, H. et al. IDH1 and IDH2 Mutations in Gliomas. *New England Journal of Medicine* **360**, 765-773 (2009).
94. Dang, L. et al. Cancer-associated IDH1 mutations produce 2-hydroxyglutarate. *Nature* **462**, 739-U752 (2009).
95. Ward, P.S. & Thompson, C.B. Metabolic Reprogramming: A Cancer Hallmark Even Warburg Did Not Anticipate. *Cancer Cell* **21**, 297-308 (2012).
96. Reitman, Z.J. et al. Profiling the effects of isocitrate dehydrogenase 1 and 2 mutations on the cellular metabolome. *Proc. Natl. Acad. Sci. U. S. A.* **108**, 3270-3275, S3270/3271-S3270/3228 (2011).
97. Jentzmik, F. et al. Sarcosine in urine after digital rectal examination fails as a marker in prostate cancer detection and identification of aggressive tumours. *Eur Urol* **58**, 12-18; discussion 20-11 (2010).
98. Sreekumar, A. et al. Metabolomic profiles delineate potential role for sarcosine in prostate cancer progression. *Nature* **457**, 910-914 (2009).
99. Jain, M. et al. Metabolite profiling identifies a key role for glycine in rapid cancer cell proliferation. *Science* **336**, 1040-1044 (2012).
100. Yang, J. et al. Diagnosis of liver cancer using HPLC-based metabonomics avoiding false-positive result from hepatitis and hepatocirrhosis diseases. *J. Chromatogr., B: Anal. Technol. Biomed. Life Sci.* **813**, 59-65 (2004).
101. Oakman, C. et al. Uncovering the metabolomic fingerprint of breast cancer. *Int. J. Biochem. Cell Biol.* **43**, 1010-1020 (2011).
102. Oakman, C. et al. Targeting Metabolomics in Breast Cancer. *Curr Breast Cancer Rep* **4**, 249-256 (2012).
103. Slupsky, C.M. et al. Urine Metabolite Analysis Offers Potential Early Diagnosis of Ovarian and Breast Cancers. *Clinical Cancer Research* **16**, 5835-5841 (2010).
104. Asiago, V.M. et al. Early Detection of Recurrent Breast Cancer Using Metabolite Profiling. *Cancer Res.* **70**, 8309-8318 (2010).
105. Oakman, C. et al. Identification of a serum-detectable metabolomic fingerprint potentially correlated with the presence of micrometastatic disease in early breast cancer patients at varying risks of disease relapse by traditional prognostic methods. *Ann Oncol* **22**, 1295-1301 (2011).
106. Gu, H. et al. Principal component directed partial least squares analysis for combining nuclear magnetic resonance and mass spectrometry data in metabolomics: Application to the detection of breast cancer. *Anal. Chim. Acta* **686**, 57-63 (2011).
107. Li, M. et al. An HR-MAS MR metabolomics study on breast tissues obtained with core needle biopsy. *PLoS One* **6**, e25563 (2011).
108. Yue, H. et al. A Metabonomics Study of Colorectal Cancer by RRLC-QTOF/MS. *J. Liq. Chromatogr. Relat. Technol.* **36**, 428-438 (2013).
109. Nishiumi, S. et al. A novel serum metabolomics-based diagnostic approach for colorectal cancer. *PLoS One* **7**, e40459 (2012).
110. Chan, E.C.Y. et al. Metabolic Profiling of Human Colorectal Cancer Using High-Resolution Magic Angle Spinning Nuclear Magnetic Resonance (HR-MAS NMR)

Spectroscopy and Gas Chromatography Mass Spectrometry (GC/MS). *J. Proteome Res.* **8**, 352-361 (2009).
111. Qiu, Y. et al. Serum Metabolite Profiling of Human Colorectal Cancer Using GC-TOFMS and UPLC-QTOFMS. *J. Proteome Res.* **8**, 4844-4850 (2009).
112. Qiu, Y. et al. Urinary Metabonomic Study on Colorectal Cancer. *J. Proteome Res.* **9**, 1627-1634 (2010).
113. Li, S. et al. Plasma choline-containing phospholipids: potential biomarkers for colorectal cancer progression. *Metabolomics* **9**, 202-212 (2013).
114. Kind, T., Tolstikov, V., Fiehn, O. & Weiss, R.H. A comprehensive urinary metabolomic approach for identifying kidney cancer. *Anal. Biochem.* **363**, 185-195 (2007).
115. Ganti, S. & Weiss, R.H. Urine metabolomics for kidney cancer detection and biomarker discovery. *Urol. Oncol.: Semin. Orig. Invest.* **29**, 551-557 (2011).
116. Kim, K. et al. Urine metabolomic analysis identifies potential biomarkers and pathogenic pathways in kidney cancer. *OMICS* **15**, 293-304 (2011).
117. Ganti, S. et al. Urinary acylcarnitines are altered in human kidney cancer. *Int. J. Cancer* **130**, 2791-2800 (2012).
118. Wang, X. et al. Urinary metabolic profiling identifies a key role for glycocholic acid in human liver cancer by ultra-performance liquid-chromatography coupled with high-definition mass spectrometry. *Clin Chim Acta* (2013).
119. Chen, T. et al. Serum and urine metabolite profiling reveals potential biomarkers of human hepatocellular carcinoma. *Mol. Cell. Proteomics* **10**, M110.004945, 004913 pp. (2011).
120. Gao, H. et al. Application of 1H NMR-based metabonomics in the study of metabolic profiling of human hepatocellular carcinoma and liver cirrhosis. *Cancer Sci.* **100**, 782-785 (2009).
121. Patterson, A.D. et al. Aberrant Lipid Metabolism in Hepatocellular Carcinoma Revealed by Plasma Metabolomics and Lipid Profiling. *Cancer Res.* **71**, 6590-6600 (2011).
122. Shariff, M.I.F. et al. Urinary metabolic biomarkers of hepatocellular carcinoma in an Egyptian population: A Validation Study. *J. Proteome Res.* **10**, 1828-1836 (2011).
123. Xue, R. et al. A serum metabolomic investigation on hepatocellular carcinoma patients by chemical derivatization followed by gas chromatography/mass spectrometry. *Rapid Commun. Mass Spectrom.* **22**, 3061-3068 (2008).
124. Yang, Y. et al. Metabonomic Studies of Human Hepatocellular Carcinoma Using High-Resolution Magic-Angle Spinning 1H NMR Spectroscopy in Conjunction with Multivariate Data Analysis. *J. Proteome Res.* **6**, 2605-2614 (2007).
125. Cho, K.R. & Shih, I.M. Ovarian Cancer. *Annual Review of Pathology-Mechanisms of Disease* **4**, 287-313 (2009).
126. Siegel, R., Naishadham, D. & Jemal, A. Cancer statistics, 2012. *CA: A Cancer Journal for Clinicians* **62**, 10-29 (2012).
127. Odunsi, K. et al. Detection of epithelial ovarian cancer using 1H-NMR-based metabonomics. *Int. J. Cancer* **113**, 782-788 (2005).
128. Zhang, T. et al. Identification of Potential Biomarkers for Ovarian Cancer by Urinary Metabolomic Profiling. *J. Proteome Res.* **12**, 505-512 (2013).
129. Hu, J.-D. et al. Prediction of gastric cancer metastasis through urinary metabolomic investigation using GC/MS. *World J. Gastroenterol.* **17**, 727-734 (2011).

130. Bertini, I. et al. Metabolomic NMR Fingerprinting to Identify and Predict Survival of Patients with Metastatic Colorectal Cancer. *Cancer Res.* **72**, 356-364 (2012).
131. Gao, H. et al. Metabonomic profiling of renal cell carcinoma: High-resolution proton nuclear magnetic resonance spectroscopy of human serum with multivariate data analysis. *Anal. Chim. Acta* **624**, 269-277 (2008).
132. Gao, H. et al. Application of ex vivo 1H NMR metabonomics to the characterization and possible detection of renal cell carcinoma metastases. *J. Cancer Res. Clin. Oncol.* **138**, 753-761 (2012).
133. Lu, X., Bennet, B., Mu, E., Rabinowitz, J. & Kang, Y. Metabolomic Changes Accompanying Transformation and Acquisition of Metastatic Potential in a Syngeneic Mouse Mammary Tumor Model. *J. Biol. Chem.* **285**, 9317-9321 (2010).
134. Cho, H.R. et al. An NMR metabolomics approach for the diagnosis of leptomeningeal carcinomatosis. *Cancer Res* **72**, 5179-5187 (2012).
135. Thysell, E. et al. Metabolomic characterization of human prostate cancer bone metastases reveals increased levels of cholesterol. *PLoS One* **5**, e14175 (2010).
136. Nishiumi, S. et al. Serum metabolomics as a novel diagnostic approach for pancreatic cancer. *Metabolomics* **6**, 518-528 (2010).
137. Denkert, C. et al. Mass spectrometry-based metabolic profiling reveals different metabolite patterns in invasive ovarian carcinomas and ovarian borderline tumors. *Cancer Res.* **66**, 10795-10804 (2006).
138. Jimenez, B. et al. (1)H HR-MAS NMR Spectroscopy of Tumor Induced Local Metabolic "Field-Effects" enables Colorectal Cancer Staging and Prognostication. *J Proteome Res* (2012).
139. Corona, G., Rizzolio, F., Giordano, A. & Toffoli, G. Pharmaco-metabolomics: An emerging "omics" tool for the personalization of anticancer treatments and identification of new valuable therapeutic targets. *J. Cell. Physiol.* **227**, 2827-2831 (2012).
140. Clayton, T.A. et al. Pharmaco-metabonomic phenotyping and personalized drug treatment. *Nature* **440**, 1073-1077 (2006).
141. Li, H.K. et al. Pharmacometabonomic phenotyping reveals different responses to xenobiotic intervention in rats. *Journal of Proteome Research* **6**, 1364-1370 (2007).
142. Clayton, T.A., Baker, D., Lindon, J.C., Everett, J.R. & Nicholson, J.K. Pharmacometabonomic identification of a significant host-microbiome metabolic interaction affecting human drug metabolism. *Proc. Natl. Acad. Sci. U. S. A.* **106**, 14728-14733 (2009).
143. Patterson, A.D. et al. Human Urinary Metabolomic Profile of PPAR alpha Induced Fatty Acid beta-Oxidation. *Journal of Proteome Research* **8**, 4293-4300 (2009).
144. West, P.R., Weir, A.M., Smith, A.M., Donley, E.L.R. & Cezar, G.G. Predicting human developmental toxicity of pharmaceuticals using human embryonic stem cells and metabolomics. *Toxicology and Applied Pharmacology* **247**, 18-27 (2010).
145. Nicholson, J.K., Wilson, I.D. & Lindon, J.C. Pharmacometabonomics as an effector for personalized medicine. *Pharmacogenomics* **12**, 103-111 (2011).
146. Abo, R. et al. Merging pharmacometabolomics with pharmacogenomics using '1000 Genomes' single-nucleotide polymorphism imputation: selective serotonin reuptake inhibitor response pharmacogenomics. *Pharmacogenetics and Genomics* **22**, 247-253 (2012).

147. Backshall, A., Sharma, R., Clarke, S.J. & Keun, H.C. Pharmacometabonomic Profiling as a Predictor of Toxicity in Patients with Inoperable Colorectal Cancer Treated with Capecitabine. *Clin. Cancer Res.* **17**, 3019-3028 (2011).
148. Tenori, L. et al. Exploration of serum metabolomic profiles and outcomes in women with metastatic breast cancer: A pilot study. *Mol. Oncol.* **6**, 437-444 (2012).

Chapter 2 OVCAR-3-derived ovarian cancer stem cells display distinct metabolic profiles

This chapter is taken from *OVCAR-3-derived ovarian cancer stem cells display distinct metabolic profiles*, which is under review in PLOS ONE.

2.1. Introduction

Ovarian cancer is the most deadly gynecological cancer and the 5th leading cause of cancer-related death in United States women. An estimated 15,500 U.S. women died from ovarian cancer in 2012.[1] Even though response to the first-line treatment is high, most patients (50-75%) relapse after the treatment.[2] Recently, side populations of cancer cells with ABC-transporter activity and ability to efflux certain compounds have been identified in many different types of tumors, including ovarian cancer.[3-5] These cells are referred to as cancer stem cells because of their many unique properties: they have self-renewal and differentiation capabilities and exhibit resistance to the effects of radiation and anticancer drugs.[6] Based on these properties, they are suspected as a primary cause of ovarian cancer recurrence.[7, 8]

We have previously established an ovarian cancer stem cell (OCSC) line as a sub-population of a widely-used ovarian cancer cell (OCC) line, OVCAR-3.[8] These cells were shown to demonstrate numerous characteristics of cancer stem cells, including self-renewal, the ability to produce differentiated progeny, increased expression of genes associated with cancer stem cells, higher invasiveness, migration potential, and enhanced chemoresistance. Transcriptional analysis identified changes in various signaling pathways including TGF-beta-dependent induction of epithelial-to-mesenchymal transition, regulation of lipid metabolism, and NOTCH and Hedgehog signaling. In addition, six pathways associated with metabolism were identified as

being enriched with genes differentially expressed between OCSCs and OCCs, suggesting a potential role of metabolic differences as a cause or consequence of the phenotypic differences between the two cell types.

Since transcriptional changes do not always directly translate to changes in metabolism, we sought to directly test the prediction that OCCs and isogenic OCSCs may display significant differences in metabolism. Metabolomics is the systems-scale analysis of the levels of small-molecule biochemical (metabolic) intermediates in the cell. Metabolomics is a field that is increasingly being brought to bear on the study of cancer, with promising results including insights into disease mechanisms as well as the identification of circulating biomarkers for potential use in diagnostics.[9-12] Metabolomics has the potential to reveal key intracellular pathways or metabolites and their related enzymes in OCSCs that may serve as potential therapeutic targets, as well as secreted or intracellular metabolites that may find potential use in diagnostic tests. However, to date metabolomics has rarely been exploited to study cancer stem cells. To our knowledge, the only reported application of metabolomics in this context was its use to study the differences between tumors derived from fresh glioma stem cells and cultured glioma stem cells *in vivo* using nuclear magnetic resonance spectroscopy.[13]

In this study, we analyzed the intracellular and extracellular metabolomic profile of both ovarian cancer cell types *in vitro* over two days using two dimensional gas chromatography-mass spectrometry (GCxGC-MS). Consistent with gene expression-driven predictions, we identified significant differences between the metabolism of these two cell types. Our findings are consistent with the hypothesis that metabolic changes may contribute to the functional differences between ovarian cancer stem cells and their more differentiated progeny that

represent the majority of bulk tumor tissue. More generally, our findings are consistent with the mounting body of evidence that altered metabolism is one of the hallmarks of cancer.[14]

2.2. Results & Discussion

2.2.1. OCCs and OCSCs have significant differences on an individual metabolite level

GCxGC-MS analysis of OCCs and OCSCs detected 211 intracellular and 203 extracellular reproducibly measurable analytes overall, including unknowns and analytes that did not map to known human metabolites (based on KEGG and HMDB identifications available in MetaboAnalyst). Differences due purely to growth media differences were removed for the intracellular data set, using the medium control experiment as a basis (as described in section 2.4.7), but could not be completely removed from the extracellular data set. Since the intracellular samples showed no medium-related artifacts and thus allowed for the most direct interpretation, moving forward we focused our attention and analysis on those data.

Once these analytes were removed, the resulting intracellular dataset contained 177 unknown and known analytes, which included 40 unique and annotated metabolites. Basic univariate analysis of metabolite levels provided insight into the differences between the two cell types. Of the 40 intracellular metabolites, 27 were significantly different (t-test, all time points, false discovery rate (FDR) < 0.05) between the two cell types, shown in Table 2.1. Nineteen of these 27 metabolites had a fold change greater than two. Based on these statistical differences, metabolism seems to be fundamentally altered in OCSCs, though it is impossible to conclude based on metabolite levels alone (without fluxes) whether this may be due to increased or decreased metabolism.

Table 2.1: List of intracellular metabolites statistically significant between OCCs and OCSCs and their fold changes. Fold changes represent the change of OCC levels with respect to OCSC levels of the metabolite.

Metabolite	p value	FDR	$\log_2$(FC)
Gamma-Aminobutyric acid	2.75E-16	1.10E-14	2.741
D-Psicose	4.96E-10	9.91E-09	1.997
Erythronic acid	4.57E-08	6.10E-07	1.411
Pyrophosphate	6.38E-08	6.38E-07	2.792
Fumaric acid	1.04E-07	8.29E-07	1.751
Erythritol	8.14E-07	5.43E-06	4.243
Putrescine	4.54E-05	2.59E-04	1.739
L-Isoleucine	6.83E-05	3.34E-04	1.187
L-Proline	7.51E-05	3.34E-04	2.736
L-Glutamate	8.80E-05	3.52E-04	1.107
L-Lysine	1.68E-04	6.11E-04	-1.155
Mannitol	2.06E-04	6.86E-04	0.702
Cholesterol	4.01E-04	1.23E-03	0.543
Glycerol	4.62E-04	1.25E-03	-0.754
Pyroglutamic acid	4.69E-04	1.25E-03	0.833
Ethanolamine	6.40E-04	1.51E-03	-0.626
L-Aspartic acid	6.15E-04	1.51E-03	1.265
Uridine 5'-monophosphate	1.09E-03	2.43E-03	0.675
3,7-Dimethyl-3-octanol	2.01E-03	4.00E-03	-0.364
Glycine	1.92E-03	4.00E-03	0.987
L-Malic acid	2.10E-03	4.00E-03	1.611
N-Decane	4.08E-03	7.09E-03	-0.536
Mannose 6-phosphate	4.05E-03	7.09E-03	0.600
Glycerol-3-phosphate	1.43E-02	2.38E-02	0.439
Citric acid	1.62E-02	2.60E-02	-0.267
Hydrogen sulfide	2.00E-02	3.08E-02	0.599
Hexadecane	2.26E-02	3.34E-02	-0.586

2.2.2. Metabolomic analysis reveals distinct metabolic profiles between OCCs and OCSCs

Unsupervised dimensional reduction using principal components analysis (PCA) showed complete separation for the intracellular metabolic profiles between OCCs and OCSCs, as seen in Figure 2.1. PCA of intracellular annotated metabolite measurements showed that the distinct metabolic profiles between the two cell types were captured mostly in principal component (PC)

1 with the second PC providing additional separation, as seen in Figure 2.1B. In both of the intracellular plots, the second PC shows some separation between different time points. The fact that this unsupervised method was able to separate sample classes so strongly in the first few PCs suggests the presence of true metabolic differences that are not artifacts of data analysis. PCA based on the entire measured dataset (including unknowns, not just the identified human metabolites) yielded similar separation (Figure 2.1A), with a number of unknowns having high loading scores in PCs 1 and 2, suggesting that the differences between the two cell types are not limited to just the well-characterized sections of cellular metabolism.

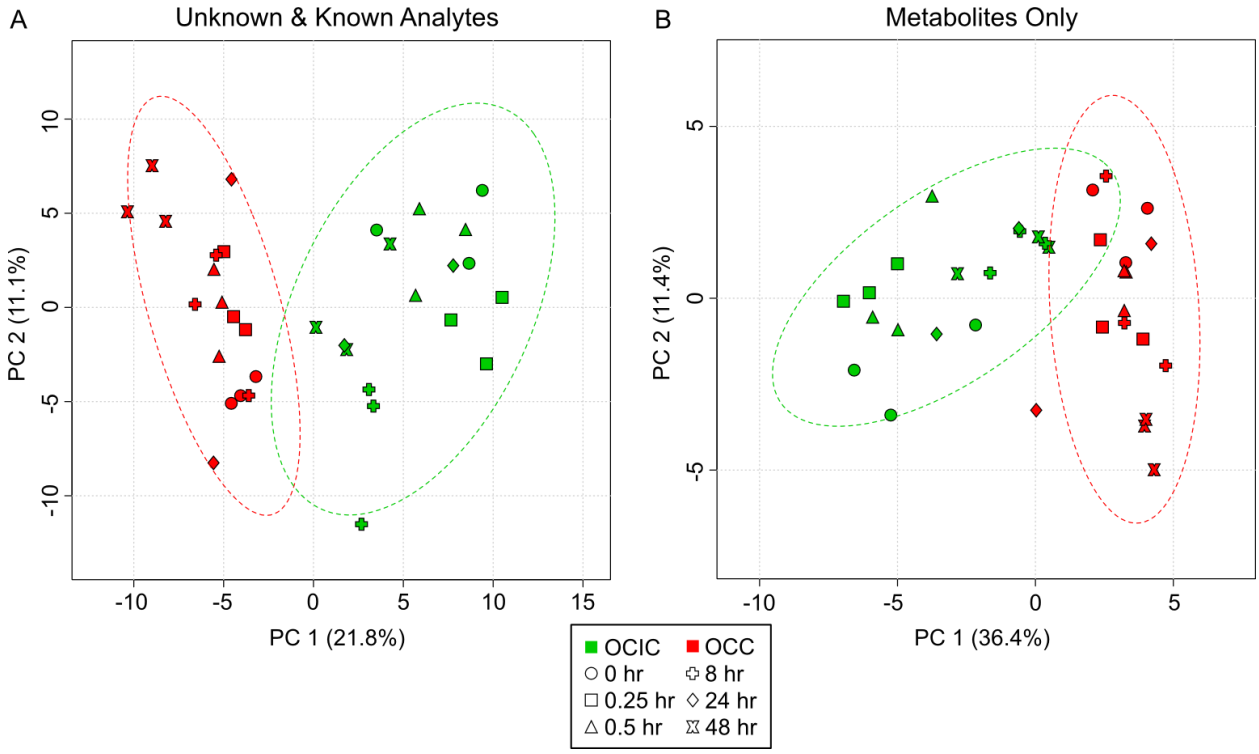

Figure 2.1: Principal components analysis easily distinguishes between the metabolic profiles of OCCs and OCSCs. Red points are OVCAR-3 cells, and green points are ovarian cancer stem cells at six different time points with three biological replicates at each time point. Principal component (PC) axes include the percentage of variation captured by each axis. A) PC 1 captures the cell type separation for the unknown and annotated analytes, with PC 2 capturing some time point separation. B) Including only the profiles of annotated metabolites shows complete cell type separation in PC 1 and some time point separation in PC 2.

Analysis of the PCA loadings revealed the metabolites that were the most important in causing the separation seen in the intracellular PCA plots. Fumarate, erythronic acid, psicose, pyrophosphate, gamma-aminobutyric acid, aspartate, isoleucine, uridine 5'-monophosphate, putrescine, and glutamate are most responsible for the cell type separation in the intracellular data set. Interestingly, putrescine, aspartate, glutamate, and fumarate are all involved in the arginine and proline pathway, which was identified in gene set enrichment analysis as significantly enriched in the OCSC phenotype (discussed in more detail below).

Hierarchically clustered heatmaps of the intracellular metabolic profiles also revealed distinct patterns, shown in Figure 2.2. The samples for OCC and OCSC cluster together tightly, showing the similarity within each specific cell type. Two main groups of analytes are evident within the clustered heatmap. Group 1 metabolites have higher levels in OCCs than OCSCs across all samples. This group consists mostly of amino acids and carbohydrates. Again, interestingly, putrescine, fumarate, glutamate, aspartate, and proline (metabolites involved in the arginine and proline pathway discussed below) all fall within group 1 of intracellular metabolites. Group 2 metabolites have higher levels in OCSCs and lower levels in OCCs across all samples, including numerous aliphatic compounds, such as diacetone alcohol, ethanolamine, N-decane, and hexadecane.

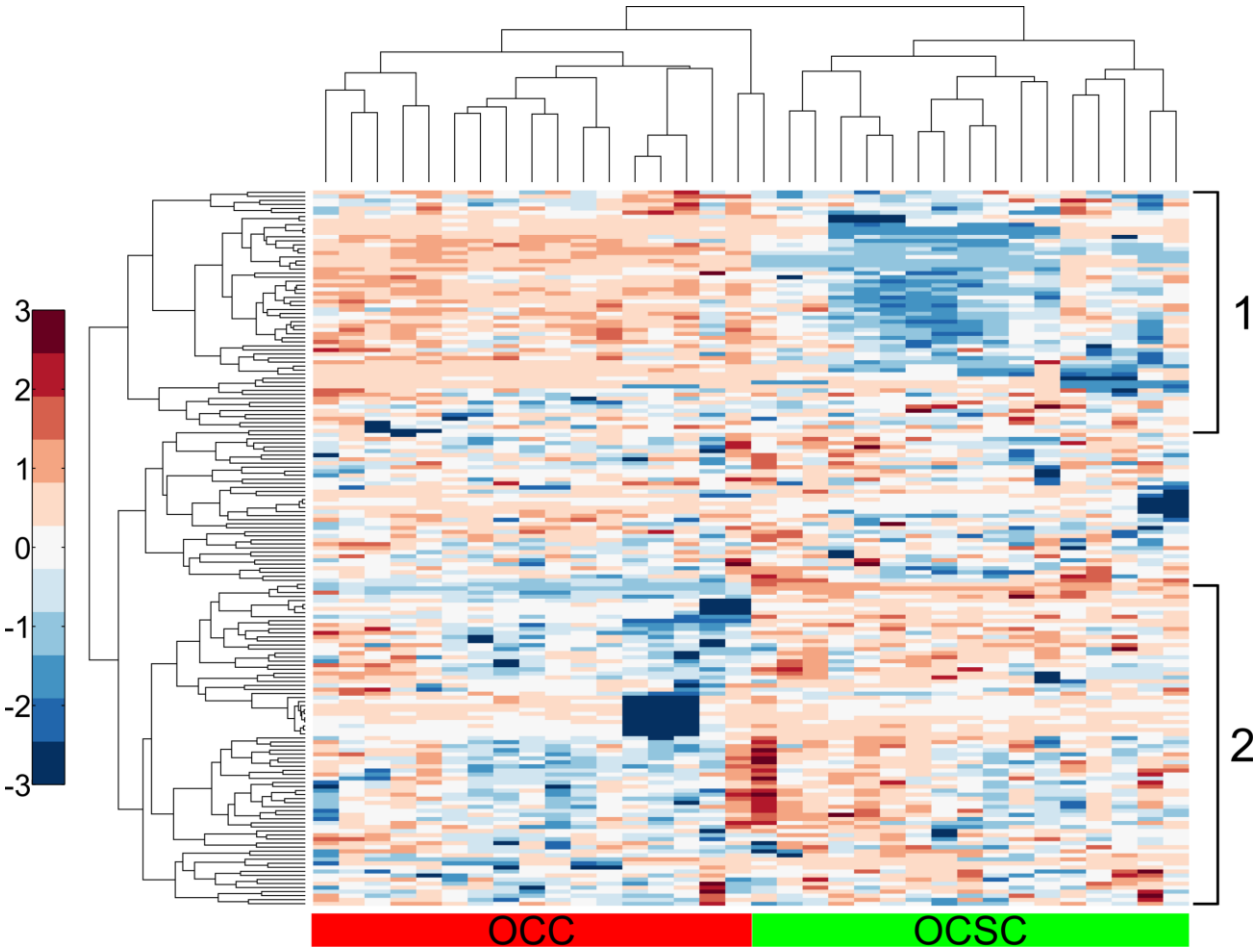

Figure 2.2: Hierarchical clustering demonstrates clear separation between cell type and major trends in analyte levels. Columns represent hierarchically clustered samples, color-coded according to cell type. Rows represent hierarchically clustered analytes. Analyte levels are mean-centered and unit-variance on a per-metabolite basis. The intracellular profile consists of two major groups with clearly separate behavior between the cell types. In group 1, OCC analyte levels are generally higher than OCSC analyte levels. Group 2 analyte levels are lower in OCCs than OCSCs.

Analysis into time series trends showed smaller clusters of metabolites whose levels varied with time (increasing or decreasing) in one cell line but did not substantially vary in the other cell line (see Figure 2.3). Further analysis into the metabolites from these clustered groups show that the metabolites have similar trends over time, as shown in Figure 2.4. In one group (Figure 2.4A), metabolites from time series cluster 1 in the hierarchical clustered heatmap, all metabolites have higher levels in OCCs than in OCSCs and this group is enriched in amino acids and carbohydrates. The second group (Figure 2.4B) consists of metabolites with higher levels in

OCSCs than OCCs (cluster group 3 from time series ordered hierarchical clustered heatmap) and is enriched in aliphatic acyclic compounds and lipids.

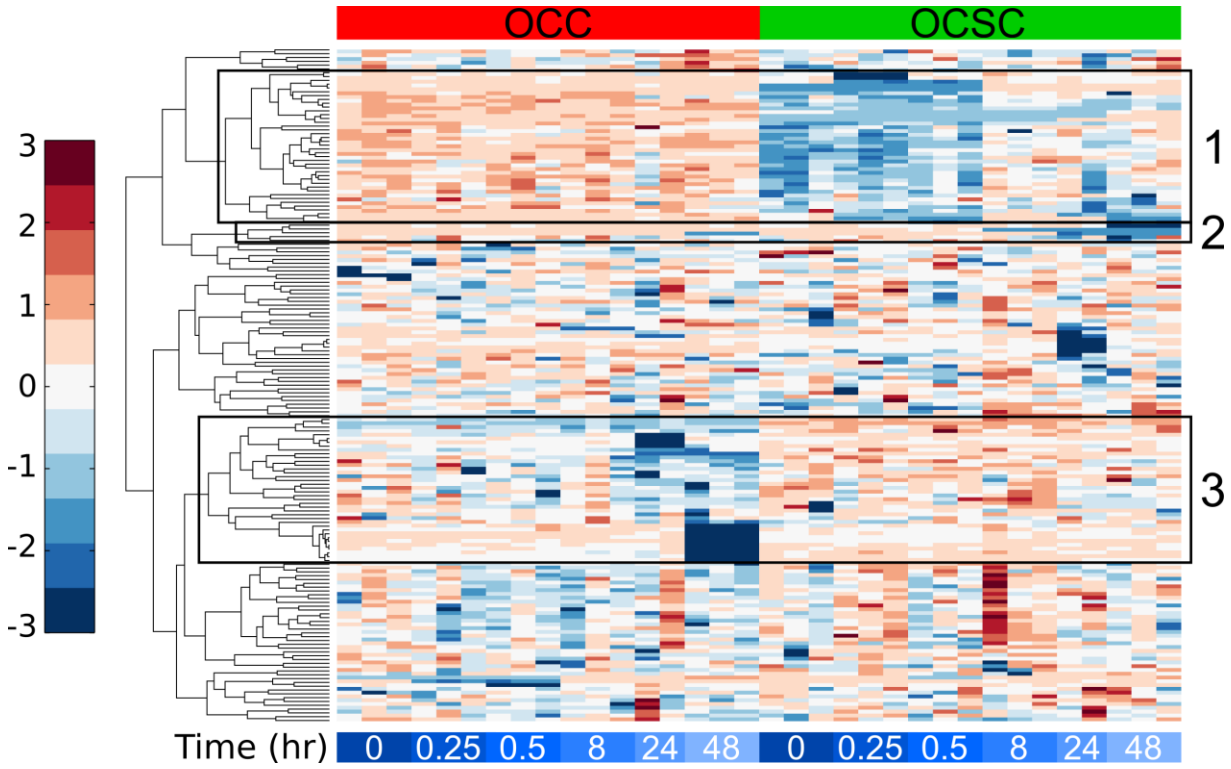

Figure 2.3: Time series ordered hierarchical clustering shows clusters of analytes with levels that increase or decrease with time. Columns represent time series ordered samples, color-coded according to cell type and time point. Rows represent hierarchically clustered analytes. Analyte levels are mean-centered and unit-variance on a per-metabolite basis. Three intracellular analyte clusters show clear temporal dependence. In group 1, OCC analyte levels are consistently high while OCSC analyte levels increase after 30 minutes. Group 2 analyte levels are consistently higher in OCCs while OCSCs start high and then start to decrease at 8 hours. Group 3 analytes are high in OCSCs while they decrease over time in OCCs.

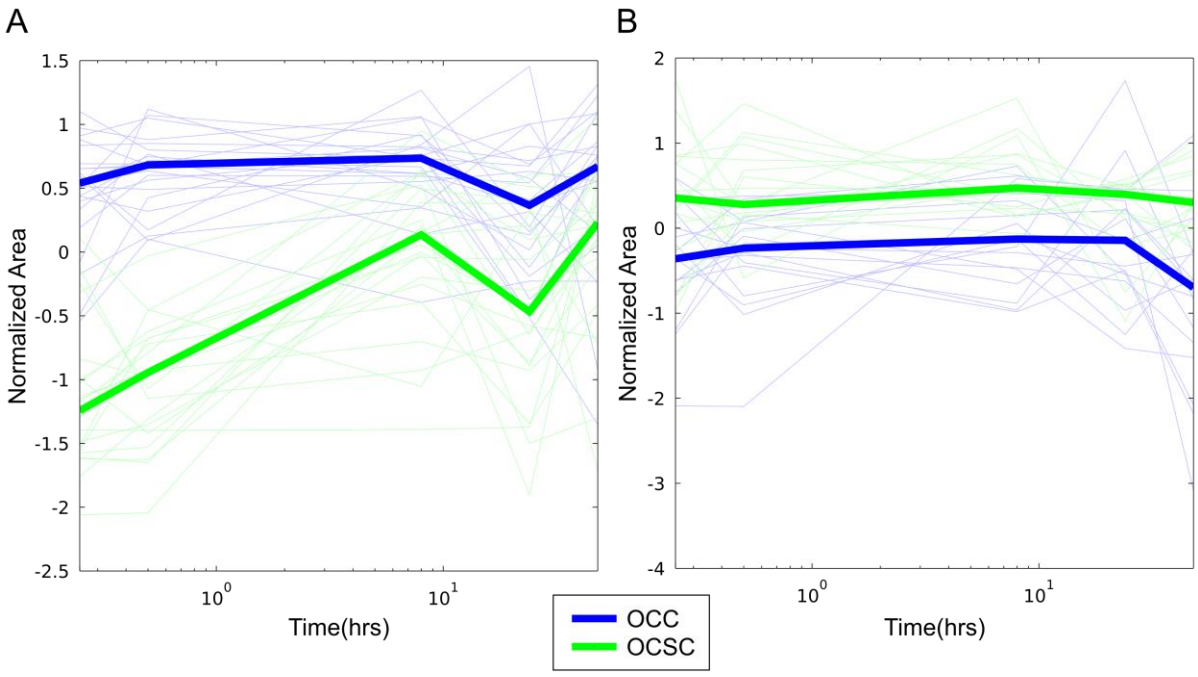

Figure 2.4: Time series plots of metabolite groups determined from clustered heatmap analysis. Plots of metabolite levels over time with groups determined from clusters assigned from heatmap analysis. Thin lines represent individual metabolite median levels and thick lines represent complied median level for the metabolite group. Normalized peak area has been log transformed and autoscaled.A) Metabolites from cluster 1 from time series ordered hierarchical clustering with OCC metabolite levels higher than OCSC metabolite levels. B) Metabolites from cluster 3 from time series ordered hierarchical clustering with OCSC metabolite levels higher than OCC metabolite levels.

2.2.3. Gene set and metabolic pathway enrichment analysis results show strong concordance

Using metabolite pathway enrichment analysis (MPEA) in MetaboAnalyst, 36 pathways were found to be significantly enriched for intracellular metabolic differences between OCCs and OCSCs, listed in Table 2.2. Gene set enrichment analysis (GSEA) revealed 11 KEGG pathways significantly enriched in OCSC phenotype, listed in Table 2.3. Out of those 11 pathways, only six include metabolic reactions that convert endogenous metabolites, four of which overlapped with the pathway results from MPEA: (i) arginine and proline metabolism, (ii) fructose and mannose metabolism, (iii) primary bile acid biosynthesis, and (iv) steroid hormone biosynthesis. This close overlap in the GSEA and MPEA results suggests strong concordance between transcriptional and metabolomic data and supports the validity of the identified differences.

Table 2.2: Significantly enriched KEGG pathways determined using metabolite pathway enrichment analysis.

KEGG Pathway	p value	FDR
Butanoate metabolism	3.19E-11	1.37E-09
beta-Alanine metabolism	1.84E-10	3.95E-09
Arginine and proline metabolism	1.32E-09	1.89E-08
Alanine, aspartate and glutamate metabolism	1.97E-09	2.12E-08
Tyrosine metabolism	1.05E-08	9.07E-08
Phenylalanine metabolism	4.50E-08	3.22E-07
Citrate cycle (TCA cycle)	5.36E-08	3.29E-07
Aminoacyl-tRNA biosynthesis	4.60E-07	2.47E-06
Nicotinate and nicotinamide metabolism	7.96E-07	3.80E-06
Glutathione metabolism	2.96E-06	1.27E-05
Lysine degradation	4.76E-06	1.71E-05
Lysine biosynthesis	4.39E-06	1.71E-05
Fructose and mannose metabolism	8.70E-06	2.88E-05
Nitrogen metabolism	3.32E-05	1.02E-04
Histidine metabolism	3.87E-05	1.11E-04
Glycerolipid metabolism	4.80E-05	1.29E-04
Primary bile acid biosynthesis	5.48E-05	1.39E-04
Valine, leucine and isoleucine biosynthesis	6.83E-05	1.47E-04
Porphyrin and chlorophyll metabolism	6.68E-05	1.47E-04
Valine, leucine and isoleucine degradation	6.83E-05	1.47E-04
D-Glutamine and D-glutamate metabolism	7.62E-05	1.56E-04
Glyoxylate and dicarboxylate metabolism	1.12E-04	2.18E-04
Biotin metabolism	1.67E-04	3.12E-04
Pantothenate and CoA biosynthesis	2.06E-04	3.69E-04
Glycerophospholipid metabolism	2.77E-04	4.76E-04
Steroid hormone biosynthesis	3.94E-04	6.52E-04
Glycine, serine and threonine metabolism	8.93E-04	1.32E-03
Pyrimidine metabolism	8.90E-04	1.32E-03
Cyanoamino acid metabolism	8.93E-04	1.32E-03
Purine metabolism	1.89E-03	2.63E-03
Thiamine metabolism	1.89E-03	2.63E-03
Pyruvate metabolism	2.93E-03	3.86E-03
Galactose metabolism	2.96E-03	3.86E-03
Cysteine and methionine metabolism	4.05E-03	5.12E-03
Methane metabolism	7.23E-03	8.89E-03
Amino sugar and nucleotide sugar metabolism	1.60E-02	1.91E-02

Table 2.3: Gene set enrichment analysis: KEGG pathways significantly enriched in OCSC phenotype

KEGG Pathway	p value	FDR q-val
Fructose and mannose metabolism	0.00000	0.01334
Metabolism of xenobiotics by cytochrome P450	0.00000	0.07636
Renin-angiotensin system	0.00960	0.09388
Glycosaminoglycan biosynthesis-keratan sulfate	0.00606	0.10337
Starch and sucrose metabolism	0.01152	0.10737
ABC transporters	0.00191	0.11004
Drug metabolism-other enzymes	0.00971	0.11724
Primary bile acid biosynthesis	0.01200	0.12187
Arginine and proline metabolism	0.01304	0.12491
PPAR signaling pathway	0.00378	0.13570
Steroid hormone biosynthesis	0.01232	0.15972

One of these pathways, arginine and proline metabolism, was particularly interesting based on the number of metabolites found within the pathway that were each individually statistically significantly different in OCSCs as compared to OCCs. These six metabolites (aspartate, fumarate, glutamate, gamma-aminobutyric acid, proline, and putrescine) were all found to be lower in OCSCs than OCCs, as seen in Figure 2.5. Two of these metabolites, proline and putrescine, demonstrated strong concordance between their levels and the levels of corresponding enzymes immediately upstream and downstream in the metabolic pathway, as shown in Figure 2.6, justifying a closer look at the role that these two metabolites can play in cancer and cancer stem cells. In order to further confirm the identity of proline and putrescine, pure standards were run on the GC-MS and compared to the intracellular samples. The retention times and mass spectra of the two standards were consistent with those of the annotated metabolites measured in the experimental samples.

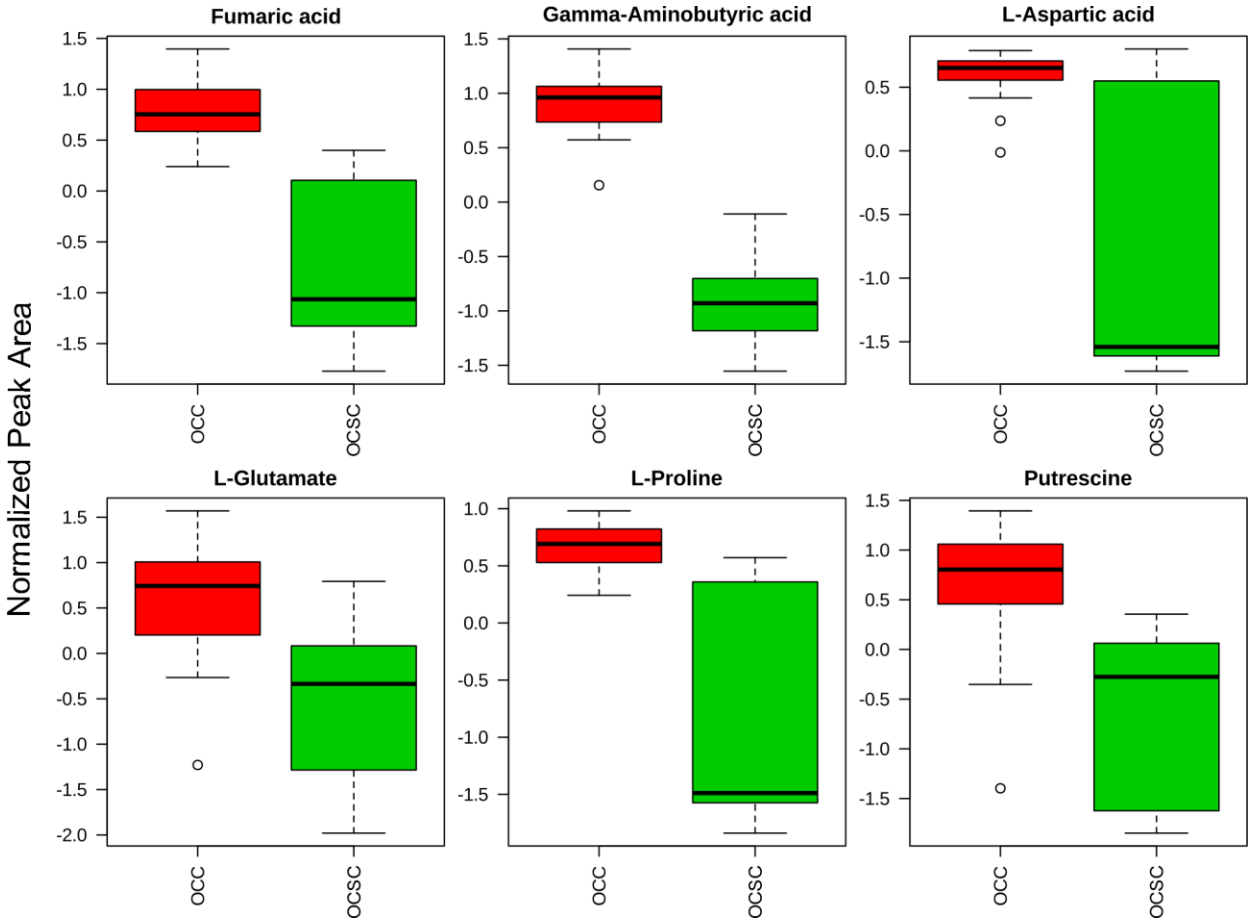

Figure 2.5: Metabolites in arginine and proline metabolism differ significantly between OCCs and OCSCs. All of the identified metabolites within the arginine and proline pathway were statistically significantly different between OCCs and OCSCs (FDR < 0.05) and were depleted in OCSCs. Box and whisker graphs depict the normalized peak area differences between the two cell types: dark black lines are the median, boxes identify the middle 50% values, dashed lines show two standard deviation bounds, and circles indicate outliers.

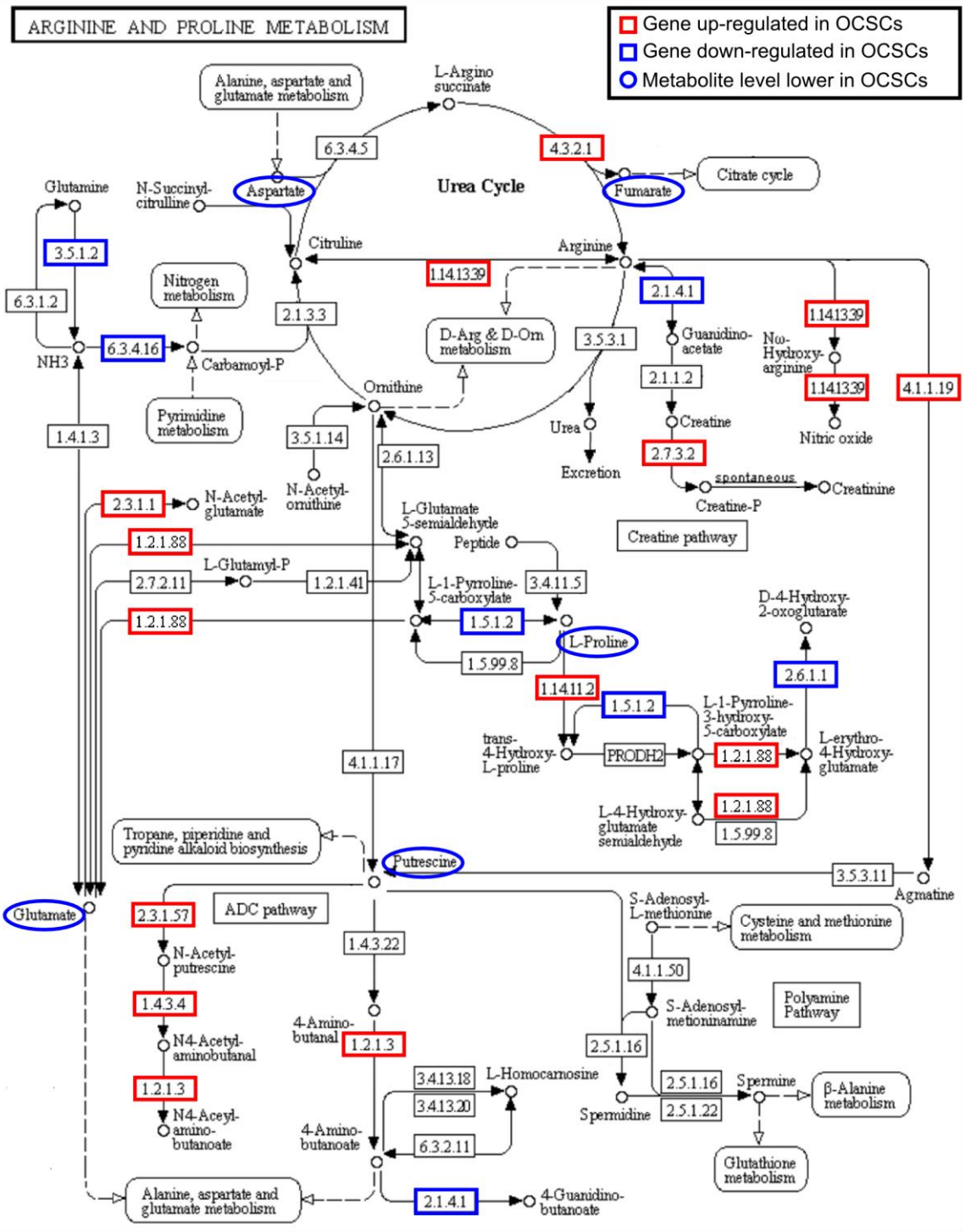

Figure 2.6: Metabolic and transcriptional differences between OCCs and OCSCs in arginine and proline metabolism. Differences are shown on the modified KEGG arginine and proline metabolism pathway (pathway is modified to show only reactions involved in human metabolism). Boxes with red and blue outlines are genes up-regulated and down-regulated, respectively, in OCSCs as compared to OCCs. Metabolites with blue ovals have lower levels in OCSCs compared to OCCs.

2.2.4. Proline & putrescine have been implicated in cancer

Putrescine is a polyamine, a class of molecules that has been shown to play an important role in cell growth and survival.[15, 16] Polyamines have been shown to affect numerous processes in normal and cancer cells, including proliferation, apoptosis, cell-cell interactions, and angiogenesis.[17] Specific mechanisms underlying these modes of action have not yet been completely elucidated; however, their critical role in DNA replication is supported by the reduced rate of DNA elongation and S-phase arrest in polyamine depleted cells.[18] Total polyamine levels are higher in highly proliferative cells, like cancer cells, and lower in cells with low proliferation rates.[16] However, we note that the medium control experiment, which induced significantly slower growth in OCCs, did not induce a change in putrescine levels, suggesting that a decrease in proliferation is not necessarily the cause of decreased putrescine levels. Polyamine catabolism has been implicated in cancer, as the process can cause DNA damage and mutation via production of reactive aldehydes, production of reactive oxygen species (ROS), or depletion of free radical scavengers.[19] Many cancer therapeutics have been targeted toward enzymes in the polyamine metabolism pathway, with promising initial results.[19, 20]

Likewise, proline metabolism is important to cellular processes, both in its catabolism and anabolism, and has been implicated in cancer.[21-23] Proline catabolism by proline dehydrogenase/oxidase (PRODH/POX) produces pyrroline-5-carboxylate, along with free electrons that can either be donated to the electron transport chain or used to generate ROS. During periods of high stress, PRODH/POX expression is induced to help rescue the cell through energy production or produce ROS to induce autophagy. Proline anabolism from glutamate has been implicated in cancer via its control by the transcription factor MYC, which represses PRODH/POX expression though microRNA control and induces expression of P5CS and PYCR, enzymes that convert glutamate to proline.[24] During glutamate conversion to proline, $NAD(P)^+$ is

regenerated from NAD(P)H for possible use in glycolysis and the pentose phosphate pathway. Knockdown of P5CS or PYCR has been shown to inhibit anaerobic glycolysis, thus indicating that proline anabolism from glutamate contributes to establishment of the Warburg effect.[24]

2.2.5. Differences in proline & putrescine levels between OCCs and OCSCs may be explained by stem cell metabolism

With both proline and putrescine and their respective pathways known to be already altered in cancer compared to normal tissues, it is perhaps surprising to find that both of these metabolites are now altered again in OCSCs relative to OCCs. The metabolic similarities between cancer stem cells and normal stem cells have already been widely commented upon – for example, both reprogram their energy metabolism to aerobic glycolysis to help support immortality.[25, 26] Reprogramming to aerobic glycolysis is characteristic of cancer cells in general, though, and therefore can not be used as a distinguishing characteristic of stem cell metabolism. Though stem cell metabolism is a field with significantly fewer published reports than cancer metabolism, recent discoveries in the field can begin to shed light on the biological meaning behind the changes of proline and putrescine in OCSCs given their previously-known alterations in cancer.

Putrescine has long been known to promote differentiation. More recently, in a study comparing mouse embryonic stem cells (mESCs), induced pluripotent stem cells (iPSCs), and fibroblasts, polyamine levels were found to be statistically significantly reduced in iPSCs, though interestingly they were similar between fibroblasts and mESCs.[27] In a systems-scale comparison of metabolite levels between mESCs and iPSCs, polyamines were one of the few metabolite groups that showed a difference between the two cell types; the others were amino acids and phosphatidylcholine and phosphatidylethanolamine lipid structures (not measured in this work). This finding suggests that OCSCs may generally occupy a state similar to iPSCs, with a shift from standard cancer metabolism towards a more stem-like metabolism, but not necessarily

identical to the normal stem cells that they in some ways emulate. In this case, the depletion of putrescine, with its role in differentiation, may help to maintain the OCSCs in a more stem-like state.

Proline has recently been shown to induce differentiation in mESCs towards an epiblast stem cell state.[28, 29] By adding biologically relevant concentrations of proline to mESC media, changes were noticed in proliferation, phenotype, and differentiation kinetics. These changes were similar to the ones caused by addition of MEDII media to the normal stem cell media, a common protocol for initiating differentiation of mESCs.[28] Further investigation showed that these changes were induced by catabolism of proline to pyrroline-5-carboxylate.[29] In addition, proline has been shown to act as a signaling molecule that controls stem cell behavior via an epigenetic mechanism.[17] This suggests that OCSCs may use proline metabolism in a similar way to stem cells and by keeping a lower intracellular concentration of proline, the OCSCs help retain their stemness.

Taken together, then, the trends identified are consistent in the context of what is known at the intersection of both the cancer metabolism and stem cell metabolism fields. While it is to be expected that proline and putrescine are accumulated in OCCs based on their roles in or correlations with proliferative phenotypes and cancer metabolism, these metabolites would display effects suppressing the observed stem cell-like phenotypes of OCSCs. Specifically, high levels of either of these metabolites may tend to promote differentiation of OCSCs into less stem-like cell types, and thus maintenance at lower levels would facilitate the stemness associated with cancer stem cells.

2.2.6. Comparison of OCSC differences to other cancer stem cell studies

An interesting picture emerges when differences in metabolite abundances between OCCs and OCSCs are compared with differences in metabolite abundances between ovarian borderline tumors and invasive ovarian carcinomas. While tissue concentrations of glycine, proline, glutamate, and fumarate are higher in invasive ovarian carcinomas relative to non-invasive borderline tumors,[30] our data show that OCSCs display lower concentrations of these metabolites relative to OCCs. Glycine plays a role in rapid proliferation of cancer cells via the glycine biosynthesis pathway[10] and the SOG pathway[31]. The SOG pathway consists of serine synthesis, one-carbon metabolism, and the glycine cleavage system and supports rapid proliferation through energy production. Considering the role of glycine in rapid proliferation of cancer cells, the role of fumarate in the malignant phenotype via aberrant activation of hypoxia response pathways,[32] and the role of glutamate in anabolic processes and replenishing of the tricarboxylic acid cycle intermediates during cell growth (anaplerosis),[33] it is somewhat intriguing that OCSCs are metabolically more similar to indolent and relatively benign borderline tumor cells with respect to these cancer-relevant metabolites. We hypothesize that certain phenotypic similarities between cancer stem cells and cells with less malignant potential (or non-malignant cells), might be associated with quiescence of these cell types and might play an important role in failure of cancer therapies designed to target aggressively growing clinical cancers. Similarly, our results imply that OCSCs are less dependent on polyamines than their more differentiated progeny, which may not be purely growth-associated (as discussed in greater detail above). This lower dependence of OCSCs on polyamines could be a more broadly applicable property of quiescent cancer stem cells that can explain the general failure of inhibitors of polyamine synthesis in clinical cancer trials.[17]

Our results are also partially consistent with a recent metabolomics study of glioma-stem cells (GSCs), specifically the cultured GSCs (CGSCs). The *in vivo* tumors formed from CGSCs were noted to have increased concentrations of glycine and choline-containing compounds and decreased concentrations of glutamine, glutamate, taurine, and total creatine.[13] In our results, we did not detect choline-containing compounds, taurine, or creatine. We did, however, notice decreasing trends in both glycine and glutamate. One caveat on comparing these two experiments, though, is that the CGSCs were compared to normal tissue, while our OCSCs were compared to cancerous cells.

2.2.7. Limitations

In this work we did not use control cells that would represent cells of origin or nonmalignant counterparts of epithelial ovarian cancer cells, since our primary interest was the identification of metabolic differences that can explain other biological differences between OCSCs and their more differentiated progeny (e.g. quiescence and drug resistance) rather than cancer vs. normal metabolomic differences that have already been more widely examined. Furthermore, identification of the appropriate normal control would be complicated, if not impossible, due to the fact that the cell of origin of epithelial ovarian cancers is still debated. Thus, the strength of our work is in that we compare the metabolism of isogenic cancer cell lines that differ only in their cell stemness and differentiation status.

We also note that the extent of biological interpretation of our data has been limited by the content of available databases and by conservative data processing decisions meant to increase confidence in the results. The metabolites used in our data analyses are not only limited by our ability to establish the biochemical identities of metabolites measured by our instrument using mass spectral databases, but also by the incompleteness of databases available for pathway-level

analysis. We have also used a high similarity threshold during chromatogram processing to ensure that, when a metabolite is assigned a name, we have high confidence that the assigned name accurately reflects the metabolite's identity. Based on these conservative decisions, we have thus potentially omitted other significant metabolites that did not meet confidence thresholds or were not available in the databases we used. Thus, there may be further support for any of the pathways discussed here, or potentially even for other pathways, as being important to OCSC metabolism; only with further refinement of pathway databases and analytical tools can a more thorough biological analysis be performed.

Finally, this work only studied one specific cancer cell line and its isogenic cancer stem cell line. It would be desirable to perform similar analyses for multiple isogenic cancer stem cell/cancer cell line pairs, as cancer is well-known to be a heterogeneous disease. However, there are very few ovarian cancer stem cell lines in existence, and none available in repositories for purchase. As such, the next steps in this work would be to derive or acquire more of such cancer stem cell lines to verify the broad applicability of the results obtained here.

2.3. Conclusions

Overall, we have shown that an OCC line and its derived OCSCs have different metabolic profiles that are consistent with predictions based on previously observed transcriptional profiles. Both multivariate and univariate data analyses indicate that there are many significant differences in the metabolism of these two isogenic cell types; however, none of these differences were previously known. Analysis of the metabolic and transcriptional differences between these OCCs and OCSCs revealed the arginine and proline metabolism pathway as playing a particularly important role in the differences between the cell types. Proline and putrescine both play important roles in cancer, and have been identified as serving important

roles in stem cell metabolism. The conflicting roles for these metabolites in these two different contexts may place them in a delicate balance in OCSCs. Proline and putrescine thus may play a major role in the maintenance of the OCSC phenotype.

2.4. Methods

2.4.1. Cell culture

The OVCAR-3 cell line was obtained from the Developmental Therapeutic Program (DTP) of the National Cancer Institute (NCI). The OVCAR-3 ovarian cancer cells (OCCs) were cultured in R10 medium: RPMI-1640 (Cellgro, Mediatech Inc., Manassas, VA) supplemented with 10% fetal bovine serum (FBS, Invitrogen, Grand Island, NY) and 1% antibiotic-antimycotic solution (Cellgro, Mediatech Inc., Manassas, VA). Authenticity of the OVCAR-3 cell line was confirmed using short tandem repeat profiling performed by IDEXX RADIL (Columbia, MO) in October 2013. Cells were grown until confluence and subcultured at a ratio of 1:4. Immediately before any time-course sampling began, OCCs were passaged and seeded in 6-well plates (Greiner Bio-One, Monroe, NC) with a surface area of 6.9 cm^2 at a density of $3x10^5$ cells/well ($4.35x10^4$ cells/cm^2) and incubated for 24 hours in 2 mL R10 medium to allow the cells to attach and recover; the medium was removed, wells were washed once with PBS, and then 2 mL of fresh R10 medium was added to begin the experiment.

Ovarian cancer stem cells (OCSCs) were previously derived from a side population of OVCAR-3. OCSCs are less adherent than OVCAR-3 cells and, unlike OVCAR-3 cells that are grown as adherent monolayers, are grown as spheroids in stem cell media to help support their stemness as previously described.[8] Briefly, the OCSCs were cultured in ultra-low attachment petri dishes (Corning Incorporated, Corning, NY) in stem cell medium: DMEM/F12 (1:1) (Cellgro, Mediatech Inc., Manassas, VA) supplemented with 0.4% bovine serum albumin (BSA, Sigma-

Aldrich, St. Louis, MO), 20 ng/mL epidermal growth factor (EGF, Invitrogen, Grand Island, NY), 10 ng/mL basic fibroblast growth factor (bFGF, Sigma-Aldrich, St. Louis, MO), 5 µg/mL insulin (Sigma-Aldrich, St. Louis, MO), and 1% antibiotic-antimycotic solution (Cellgro, Mediatech Inc., Manassas, VA). The spheroids were dissociated and reseeded at a density of 10^5 cells/mL each week. To begin the time-course experiment, OCSCs were dissociated and seeded into ultra-low attachment 6-well plates (Corning Incorporated, Corning, NY) with a surface area of 6.9 cm^2 containing 2mL of fresh stem cell medium at a density of $3x10^5$ cells/well. Both the OCC and OCSC experiments were performed in biological triplicate.

2.4.2. Sampling Protocols

Samples were taken at 0 minutes, 15 minutes, 30 minutes, 8 hours, 24 hours, and 48 hours to capture both short- and long-term metabolic profiles. For OCCs, medium was removed and snap frozen in liquid nitrogen for extracellular analysis. Cells were then quickly washed with 1mL PBS at 37°C, which was aspirated off, and then 700 µL of 80:20 methanol/water solution at -80°C was added immediately. The plate was then incubated at -80°C for 15 minutes. After incubation, remaining cellular debris were harvested using a cell scraper (BD Falcon, San Jose, CA) for intracellular analysis. For OCSC cells, the media-cell mixture was transferred to a 15 mL centrifuge tube and centrifuged at 1,900 *g* for 30 seconds at room temperature. The supernatant was removed and snap frozen in liquid nitrogen for extracellular analysis. The cell pellet was quickly resuspended in 1mL PBS at 37°C and then immediately centrifuged again at 1,900 *g* for 30 seconds at room temperature. The wash solution was discarded and the cell pellet was resuspended in 700 µL of 80:20 methanol/water at -80°C. The samples were then incubated at -80°C for 15 minutes.

For both cell types, the intracellular solution was then transferred to a microcentrifuge tube in a cold ethanol bath and centrifuged at 5,000 *g* for 5 minutes at -4°C. The supernatant was retained, and the pellet was subsequently re-extracted twice in 100 µL of the cold 80:20 methanol/water solution, with all supernatants being pooled.[34] Intracellular and extracellular samples were stored at -80°C and -20°C, respectively, until analysis.

2.4.3. Media Control

To control for the differences in media, a secondary experiment was performed where OCCs were grown in parallel in their normal media and OCSC media (both media formulations are described above) for 48 hours. Intracellular and extracellular samples were taken at 0, 24, and 48 hours in the same manner as described above for the OCCs. Cell counts were also taken (data not shown) and it was discovered that OCCs grow slower in the OCSC medium than they do in their normal medium, mimicking the slower growth rate of OCSCs. Intracellular and extracellular samples were analyzed and on the GCxGC-MS and processed with the OCC and OCSC data (as described in section 2.4.7).

2.4.4. Extracellular Sample Extraction

Immediately before two dimensional gas chromatography-mass spectrometry (GCxGC-MS) analysis, an acetonitrile precipitation was performed on the extracellular samples to remove protein.[35] Briefly, the extracellular samples were thawed on ice and 75 µL was removed for GCxGC-MS analysis. 150 µL of ice-cold acetonitrile was added to the sample, and the sample was vortexed for one minute. The sample was then centrifuged at 21,100 *g* for 7 minutes, and the supernatant removed for GCxGC-MS analysis.

2.4.5. GCxGC-MS Analysis

Before derivatization, both intracellular and extracellular samples were vacuum concentrated in a CentriVap at 40°C until completely dry. For the intracellular samples, a volume equated to

$7.5x10^4$ cells for each sample was vacuum concentrated in order to achieve a concentration of $3x10^4$ cells equivalents/µL after derivatization. For the extracellular samples, the entire supernatant from the extracellular extraction was vacuum concentrated.

The samples were derivatized following the protocol laid out by Fiehn, *et. al*.[36] Briefly, 10 µL (extracellular) or 2.5 µL (intracellular) of 40 mg/mL *O*-methylhydroxylamine hydrochloride (MP Biomedicals, LLC, Santa Ana, CA) in pyridine was added to the dried sample and shaken at 1400 rpm for 90 minutes at 30°C. 90 µL (extracellular) or 22.5 µL (intracellular) of *N*-methyl-*N*-(trimethylsilyl) trifluoroacetamide (MSTFA) + 1% trimethylchlorosilane (TMCS) (Thermo Scientific, Lafayette, CO) was then added to the samples which were then shaken at 1400 rpm for 30 minutes at 37°C. Samples were centrifuged at 21,100 *g* for 3 minutes and 50 µL (extracellular) or 15 µL (intracellular) of the supernatant was added to an autosampler vial. Samples were spiked with 0.25 µL (extracellular) or 0.10 µL (intracellular) of a retention time standard solution consisting of fatty acid methyl esters (FAMEs) and an internal standard of nonadecanoic acid methyl ester dissolved in dimethylformamide.

A LECO Pegasus 4D instrument with an Agilent 7683B autosampler, Agilent 7890A gas chromatograph and time-of-flight mass spectrometer (TOF-MS) was used to analyze the samples. The first column was an HP-5, 30 m long x 0.320 mm ID x 0.25 µm film thickness (Agilent, Santa Clara, CA), and the second was an Rtx-200, 2 m long x 0.25 mm ID x 0.25 µm film thickness (Restek, Bellefonte, PA). Specific autosampler, gas chromatography, and mass spectrometry methods can be found in Appendix A.

2.4.6. Data Analysis

Sample runs were first analyzed in ChromaTOF (LECO, St. Joseph, MI) to determine baseline, peak area, and peak identification. Briefly, settings included a baseline offset of 0.5, automatic

smoothing, 1st dimension peak width of 10 seconds, 2nd dimension peak width of 0.10 seconds, and a match of 700 required to combine peaks with a minimum signal-to-noise (S/N) of 5 for all subpeaks. Peaks were required to have a S/N of 10 and have a minimum similarity score of 800 before assigning a name. Unique mass was used for area and height calculation.

To align the samples, MetPP (http://metaopen.sourceforge.net/metpp.html) was used.[37] Sample files and a derivatization reagent blank file were uploaded from ChromaTOF. Unknowns were retained during the peak alignment process. The derivatization reagent blank file was used to subtract peaks attributable only to derivatization reagents from the sample files. On-the-fly alignment was used with quality control samples manually selected as the peak list for primary alignment. Peak alignment was performed using the default criteria.

After alignment, further processing of the data was done following the procedure laid out by Dunn, *et. al*.[38] Batch effects were removed from the intracellular data set using LOESS. During LOESS correction, one of the OCC and OCSC 24 hour biological replicates were identified as an outlier and removed. LOESS was also performed on the extracellular data set, but batch effects were amplified in the samples after correction due to quality control (QC) sample run errors so the original data set was used for subsequent analysis. To remove analytes that were not reproducibly detected, analytes for which more than half of the values were missing in the QC samples or for which the QC samples had a coefficient of variance larger than 0.5 (excluding missing values) were removed from the data set. Then, missing values were manually corrected using small value correction only if all the values were missing in a set of biological replicates.

Finally, MetaboAnalyst (http://metaboanalyst.ca/) was used for statistical and enrichment analysis, applying both the statistical analysis and time series analysis modules.[39] For both

analyses, remaining missing values were k-nearest neighbors (KNN) imputed. Data was filtered using the interquantile range method and then log-transformed using generalized logarithm transformation (base 2) and autoscaled.

For removal of media effects, the media control samples were isolated from the OCC and OCSC samples and analyzed using MetaboAnalyst. Any metabolites found to have significant differences (t-test, all time points, FDR < 0.05) in the media control experiment were then removed from the main data set to eliminate any metabolic changes due to media differences. This was done for both the intracellular and extracellular data sets.

For enrichment analysis, both metabolite set enrichment analysis (MSEA) and metabolite pathway enrichment analysis (MPEA) yielded similar results, so only MPEA results were considered further. The entire time series was uploaded as discrete data with compound names. Metabolites were properly matched to their HMDB codes before processing the data. Data processing followed the same steps as listed above for missing value imputation and data normalization. The *Homo sapiens* pathway library was used for analysis and an in-house metabolite reference library based on detectable metabolites for our system was uploaded. Global test was used for pathway enrichment analysis, with relative-betweeness centrality as the pathway topology analysis. Pathways with an FDR < 0.05 were considered significantly enriched.

For gene set enrichment analysis (GSEA) of OCSC and OCC gene expression data, .CEL files corresponding to 3 replicated cultures of OCSC and OCC (GeneChip® Human Genome U133 Plus 2.0 Array), generated as previously described[8], were processed and normalized by GCRMA method (http://arrayanalysis.org) and used for GSEA

(http://www.broadinstitute.org/gsea/index.jsp) without pre-filtering of probe sets using the following parameters: OCC vs. OCSC as categorical phenotypes; signal-to-noise metric; gene set permutation type; curated KEGG gene sets (186 gene sets, Molecular Signatures Database v4.0). Gene sets were considered significantly enriched in a given phenotype if their FDR q value was < 0.20. The dataset employed in this analysis is available in the Gene Expression Omnibus (GEO, http://www.ncbi.nlm.nih.gov/geo/) as series GSE28799.

2.4.7. Effects due to growth media differences successfully removed from OCC vs OCSC intracellular metabolomics data

OCSCs require stem cell medium to retain their stem-like properties and therefore, they are grown in different media than the OCCs. Since growth in different media could cause metabolic changes and confound the metabolic differences seen between the two cell types, we designed a media control experiment that would allow us to remove any metabolic changes due purely to media effects. OCCs were grown in their normal R10 medium and in stem cell medium and intracellular and extracellular samples were taken at 0, 24, and 48 hours. These samples were analyzed and processed with the OCC and OCSC intracellular and extracellular samples. The media control samples were then isolated from the OCC and OCSC samples and analyzed on their own. Any analyte identified as statistically different between only the media control samples was removed from the entire data set.

Before removing the analytes with statistically significant differences from the intracellular dataset, the samples from the two different media types separated in principal component (PC) 2, seen in Figure 2.7A. Even though separation is seen between these two media controls, it is captured in PC2, which represents a smaller proportion of the overall variance than the separation between OCCs and OCSCs, captured in PC1. Once the significant analytes were removed, the separation decreased between the two media controls in the all analyte dataset

(Figure 2.7B) and no principal components analysis (PCA)-based separation could be found based on annotated metabolites only (Figure 2.7C), showing that the differences between OCC and OCSC intracellular metabolism are not simply due to growth in different media. The intracellular datasets with media effects removed are the basis for all of the biologically-related discussion following, and so any differences in these analytes between OCCs and OCSCs should not be attributed to medium differences.

In the extracellular dataset, a large difference between the OCCs in R10 medium and OCCs in stem cell medium was seen before removal of the statistically different analytes, as seen in Figure 2.8A. After removal, in both the unknown and known compound data set and the metabolite only data set, there is still separation visible between the two media control samples (Figure 2.8B and C). This separation is less than that seen between the OCC and OCSC extracellular samples, but because the media effect was not completely removed, we will focus only on the intracellular samples.

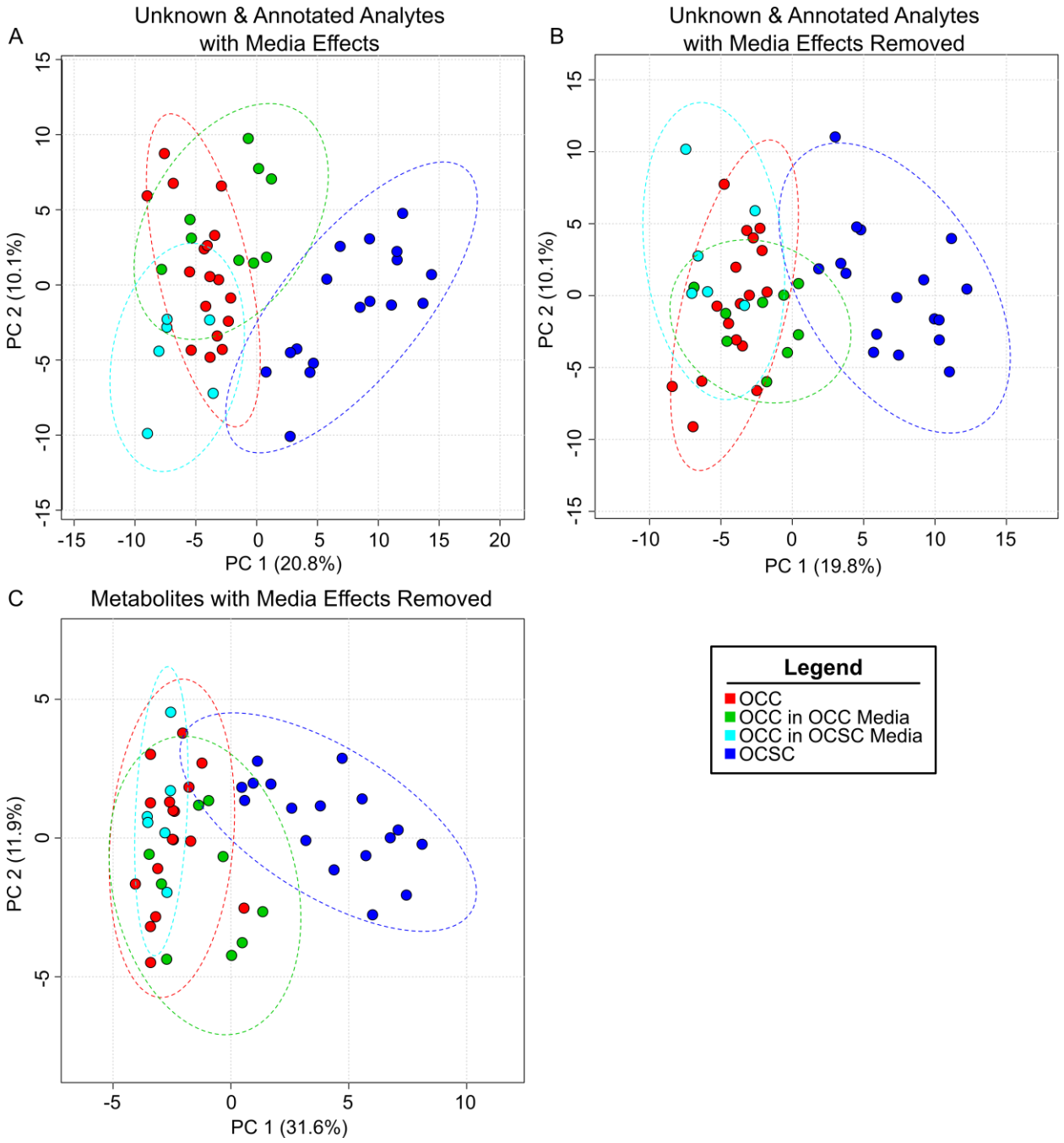

Figure 2.7: Intracellular media effects are successfully removed from OCC vs OCSC comparisons. Principal components analysis of OCC (red), OCSC (blue), and the two media control (OCCs grown in R10 medium (green) and stem cell medium (cyan)) intracellular samples. OCCs (red) and OCCs grown in R10 medium (green) are similar samples, but the OCCs grown in R10 medium were grown at a different time than OCCs and only have three time points instead of six. (A) Media effects are clearly seen in PC 2 through the separation of two media control samples. (B) After removing media effects, the two media control samples are overlapping, showing the reduction of media effects in the intracellular analysis. (C) Focusing only on annotated metabolites, the media effects are further reduced.

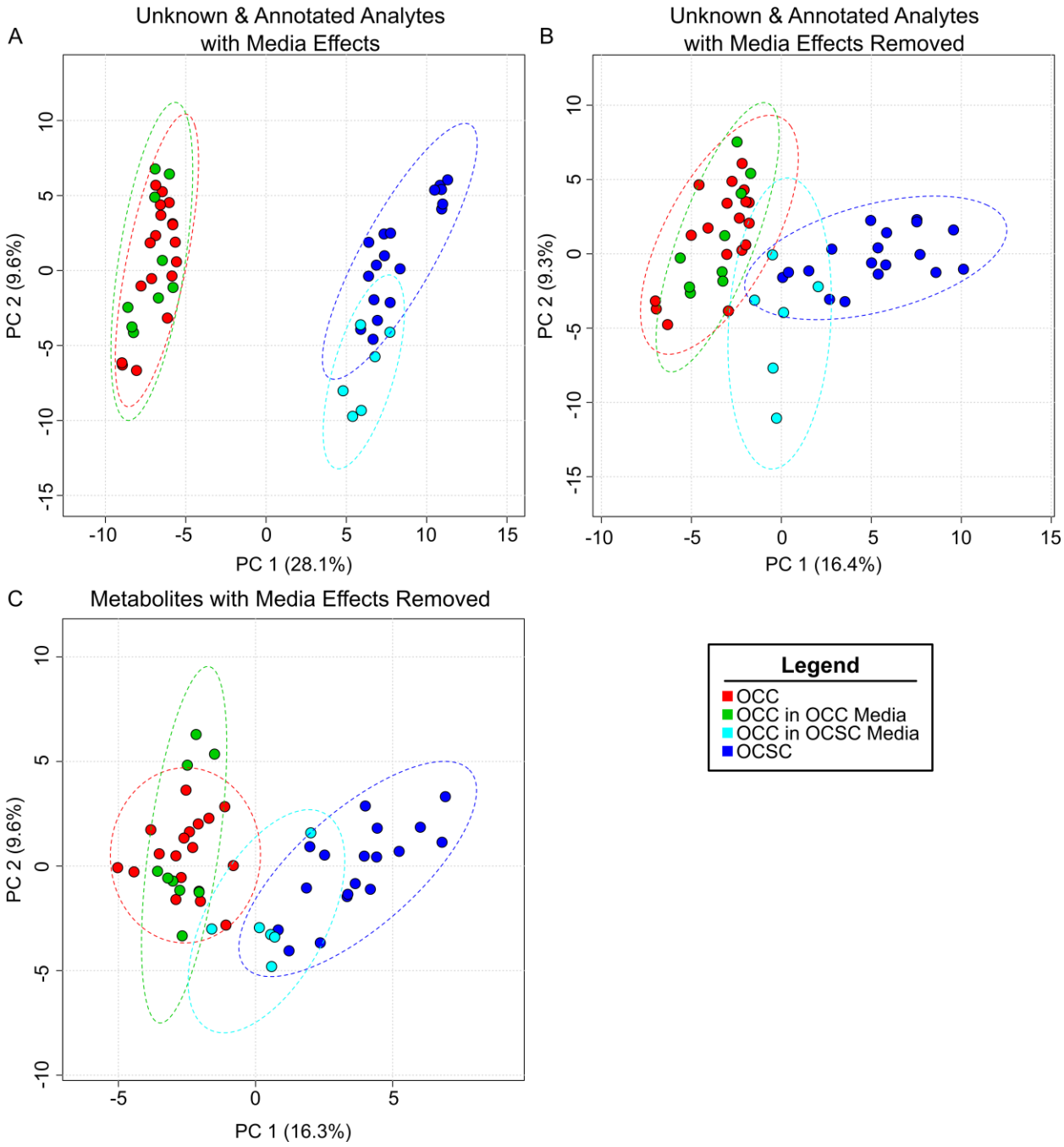

Figure 2.8: Extracellular media effects cannot be removed through simple removal of statistically significantly different analytes. Principal components analysis of OCC (red), OCSC (blue), and the two media control (OCCs grown in OCC media (green) and OCSC media (cyan)) extracellular samples. (A) OCCs (red) and OCCs grown in R10 medium (green) are similar samples, but the OCCs grown in R10 medium were grown at a different time than OCCs and only have three time points instead of six. Media effects are clearly seen in PC 1 through the separation of two media control samples. (B) After removing media effects, the two media control samples are closer, showing the reduction of media effects, but are still separated. (C) Focusing on annotated metabolites only, the media effects are still noticeable.

2.5. References

1. Siegel, R., Naishadham, D. & Jemal, A. Cancer statistics, 2012. *CA: A Cancer Journal for Clinicians* **62**, 10-29 (2012).
2. Herzog, T.J. Recurrent Ovarian Cancer: How Important Is It to Treat to Disease Progression? *Clinical Cancer Research* **10**, 7439-7449 (2004).
3. Fong, M.Y. & Kakar, S.S. The role of cancer stem cells and the side population in epithelial ovarian cancer. *Histology and Histopathology* **25**, 113-120 (2010).
4. Gao, Q.L., Geng, L., Kvalheim, G., Gaudernack, G. & Suo, Z.H. Identification of Cancer Stem-like Side Population Cells in Ovarian Cancer Cell Line OVCAR-3. *Ultrastruct. Pathol.* **33**, 175-181 (2009).
5. Goodell, M.A., Brose, K., Paradis, G., Conner, A.S. & Mulligan, R.C. Isolation and functional properties of murine hematopoietic stem cells that are replicating in vivo. *J Exp Med* **183**, 1797-1806 (1996).
6. Visvader, J.E. & Lindeman, G.J. Cancer stem cells in solid tumours: accumulating evidence and unresolved questions. *Nat. Rev. Cancer* **8**, 755-768 (2008).
7. Alvero, A.B. et al. Molecular phenotyping of human ovarian cancer stem cells unravels the mechanisms for repair and chemoresistance. *Cell Cycle* **8**, 158-166 (2009).
8. Wang, L., Mezencev, R., Bowen, N.J., Matyunina, L.V. & McDonald, J.F. Isolation and characterization of stem-like cells from a human ovarian cancer cell line. *Mol Cell Biochem* **363**, 257-268 (2012).
9. Dang, L. et al. Cancer-associated IDH1 mutations produce 2-hydroxyglutarate. *Nature* **462**, 739-U752 (2009).
10. Jain, M. et al. Metabolite profiling identifies a key role for glycine in rapid cancer cell proliferation. *Science* **336**, 1040-1044 (2012).
11. Zhou, M. et al. Rapid Mass Spectrometric Metabolic Profiling of Blood Sera Detects Ovarian Cancer with High Accuracy. *Cancer Epidemiology Biomarkers & Prevention* **19** (2010).
12. Zhang, T. et al. Identification of Potential Biomarkers for Ovarian Cancer by Urinary Metabolomic Profiling. *J. Proteome Res.* **12**, 505-512 (2013).
13. Mlynarik, V. et al. In vivo metabolic profiling of glioma-initiating cells using proton magnetic resonance spectroscopy at 14.1 Tesla. *NMR in biomedicine* **25**, 506-513 (2012).
14. Hanahan, D. & Weinberg, R.A. Hallmarks of Cancer: The Next Generation. *Cell* **144**, 646-674 (2011).
15. Wallace, H., Fraser, A. & Hughes, A. A perspective of polyamine metabolism. *Biochem. J* **376**, 1-14 (2003).
16. Igarashi, K. & Kashiwagi, K. Modulation of cellular function by polyamines. *The International Journal of Biochemistry & Cell Biology* **42**, 39-51 (2010).
17. Gerner, E.W. & Meyskens, F.L., Jr. Polyamines and cancer: old molecules, new understanding. *Nat Rev Cancer* **4**, 781-792 (2004).
18. Oredsson, S.M., Nicander, B. & Heby, O. Implications for a reduced DNA-elongation rate in polyamine-depleted cells. *European journal of biochemistry / FEBS* **190**, 483-489 (1990).
19. Battaglia, V., DeStefano Shields, C., Murray-Stewart, T. & Casero, R.A. Polyamine catabolism in carcinogenesis: potential targets for chemotherapy and chemoprevention. *Amino Acids* (2013).

20. Casero, R.A. & Marton, L.J. Targeting polyamine metabolism and function in cancer and other hyperproliferative diseases. *Nature Reviews Drug Discovery* **6**, 373-390 (2007).
21. Phang, J.M., Donald, S.P., Pandhare, J. & Liu, Y. The metabolism of proline, a stress substrate, modulates carcinogenic pathways. *Amino Acids* **35**, 681-690 (2008).
22. Phang, J.M., Liu, W. & Hancock, C. Bridging epigenetics and metabolism: Role of non-essential amino acids. *Epigenetics* **8** (2013).
23. Phang, J.M. & Liu, W. Proline metabolism and cancer. *Frontiers in Bioscience-Landmark* **17**, 1835-1845 (2012).
24. Liu, W. et al. Reprogramming of proline and glutamine metabolism contributes to the proliferative and metabolic responses regulated by oncogenic transcription factor c-MYC. *Proceedings of the National Academy of Sciences* **109**, 8983-8988 (2012).
25. Menendez, J.A. et al. The Warburg effect version 2.0: Metabolic reprogramming of cancer stem cells. *Cell cycle (Georgetown, Tex)* **12**, 1166-1179 (2013).
26. Pecqueur, C., Oliver, L., Oizel, K., Lalier, L. & Vallette, F.M. Targeting Metabolism to Induce Cell Death in Cancer Cells and Cancer Stem Cells. *International Journal of Cell Biology* **2013**, 1-13 (2013).
27. Meissen, J.K. et al. Induced Pluripotent Stem Cells Show Metabolomic Differences to Embryonic Stem Cells in Polyunsaturated Phosphatidylcholines and Primary Metabolism. *PLoS ONE* **7**, e46770 (2012).
28. Washington, J.M. et al. L-Proline induces differentiation of ES cells: a novel role for an amino acid in the regulation of pluripotent cells in culture. *AJP: Cell Physiology* **298**, C982-C992 (2010).
29. Casalino, L. et al. Control of embryonic stem cell metastability by L-proline catabolism. *Journal of Molecular Cell Biology* **3**, 108-122 (2011).
30. Denkert, C. et al. Mass spectrometry-based metabolic profiling reveals different metabolite patterns in invasive ovarian carcinomas and ovarian borderline tumors. *Cancer Res.* **66**, 10795-10804 (2006).
31. Tedeschi, P.M. et al. Contribution of serine, folate and glycine metabolism to the ATP, NADPH and purine requirements of cancer cells. *Cell Death Dis* **4**, e877 (2013).
32. Sudarshan, S. et al. Reduced expression of fumarate hydratase in clear cell renal cancer mediates HIF-2alpha accumulation and promotes migration and invasion. *PLoS One* **6**, e21037 (2011).
33. DeBerardinis, R.J. & Cheng, T. Q's next: the diverse functions of glutamine in metabolism, cell biology and cancer. *Oncogene* **29**, 313-324 (2010).
34. Lu, X., Bennet, B., Mu, E., Rabinowitz, J. & Kang, Y. Metabolomic Changes Accompanying Transformation and Acquisition of Metastatic Potential in a Syngeneic Mouse Mammary Tumor Model. *J. Biol. Chem.* **285**, 9317-9321 (2010).
35. Teja-Isavadharm, P. et al. A Simplified Liquid Chromatography-Mass Spectrometry Assay for Artesunate and Dihydroartemisinin, Its Metabolite, in Human Plasma. *Molecules* **15**, 8747-8768 (2010).
36. Kind, T. et al. FiehnLib: Mass Spectral and Retention Index Libraries for Metabolomics Based on Quadrupole and Time-of-Flight Gas Chromatography/Mass Spectrometry. *Anal. Chem.* **81**, 10038-10048 (2009).
37. Wei, X. et al. MetPP: a computational platform for comprehensive two-dimensional gas chromatography time-of-flight mass spectrometry-based metabolomics. *Bioinformatics (Oxford, England)* **29**, 1786-1792 (2013).

38. Dunn, W.B. et al. Procedures for large-scale metabolic profiling of serum and plasma using gas chromatography and liquid chromatography coupled to mass spectrometry. *Nat Protoc* **6**, 1060-1083 (2011).
39. Xia, J.G., Mandal, R., Sinelnikov, I.V., Broadhurst, D. & Wishart, D.S. MetaboAnalyst 2.0-a comprehensive server for metabolomic data analysis. *Nucleic Acids Research* **40**, W127-W133 (2012).

Chapter 3 Chemotherapeutic and environmental perturbations cause different metabolic responses in an ovarian cancer stem cell line compared to its isogenic parental cell line

3.1. Introduction

Since 1924, when Warburg discovered anaerobic glycolysis, it has been known that cancer cellular metabolism is distinct from normal cellular metabolism.[1, 2] It is only recently that the important role metabolism plays in cancer has become more generally recognized. Dysfunctional metabolism is now acknowledged as a hallmark of cancer, and multiple different examples of altered metabolism in cancer cells have been demonstrated.[3, 4] Most cancer cellular metabolism studies are usually performed using *in vitro* cell culture. Cell culture conditions are ideal: an overabundance of an energy source (usually in the form of glucose) is supplied, oxygen concentration is kept high, and cells are grown in monolayers to keep nutrient and oxygen transfer high to all cells. Unfortunately, these *in vitro* conditions drastically differ from the conditions found *in vivo* in the tumor environment, which are far from ideal. With the fast growth of tumors, angiogenesis cannot occur quickly enough to supply the entire tumor with capillaries, resulting in nutrient fluctuations, hypoxia, and ischemia (a state of depleted oxygen and glucose) – particularly in the center of tumor. Along with poor cellular growth conditions, most tumors are also treated with chemotherapeutics to attempt to eradicate the tumor. These differences in environmental conditions can actually be critical in correctly understanding and treating cancer cells. For example, differences between *in vitro* cellular growth conditions and the *in vivo* tumor environment have been identified as responsible for the inconsistency in

clinical and *in vitro* lethal concentration for metformin.[5] It is thus critical to attempt to study cancer cells under conditions relevant to their natural tumor environment.

Another important characteristic of tumors that may not be well represented in *in vitro* models is the heterogeneous population of cancer cells. Part of the heterogeneous population are cells referred to as cancer stem cells due to their stem-like properties: they can differentiate and self-renew, and they are chemo and radio-resistant. Thus, to fully understand tumor metabolism we must characterize the metabolism of both cancer cells and cancer stem cells. Any differences in metabolic behaviors between these two cells types could allow us to start to understand how the two different cell types handle some of the stresses encountered in a tumor. Understanding the metabolic effects of these stresses could lead to a more complete model of cancer pathology and the development of metabolism-targeted cancer therapies.

Here, we use ovarian cancer cells (OCCs) and ovarian cancer stem cells (OCSCs) as a model system for isogenic cancer cells and cancer stem cells. We subjected them to biologically inspired environmental *in vitro* perturbations and measured their metabolic responses. Since OCCs and OCSCs are already known to exhibit significant metabolic differences during normal growth,[6] we hypothesized that these two cell types may also have differing metabolic responses to the environmental perturbations. The perturbations used in this study are glucose deprivation, hypoxia, ischemia, and chemotherapeutic treatment. Docetaxel, a common first line treatment for ovarian cancer, was chosen as the chemotherapeutic. These perturbations are applied over a period of 48 hours with metabolomics measurements being made throughout that period using two-dimensional gas chromatography-mass spectrometry (GCxGC-MS).

3.2. Results & Discussion

3.2.1. Univariate analysis and time series analysis reveals no metabolic change for OCSCs upon docetaxel treatment

To profile cellular metabolism, GCxGC-MS was used to analyze the intracellular samples collected during the docetaxel treatment for both the OCCs and OCSCs. Both unknown analytes and annotated analytes result from this data processing pipeline. Because of the limited scope of metabolite mass spectrum databases and the conservative identification cutoff we employ in data processing, some of the unannotated analytes may be endogenous metabolites that have not yet had a mass spectrum deposited in a database, or their mass spectral similarities to library spectra may fall under our conservative naming cutoff. Therefore, these unknown analytes can still be important to the metabolic profile of the cells, and so they were included for most downstream analyses except enrichment analyses (which require metabolite identifies). Lists of annotated metabolites in this work come from unique matches to known human metabolites in either the Kyoto Encyclopedia of Genes and Genomes (KEGG) or the Human Metabolome Database (HMDB), followed by a manual confirmation of similarity between the annotated peak spectrum and the library spectrum. For the OCCs, 198 reproducible analytes were detected, including unknown analytes and annotated analytes that were not included in human metabolic databases, with 46 unique metabolites were annotated as known human metabolites. For the OCSCs, 115 reproducible analytes were detected overall and 31 unique metabolites were mapped to either KEGG or HMDB.

For OCSCs, univariate analysis in MetaboAnalyst revealed no statistically significant differences (FDR corrected p value < 0.05) between the control and docetaxel treated cells overall (*t* test across all time points). When looking at the individual time points, only one unknown analyte was found to be statistically significantly different between the control and docetaxel treated

cells, at 48 hours. For the OCCs, on the other hand, significant metabolome-scale changes were apparent during univariate analysis. Analysis of variance (ANOVA) was used to determine the differences between the three treatments: docetaxel at IC_{50}, docetaxel at 1.5x IC_{50}, and control. The number of statistically significant analytes found during ANOVA is shown in Table 3.1. Two-sample *t* tests were also performed on each individual docetaxel treatment versus control, with the number of statistically significant analytes shown in Table 3.1.

Table 3.1: Number of statistically significant analytes found in OCC analysis. The number of statistically significant analytes (FDR < 0.05) found during ANOVA (Control vs IC_{50} vs 1.5x IC_{50}) or t-test analysis (Control vs IC_{50} and 1.5x IC_{50}).

Time Points	Control vs IC_{50} vs 1.5x IC_{50}	Control vs IC_{50}	Control vs 1.5x IC_{50}
All	31	18	24
24	22	15	14
48	22	8	8

Two-way ANOVA was used to identify FDR-corrected p values for group, time, and interaction effects. Group effects relate to the difference in analytes between the experiment conditions, the time effect measures how the analyte changes with time across all the conditions, and the interaction effect captures effects where the combination of time and group effects are not additive. Analysis of the OCSC intracellular data using two-way ANOVA again demonstrated very little change over time between the control and docetaxel treated cells, with only two analytes showing statistically significant differences in the group category; neither of these were analytes that mapped to an annotated metabolite. Two-way ANOVA on OCC intracellular data revealed many more analytes that were statistically significantly different between the two docetaxel treatments and control cells than were found using one-way ANOVA. The numbers of metabolites with statistically significant effects are shown in Table 3.2.

Table 3.2: Number of statistically significantly different analytes in OCC using two-way ANVOA time series analysis. The number of statistically significant analytes (FDR < 0.05) found during time series analysis using two-way ANOVA.

Category	Control vs IC_{50} vs 1.5x IC_{50}	Control vs IC_{50}	Control vs 1.5x IC_{50}
Group	42	31	41
Time	67	48	51
Interactions	36	29	29

The annotated metabolites identified as having statistically significant group effects are shown in Table 3.3 for both docetaxel concentrations and for each concentration individually. All of the metabolites identified as statistically significant via one-way ANOVA for both docetaxel concentrations were also found as statistically significant via *t* tests for at least one of the concentrations individually. All of the metabolites with significant group effects for either concentration also had significant group effects for both docetaxel concentrations together. For the 1.5x IC_{50} concentration, three metabolites, including gamma-aminobutyric acid (GABA), were identified as having significant group effects that had not been detectable when analyzing both docetaxel concentrations together, suggesting that docetaxel at 1.5x IC_{50} has greater metabolic effects over 48 hours than docetaxel at IC_{50}.

Table 3.3: Metabolites identified as statistically significantly different during chemotherapeutic treatment using two-way ANOVA for OCCs.

	Metabolite	Group	Time	Interactions
Control vs IC_{50} vs 1.5x IC_{50}	Uracil	2.12E-04	3.65E-12	2.48E-07
	Phosphoric acid	5.77E-04	1.90E-06	3.24E-06
	Arachidonic acid	5.77E-04	1.75E-05	3.24E-06
	Ethanolamine	3.24E-03	1.33E-08	1.11E-04
	D-Glucose	3.38E-03	5.24E-03	6.43E-04
	Mannose 6-phosphate	0.010	0.187	0.337
Control vs IC_{50}	Uracil	0.019	5.08E-09	1.79E-06
	Phosphoric acid	0.030	1.61E-04	5.39E-04
	Ethanolamine	0.036	4.64E-06	6.99E-04
	D-Glucose	0.036	8.18E-04	4.90E-03
Control vs 1.5x IC_{50}	Uracil	3.85E-04	4.65E-07	6.66E-05
	Arachidonic acid	7.39E-03	6.00E-05	9.66E-05
	Hexadecane	0.025	0.287	0.522
	D-Glucose	0.029	0.016	3.59E-03
	Mannose 6-phosphate	0.038	0.320	0.491
	4-Hydroxy-L-proline	0.039	0.262	0.793

Uracil, a nucleobase used for RNA production, allosteric regulation, and as a coenzyme, always showed the most significant group effect, most significant time effect, and the most or second most significant interaction effect in the three data sets of analyses. Uracil levels in docetaxel treated cells spiked at 24 hours (with over 700-fold change from the control) and then leveled off at 48 hours, at which time the uracil in the control cells reached similar levels. The quicker spiking of uracil levels in docetaxel treated OCCs could be the cell reacting to the stress by increasing production of uracil or the docetaxel treatment blocking pathways that utilize uracil. These docetaxel-induced changes in uracil levels are particularly noteworthy, as recent clinical studies have shown that synthetic analogs of uracil (such as 5-flurouracil or tegafur/uracil), which inhibit enzymes using uracil as a substrate, when administered in combination with docetaxel cause improved treatment results for gastric cancer, prostate cancer, and lung

metastases.[7-10] Therefore, if docetaxel treatment does increase cellular dependence on uracil in the cells that are somewhat docetaxel resistant, then this would help explain why the addition of a competitive inhibitor for uracil improves patient treatment results.

3.2.2. PCA further confirms metabolic change in OCCs but not in OCSCs upon docetaxel treatment

Principal components analysis (PCA) allows for graphical interpretation of data through unsupervised dimensional reduction. PCA on OCSCs alone further supported the results from the basic and time series univariate analysis. No separation is evident between control and docetaxel treated cells, with the only separation seen between the initial time point and the later time points (24 and 48 hours), as shown in Figure 3.1A, and PC1 fully responsible for capturing this separation. PCA loading scores indicate that fumarate, psicose, and other unknown analytes are responsible for the separation seen in PC1. PCA on only the 24 or 48 hour time points showed the same lack of separation between control and docetaxel treated OCSCs. Previous work has shown that OCSC viability does not vary greatly over 96 hours of docetaxel treatment.[11] Overall, this non-perturbation of metabolism suggests quite powerful resistance of the OCSCs to docetaxel. Cancer stem cells are generally less susceptible to chemotherapeutic treatments than their cancer cell counterparts, but it is not known how susceptible their cellular metabolism is to chemotherapeutics. Here, it seems that OCSCs are able prevent any systematic change in metabolism, whether through an active role (removing docetaxel or inhibiting docetaxel uptake) or through a passive role (such as their low division rate). Either way, the OCSCs exhibit no metabolic stress.

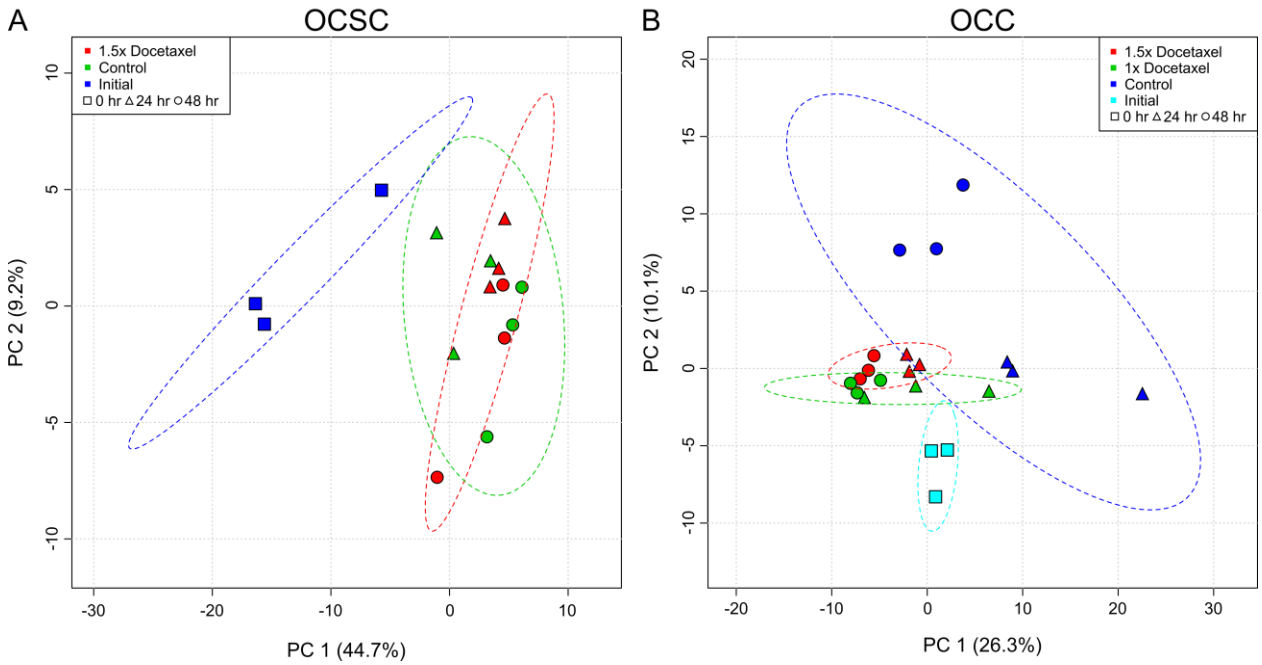

Figure 3.1: PCA of docetaxel perturbations highlights the different metabolic responses of OCCs and OCSCs. PCA of metabolic profiles of OCSCs (A) and OCCs (B) in response to docetaxel over 48 hours. Dotted ovals represent 95% confidence intervals of the membership of each sample class. (A) PC1 separates the initial time point and the later times points, but there is no separation between control and docetaxel treated cells, suggesting that docetaxel has little to no effect on the metabolism of OCSCs over a 48 hour period. (B) PCA shows clear separation between control and docetaxel treated OCCs, as well as separation between the two treatment levels, and separation between the time points for all treatments and controls. PCI and PC2 both are responsible for the separation between different experimental groups as well as time.

The clear effect of docetaxel on OCC metabolism is further supported with PCA, as seen in Figure 3.1B. Docetaxel-treated samples cluster together away from both the control and initial samples with distinct separation between the different concentrations and time points. Even though the separation is small between the different time points and between the different treatment levels (each in different PCs), the differences are clear and consistent. The control samples cluster together high in PC1 or PC2, with large variation between the 24 hour samples, which lie closer to the initial samples, and the 48 hour samples. The control OCCs have a much larger variance between the 24 and 48 hour time points compared to the variance between docetaxel treated OCCs. PC1 and 2 seem to be equally responsible for capturing the separation between treatment and time points. Unknown analytes, leucine, and fumarate are most important

in PC1 separation. For PC2, unknown analytes and glucose are largely responsible for separation.

3.2.3. Metabolite pathway enrichment analysis reveals important pathways in metabolic docetaxel response for OCCs

Metabolic pathway enrichment analysis (MPEA) in MetaboAnalyst found 14 pathways statistically significantly enriched for differences between control and docetaxel treated OCCs. In order to find only the pathways enriched for docetaxel differences and not between the initial state and these treatments, only the 24 and 48 hour time points were included in this analysis. Table 3.4 shows the pathways that were enriched. Most of the pathways affected by docetaxel are amino acid and carbohydrate metabolism pathways, but pathways involved in nucleotide metabolism, cofactor and vitamin metabolism, and lipid metabolism have also been altered. Pantothenate and CoA biosynthesis and pyrimidine metabolism both involve uracil, further highlighting that docetaxel treatment causes a perturbation in uracil metabolism.

Table 3.4: Metabolic pathways significantly enriched for differences between control and docetaxel treated OCCs.

KEGG Pathway	Raw p	FDR
Amino sugar and nucleotide sugar metabolism	0.002	0.033
Citrate cycle (TCA cycle)	0.002	0.033
Glycerophospholipid metabolism	0.004	0.033
Butanoate metabolism	0.004	0.033
Nicotinate and nicotinamide metabolism	0.005	0.033
Alanine, aspartate and glutamate metabolism	0.005	0.033
Arginine and proline metabolism	0.005	0.033
Glutathione metabolism	0.007	0.040
Pyrimidine metabolism	0.010	0.047
Arachidonic acid metabolism	0.011	0.047
Pantothenate and CoA biosynthesis	0.013	0.050
beta-Alanine metabolism	0.014	0.050
Fructose and mannose metabolism	0.015	0.050

Unsurprisingly, MPEA identified no pathways significantly enriched for differences between control and docetaxel treated OCSCs, further supporting all previous findings that docetaxel does not affect OCSC metabolism over a 48 hour period.

3.2.4. Glucose deprivation, hypoxia, and ischemia affect OCC and OCSCs in a time-dependent manner

GCxGC-MS analysis was used to profile the metabolism of the OCCs and OCSCs over the 48 hour period. For OCCs, 98 intracellular analytes were reproducibly detected with 35 of these analytes annotated to unique metabolites. For OCSCs, 81 reproducibly measured intracellular analytes were detected with 32 annotated to unique metabolites.

Two-way ANOVA was used to analyze the data to account for changes as a function of both time and treatment. OCC and OCSC samples were analyzed with all conditions together, and with each of the conditions individually compared against the normal condition. The number of analytes with statistically significant effects indicated by these analyses (FDR < 0.05) is shown in Table 3.5.

Table 3.5: Number of statistically significant analytes for OCCs and OCSCs using two-way ANOVA.

		All Analytes			Metabolites		
		Group	Time	Interaction	Group	Time	Interaction
OCCs	All Conditions	40	69	45	14	22	12
	Glucose Deprived vs Control	14	49	20	1	15	5
	Hypoxic vs Control	23	52	23	7	15	4
	Ischemia vs Control	26	42	34	9	13	10
OCSCs	All Conditions	21	52	27	7	19	5
	Glucose Deprived vs Control	11	33	17	3	14	5
	Hypoxic vs Control	4	34	9	0	10	2
	Ischemia vs Control	12	31	15	5	12	3

Individual annotated metabolites found to have statistically significant group effects for all conditions or for any individual condition are shown in Figure 3.2 for OCCs and OCSCs. Five metabolites had significant group effects for both OCCs and OCSCs when including all conditions, representing a core of conserved metabolites with a major role in responding to one or more of these environmental stressors. One of these metabolites, phosphoethanolamine, is a substrate for many cell membrane phospholipids that has recently been shown to induce both cell cycle arrest and apoptosis in cancer cells.[12, 13] Here, intracellular phosphoethanolamine levels for both OCCs and OCSCs stay fairly consistent over 48 hours for the control cells, but for the metabolic perturbations, the levels steadily increase over 48 hours. Because the phosphoethanolamine levels increase slightly but consistently for all metabolic perturbations, the reaction seems to be a generalized metabolic stress response. This reaction could be indicative of increased phospholipid membrane turnover or an apoptotic response to the increasing stress levels. Thus far, the apoptotic effects of phosphoethanolamine have only been studied in a controlled dose manner;[12, 13] it would be interesting to determine if the cells themselves use phosphoethanolamine as an apoptotic inducer.

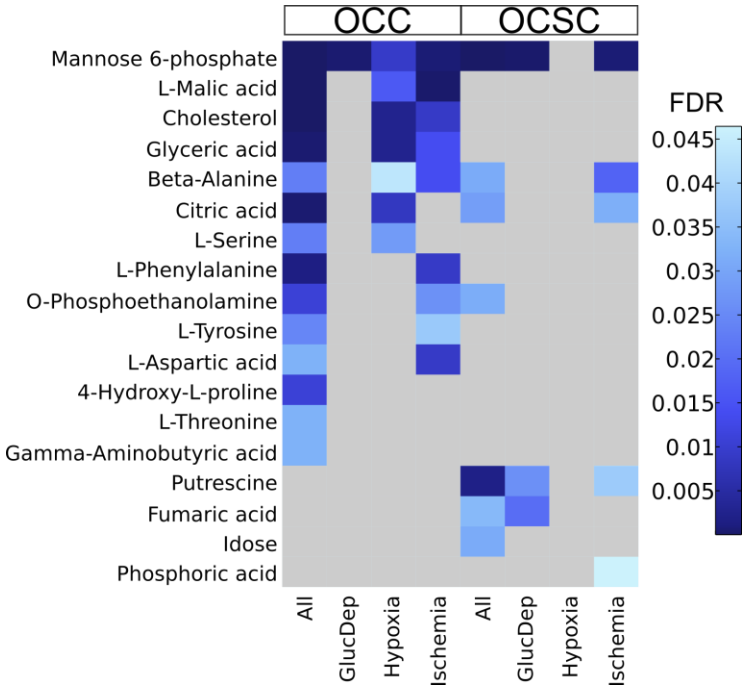

Figure 3.2: Environmental perturbations cause different metabolite-level changes in OCCs and OCSCs. Heatmap displays false discovery rate corrected p values for OCC and OCSC group effects for different metabolites during two-way ANOVA. Metabolites are shown in the rows, with the conditions represented in the columns. The darker the blue, the more statistically significantly different the metabolite differences are between the stated condition and the control. The five metabolites at the top represent a core, conserved set of metabolites with overall significance in both cell types.

Other types of stress-responsive analytes are also evident in this analysis. For example, there are numerous analytes that would not have been detectable as having significant group effects without the combination of all of the metabolic perturbations studied herein. This group, which includes 4-hydroxy-L-proline, GABA, and threonine for OCCs, can be seen as a "weak core response": not like the strong, individually significant core response observed for mannose-6-phosphate across all perturbations for OCCs, but nonetheless consistent in its small effect across all perturbations so as to yield an overall significant effect.

3.2.5. PCA shows separation between environmental perturbations for both OCCs and OCSCs

To assess the differences between cell types for the perturbations, PCA was used to examine the results of each perturbation individually, for OCCs and OCSCs together. Again, analytes whose

differences were due to the differences in media or extraction method were removed as discussed in the methods. PCA revealed separation between OCCs and OCSCs for each individual condition as shown in Figure 3.3, with the hypoxic perturbation showing the most distinct separation between the cell types. PC1 and PC2 are both responsible for separation of the OCC and OCSC samples as well as time point separation in different perturbations. For the control, the analytes most responsible for separation between OCCs and OCSCs are unknowns, myristic acid, and threonine. Unknowns, threonine, tyrosine, leucine, and valine are the analytes important for separation in glucose deprivation. The analytes most important for hypoxic separation are unknowns, 3,8-dimethylundecane, and ribose. Unknowns, n-dodecane, 4,6-dimethyldodecane, and 2,3,5,8-tetramethyl-decane are the most important analytes for separation between OCCs and OCSCs in ischemia. It is clear that both hypoxia and ischemia amplify the differences between OCCs and OCSCs evident in the normoxic condition; the effects of glucose deprivation are less evident in this analysis, though the differences become more evident in later analyses.

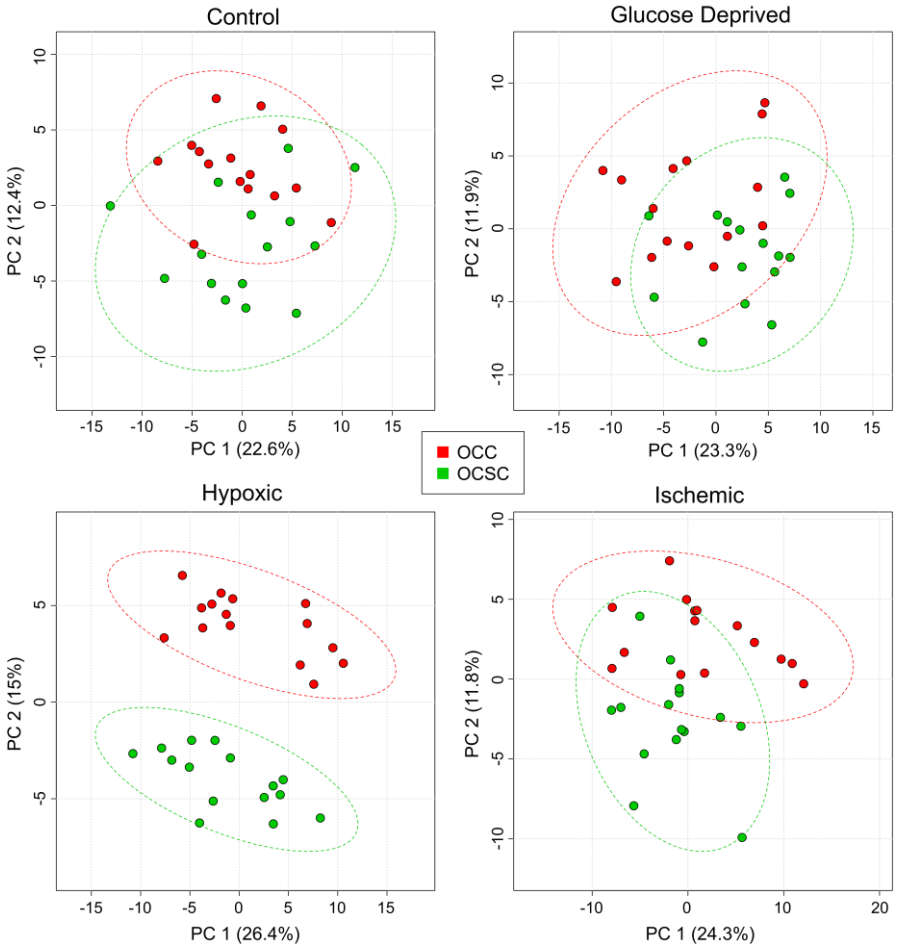

Figure 3.3: Control, glucose deprived, hypoxic, and ischemic conditions show varying effects on the differences between the two cell types. PCA of both cell types and all time points for four environmental conditions captured varying separation between OCCs and OCSCs. The greatest metabolic difference between the two cell types is during hypoxia; both hypoxia and ischemia amplify the differences between OCCs and OCSCs compared to control. PC1 and PC2 both capture separation between the cell types as well as time point separation in the different conditions. Dotted ovals represent 95% confidence intervals of the membership of each sample class.

To further characterize the effects of the perturbations on OCC and OCSC metabolism, PCA was performed on each cell type individually for all perturbations together. Plotting all conditions across all time points showed differences between the different conditions for both cell types, but only at later time points (data not shown). This suggests that the effects of these perturbations are not extremely fast, even though they are each tied closely to cellular metabolism; the impacts of these perturbations are best observed accumulated over days. For clarity and to facilitate

interpretation, time points at 2, 4, and 8 hours were removed from further visualizations and analyses, and PCA was performed for all conditions at 0, 24 and 48 hours, as seen in Figure 3.4.

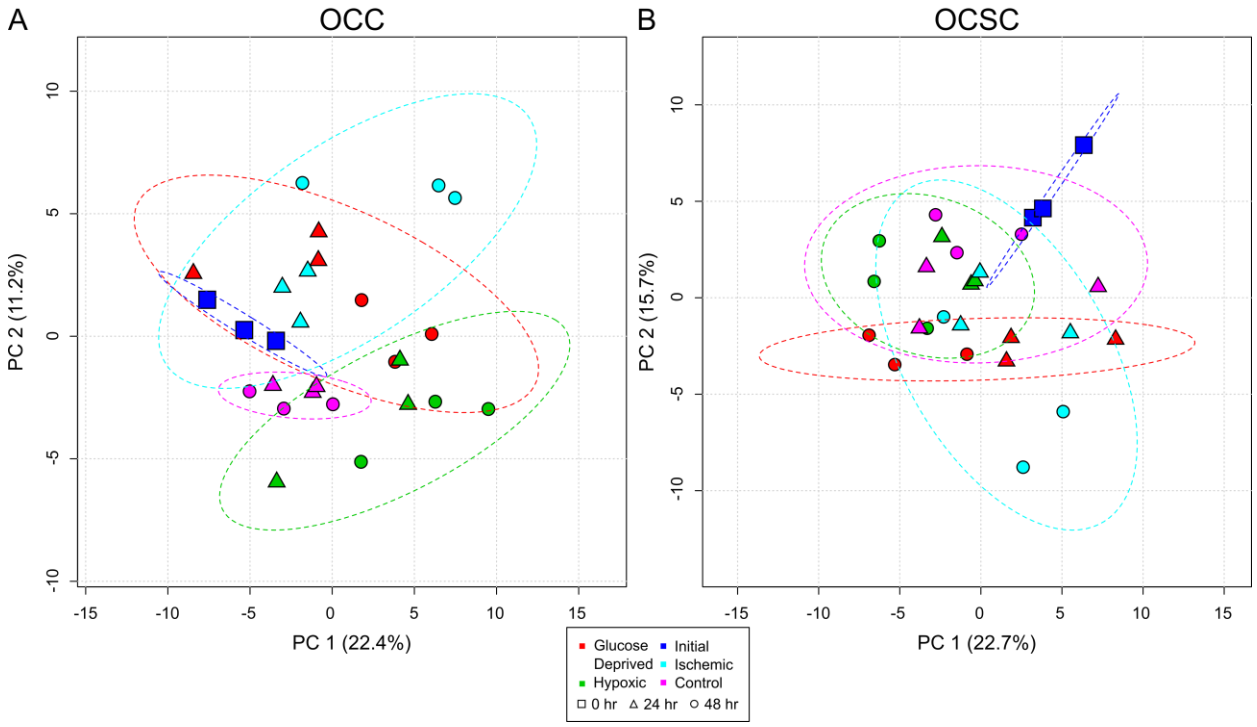

Figure 3.4: PCA for OCCs and OCSCs shows differences between environmental perturbations at later time points for each cell type. PCA shows separation between conditions and time points at later time points. In both cell types, PC1 plays a large role in separating time points, and PC2 captures variation between the conditions. Dotted ovals represent 95% confidence intervals of the membership of each sample class. A) Control samples show little temporal variation in OCCs. Effects of ischemia are not additive based on the effects of glucose deprivation and hypoxia individually at 48 hours, but are much more similar to the effects of glucose deprivation than they are to hypoxia. B) OCSC control samples display much greater temporal variation compared to OCCs. There is no metabolic distinction between control and hypoxic cells, and 48-hour ischemia samples again show non-additive effects compared to glucose-deprived and hypoxic conditions.

For OCCs, shown in Figure 3.4A, PC1 plays a large role in separating the different time points, with hydroxyproline, threonine, and tyrosine being most important analytes for the separation. PC2 plays a large role in separating the treatment conditions, with unknown analytes causing most of the separation between conditions. The control and initial samples are more similar to each other than the other conditions based on their close clustering, showing that the applied perturbations induce significant changes in metabolism. The effects of ischemia, even though it

is a combination of the glucose deprived and hypoxic conditions, are not additive based on the effects of glucose deprivation and hypoxia individually; instead, the 48 hour time points experience much greater differences for ischemia than for either of the two individual treatments. The overall proximity of the ischemia treatment to the glucose deprivation suggests that the metabolic impacts of ischemia are driven more strongly by glucose deprivation than by hypoxia.

PCA of OCSC samples again shows differences between conditions during the later time points, as seen in Figure 3.4B. PC1 captures significant time variance, with an unknown, phenylalanine, pyroglutamate, and tyrosine responsible for most of the variance. PC2 captures significant separation between the treatments, with 2,9-dimethyldecane, hexadecane, and cis-1,4-dimethylcyclooctane most responsible for separation. Similar to the OCCs, glucose deprivation shifted the OCSCs' metabolic profile away from the control, and ischemia showed a nonadditive extra effect on metabolism at 48 hours. Unlike OCCs, though, the control samples display substantial changes and variability between time points; this is to be expected based on previous work indicating temporal changes in metabolism of OCSCs.[6] In addition, the hypoxic samples completely overlap the control, showing that hypoxia did not substantially alter the metabolic profile of the OCSCs from its normal state as it did to OCCs. Hypoxic conditions have been shown to support stemness within cancer stem cells *in vitro* and cancer stem cells have been located in hypoxic niches within the tumor.[14, 15] Therefore, it is possible that OCSCs have adapted to hypoxic environments to the point where hypoxia no longer puts more stress on their metabolism compared to growth under normal oxygen concentrations.

3.2.6. MPEA further supports that OCCs and OCSCs respond to hypoxia and glucose deprivation differently

Using MPEA in MetaboAnalyst, 21 KEGG pathways for OCCs and 23 KEGG pathways for OCSCs were identified as being statistically significantly enriched (FDR < 0.05) in differences

between the normal, glucose deprived, hypoxic, and ischemic conditions across all time points. Figure 5 breaks the pathway responses into three categories: “strong core” responses in either cell type are significant for multiple individual conditions as well as all individual conditions together. “Weak core” responses are significant only for all conditions together, but never for any individual condition, suggesting the combination of many small, individually insignificant effects to reflect a significant core response. The remaining class of pathways are “perturbation-specific” responses: they are significant for only one perturbation in a cell type, which may or may not drive overall significance for all conditions. Within these subtypes, we can then further identify which of these responses are conserved between cell types, and which are unique to cell types.

Overall, 18 of the statistically significantly enriched pathways overlap between OCCs and OCSCs, indicating that many of the changes caused by the metabolic perturbations are similar between the two cells. However, 6 pathways were exclusively enriched in the OCCs and 5 pathways were exclusive for OCSCs. Detailed investigation of why these pathways were only altered in one cell type during all the perturbations may help to further explain the differences in metabolism between OCCs and OCSCs.

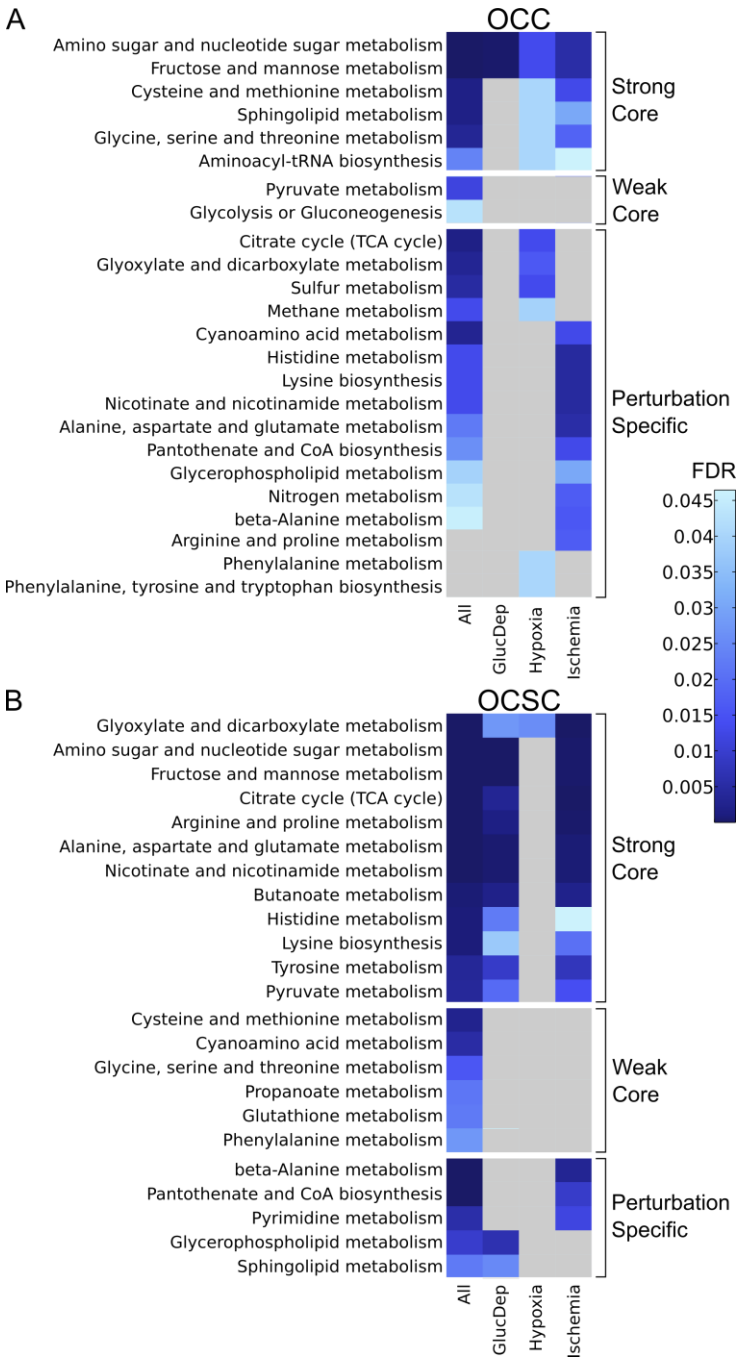

Figure 3.5: MPEA results show different trends in enriched pathways for OCCs, OCSCs, and both. Heatmap displays false discovery rate corrected p values for metabolite pathway enrichment analysis results for (A) OCCs, and (B) OCSCs. KEGG pathways are shown in the rows with the conditions represented in the columns. Strong core response pathways are those with significant enrichment in all conditions and in at least one individual condition; weak core response pathways are those enriched only in all conditions; perturbation specific pathways are those that are only enriched for a unique individual condition. The darker the blue, the more statistically significantly enriched the pathway is for metabolic differences. Grey boxes represent pathways with FDR > 0.05. All: glucose deprived vs hypoxia vs ischemia vs control; GlucDep: glucose deprived vs control; Hypoxia: hypoxia vs control; Ischemia: ischemia vs control.

To determine which pathways are most affected by each perturbation, each individual condition was compared against the control condition using MPEA. In OCCs, glucose deprivation resulted in only two pathways significantly enriched, amino sugar and nucleotide sugar metabolism and fructose and mannose metabolism pathways, both strong core responses. Therefore, it appears that glucose deprivation in OCCs only directly affects sugar metabolism pathways and the cells adjust their metabolism to meet their energy and other requirements without systems-scale metabolic impact. In contrast, glucose deprivation resulted in 14 significantly enriched pathways in OCSCs that are widespread throughout metabolism, including amino acid metabolism, carbohydrate metabolism, lipid metabolism, and cofactor and vitamin metabolism. The differences in lipid metabolism pathways, glycerophospholipid metabolism and sphingolipid metabolism, are largely driven by differences in phosphoethanolamine levels between the control and glucose deprived cells, discussed previously. Overall, these findings suggest that OCSCs might be more dependent on glucose than OCCs, since glucose deprivation has a much larger effect on OCSC metabolism than OCC metabolism. This is particularly surprising given the substantially lower proliferation rate of OCSCs and the known significant glycolytic flux of the Warburg effect in bulk cancer cells.

Under hypoxic conditions, 12 pathways were significantly enriched for metabolic differences for OCCs. Out of these 12, two pathways were perturbation-specific responses, phenylalanine metabolism and phenylalanine, tyrosine and tryptophan biosynthesis, both of which are amino acid metabolism pathways. Tyrosine and phenylalanine are the metabolites most responsible for the differences in these two pathways, both of which have lower levels in hypoxic conditions. Along with these two pathways, there are three other amino acid metabolism pathways enriched for statistically significant differences along with aminoacyl-tRNA biosynthesis, which prepares

for translation. In all of these pathways, the amino acids driving the differences have lower levels in hypoxia than the control. Therefore, hypoxic conditions seem to be causing significant overall changes in amino acid metabolism, whether via decreased production or increased consumption. Hypoxia also has an observable effect on sulfur metabolism; the sulfur metabolism pathway supplies sulfur for cysteine and methionine metabolism, both of which are enriched for metabolites with lower levels in hypoxia. The only metabolites with higher levels in hypoxia are citric acid and malic acid, both of which play a major role in the TCA cycle. For OCSCs, in contrast, hypoxia only resulted in one pathway being significantly enriched (glyoxylate and dicarboxylate metabolism), thus reinforcing the idea that OCSCs have fairly completely adapted to a hypoxic environment.

Ischemia caused 16 pathways to be significantly enriched for metabolic differences for the OCCs, ten of which are perturbation-specific responses (though nine of them drive significance in the overall analysis as well). For OCSCs, 15 pathways were statistically significantly enriched. 9 of these pathways are in common between the two cell types, showing a surprisingly well-conserved ischemia response conserved between the two cell types, especially considering that the responses to hypoxia and glucose deprivation alone are not at all conserved, being very cell type-specific. Interestingly, for both cells there are some metabolic pathways that are enriched for differences under glucose deprived or hypoxic conditions that are not seen under ischemic conditions, which suggests that the effect ischemia has on the cells is not an additive affect of glucose deprivation and hypoxia.

Overall, OCCs and OCSCs have different trends in pathway response to the environmental perturbations, but do display some level of conservation. The conserved strong core response module consists of amino sugar and nucleotide sugar metabolism and fructose and mannose

metabolism, which are in the strong core modules of both cell types. The conserved core response module can be broadened to also include cysteine and methionine metabolism; glycine, serine, and threonine metabolism; and pyruvate metabolism. Each of these display strong core responses across the perturbations in one cell type and weak core responses across the perturbations in the other cell type. These five pathways are the ones that the two cell types use very similarly in responding to these environmental stresses, representing a core, conserved response between the cell types. This leaves three (weak or strong) core responses in OCCs and thirteen (weak or strong) core responses in OCSCs as the cell type-specific core responses; many of these core responses pathways in one cell type may be perturbation-specific in the other, though some (for example, tyrosine metabolism) are core in one but not at all significant in the other. Taken together, though, the set of core responses is much larger in OCSCs, indicating that OCSCs are responding more similarly to the different environmental perturbations while OCCs are dominated by more perturbation-specific responses.

3.2.7. Limitations

For this work, only one isogenic cancer cell and cancer stem cell line pair was used. Therefore, the results found here only correspond to differences between these two particular ovarian cancer cell lines. It would be desirable to expand this study to other isogenic cancer cell and cancer stem cell line pairs, but, unfortunately, there are very few such cell lines, and they are not easily obtainable. As such cell line pairs become more widely available, these metabolic experiments should be expanded to additional cell lines to determine if the results shown here are characteristic of this specific isogenic pair or if they are indicative of broader isogenic (ovarian) cancer cell and cancer stem cell line differences.

Another limitation of this study is the constraint of biological interpretation due to metabolite identification. Over half of the analytes that are retained in the final data set are labeled as unknown analytes, due to low match scores during our conservative metabolite identification step during processing. Additionally, the database used for metabolite pathway enrichment analysis does not include all of the metabolites identified within our data set. Therefore, there may be additional changes, especially in the metabolite pathway enrichment analysis, that are not currently detected because of lack of metabolite identification. Greater efforts must be made toward increasing the number of metabolites available within these databases in order for a complete understanding of the changes detected in these experiments. And, as previously noted, even conservative annotation score thresholds can yield false identifications on occasion.

Finally, our chemotherapeutic perturbation was only applied under normal cell culture conditions, which, as discussed for metformin, can cause different results than what would be seen under tumor conditions. To further explore the metabolic changes caused by chemotherapeutics, future work will include applying chemotherapeutic and environmental perturbations at the same time.

3.3. Conclusions

In this study, OCC and OCSC were shown to have different metabolic reactions to biologically based perturbations applied *in vitro* to mimic *in vivo* tumor conditions. Docetaxel treatment did not affect the metabolism of OCSCs, showing that these cells are chemo-resistant even on a metabolic level. Docetaxel had a substantial effect on OCCs, especially in amino acid metabolism and carbohydrate metabolism. Docetaxel also caused increased levels of uracil compared to the control, which may help explain why treatment with competitive inhibitors of uracil in conjunction with docetaxel improves tumor treatment. OCCs and OCSCs also reacted

differently to glucose deprivation, hypoxia, and ischemia perturbations. Glucose deprivation alone did not have a large affect on OCC metabolism, but did perturb many pathways in the OCSCs, a surprising result based on the relative proliferation rates of the cells and the known high glycolytic flux associated with the Warburg effect and cancerous proliferation. Hypoxia had the reverse affect, affecting the metabolism of OCCs but not OCSCs, likely indicative of the ability of hypoxic conditions to support CSC stemness *in vivo*. Ischemia affected the metabolism of both cell types in many of the same pathways, suggesting that OCCs and OCSCs respond to this stress in a similar way. However, the ischemia response in both cells is not simply an additive response of the glucose deprivation and hypoxia conditions, especially since one of those conditions essentially yielded no response in each cell type. Both pathway-level analysis and metabolite-level analyses helped to identify core metabolic responses to multiple perturbations common across both cell types, including an increase in phosphoethanolamine levels for all perturbations for both cell types as a generic stress response. Five metabolic pathways were identified as a conserved core response module, responding to multiple environmental perturbations in each cell type. Overall, these metabolic differences seen during chemotherapeutic and environmental perturbations *in vitro* help to provide much-needed detail to characterize the inherent differences in metabolism between OCCs and OCSCs; this information could potentially be used in the development of targeted treatments against OCSCs.

3.4. Methods

3.4.1. Cell culture

The OVCAR-3 cell line was obtained from the Developmental Therapeutic Program (DTP) of the National Cancer Institute (NCI). The OVCAR-3 ovarian cancer cells (OCCs) were cultured in R10 medium: RPMI-1640 (Cellgro, Mediatech Inc., Manassas, VA) supplemented with 10% fetal bovine serum (FBS, Invitrogen, Grand Island, NY) and 1% antibiotic-antimycotic solution

(Cellgro, Mediatech Inc., Manassas, VA). Authenticity of the OVCAR-3 cell line was confirmed using short tandem repeat profiling performed by IDEXX RADIL (Columbia, MO) in October 2013. Cells were grown until confluence and subcultured at a ratio of 1:4.

Ovarian cancer stem cells (OCSCs) were previously derived from a side population of OVCAR-3. OCSCs are less adherent than OVCAR-3 cells and, unlike OVCAR-3 cells that are grown as adherent monolayers, are grown as spheroids in stem cell media to help support their stemness as previously described.[11] Briefly, the OCSCs were cultured in ultra-low attachment petri dishes (Corning Incorporated, Corning, NY) in stem cell medium: DMEM/F12 (1:1) (Cellgro, Mediatech Inc., Manassas, VA) supplemented with 0.4% bovine serum albumin (BSA, Sigma-Aldrich, St. Louis, MO), 20 ng/mL epidermal growth factor (EGF, Invitrogen, Grand Island, NY), 10 ng/mL basic fibroblast growth factor (bFGF, Sigma-Aldrich, St. Louis, MO), 5 µg/mL insulin (Sigma-Aldrich, St. Louis, MO), and 1% antibiotic-antimycotic solution (Cellgro, Mediatech Inc., Manassas, VA). The spheroids were dissociated and reseeded at a density of 10^5 cells/mL each week.

3.4.2. Environmental perturbation experiments

There were four environmental perturbations used in these experiments: chemotherapeutic, glucose deprived, hypoxia, and ischemia. According to the American Cancer Society, the common first line chemotherapeutic treatment for ovarian cancer is a combination of a platinum compound, like cisplatin, and a taxane compound, such as docetaxel. Docetaxel was chosen as the chemotherapeutic treatment because it interrupts cellular division and thus would more likely have a direct effect on metabolism over cisplatin, which causes DNA crosslinking. Docetaxel disrupts cellular division through suppression of microtubule dynamics in the cells, which eventually leads to apoptosis.[16] For OCCs, two different concentrations of docetaxel dissolved in

dimethylsulfoxide (DMSO) were given to the cells, the IC_{50} value (10nM) and 50% above the IC50 value (1.5x IC_{50}) (15nM). IC_{50} values for OCCs were reported in previous work.[11] For the OCSCs, only the higher concentration of docetaxel (1.5x IC_{50} of the OCCs) was given to the cells since the higher concentration would be more likely to have an impact on the OCSCs. Solutions of docetaxel dissolved in DMSO at 100μM and 150μM were used to obtain the desired final required concentrations for IC_{50} and 1.5x IC_{50}. An equivalent amount of DMSO was added to control media to account for effects of DMSO.

For glucose-deprived conditions, RPMI-1640 (Cellgro, Mediatech Inc., Manassas, VA) and DMEM-F12 (US Biological, Massachusetts, MA) without glucose were obtained and used to make glucose-free R10 and stem cell media as described above. For hypoxic conditions, cells were placed in a hypoxic chamber with 2% oxygen at the beginning of the experiment. Ischemic conditions were a combination of glucose deprived and hypoxic conditions.

Immediately before applying the environmental perturbations, OCCs were passaged and seeded in 6-well plates (Greiner Bio-One, Monroe, NC**)** with a well surface area of 6.9 cm^2 at a density of $3x10^5$ cells/well in 2mL of R10 medium and incubated for 24 hours to allow the cells to attach and recover. The medium was then removed, wells were washed once with PBS, and then 2mL of fresh experimental medium (prepared as described above) was applied to begin the experiment. OCSCs were dissociated and seeded into ultra-low attachment 6-well plates (Corning Incorporated, Corning, NY) containing 2mL of fresh experimental stem cell medium (prepared as described above) at a density of $3x10^5$ cells/well with a well surface area of 6.9 cm^2. Both the OCC and OCSC experiments were performed in biological triplicate.

3.4.3. Sampling protocols

For the chemotherapeutic perturbation, samples were taken at 0 minutes, 24 hours, and 48 hours. For the hypoxic and glucose deprived perturbation, samples were taken at 0 minutes, 2 hours, 4 hours, 8 hours, 24 hours, and 48 hours. The additional short-term time points were taken since the direct metabolic nature of the perturbations might cause a fairly rapid metabolic response. For OCCs, medium was removed and cells were quickly washed with 1mL PBS at 37°C, which was aspirated off, and then 700 µL of 80:20 methanol/water solution at -80°C was added immediately. The plate was then incubated at -80°C for 15 minutes. After incubation, remaining cellular debris were harvested using a cell scraper (BD Falcon, San Jose, CA) for intracellular analysis. For OCSCs, the media-cell mixture was transferred to a filter cup (Microcheck II beverage monitor, Pall, Port Washington, NY) with a pre-wetted membrane (0.45 µm pore Express PLUS Polyethersulfone membrane, Millipore, Billerica, MA) and the medium was filtered from the cells. The cells were then quickly washed with 4mL PBS at 37°C. The filter was then removed and placed upside down in a petri dish containing 1.5mL of 80:20 methanol/water solution at -80°C. The samples were then incubated at -80°C for 15 minutes. After 15 minutes, the petri dish was removed and the filter was flipped over and washed using the 1.5mL 80:20 methanol/water solution to remove any debris still caught in the filter. An extraction blank was made for the OCSCs following the same procedure above but only 4mL PBS was washed through the filter.

For both cell types, the intracellular solution was then transferred to a microcentrifuge tube in a cold ethanol bath and centrifuged at 5,000 *g* for 5 minutes at -4°C. The supernatant was retained, and the pellet was subsequently re-extracted twice in 100 µL of the cold 80:20 methanol/water solution, with all supernatants being pooled.[17] Intracellular and extracellular samples were stored at -80°C and -20°C, respectively, until analysis.

3.4.4. Growth media experiment

To control for the differences in media between the two cell types, a secondary experiment was performed where OCCs were grown in parallel in R10 media and stem cell media for 48 hours. Intracellular samples were taken at 0, 24, and 48 hours in the same manner as described above for the OCCs. Cell counts were also taken (data not shown) and showed that OCCs grow slower in the OCSC medium than they do in their normal medium, mimicking the slower growth rate of OCSCs.

3.4.5. GCxGC-MS analysis

Before derivatization, intracellular samples were vacuum concentrated in a CentriVap at 40°C until completely dry. The volume that was vacuum concentrated was varied for each sample in order to yield a final concentration of $3x10^3$ live cell equivalents/µL after derivatization, based on the cell density at the sample time. The samples were derivatized following the protocol laid out by Fiehn, *et. al*.[18] Briefly, 2.5 µL of 40 mg/mL *O*-methylhydroxylamine hydrochloride (MP Biomedicals, LLC, Santa Ana, CA) in pyridine was added to the dried sample and shaken at 1400 rpm for 90 minutes at 30°C. 22.5 µL of *N*-methyl-*N*-(trimethylsilyl) trifluoroacetamide (MSTFA) + 1% trimethylchlorosilane (TMCS) (Thermo Scientific, Lafayette, CO) was then added to the samples which were then shaken at 1400 rpm for 30 minutes at 37°C. Samples were centrifuged at 21,100 *g* for 3 minutes and 10 µL of the supernatant was added to an autosampler vial. Samples were spiked with 0.10 µL of a retention time standard solution consisting of fatty acid methyl esters (FAMEs) and an internal standard of nonadecanoic acid methyl ester dissolved in dimethylformamide.

A LECO Pegasus 4D instrument with an Aglient 7683B autosampler, Agilent 7890A gas chromatograph and time-of-flight mass spectrometer (TOF-MS) was used to analyze the samples. The first column was an HP-5, 30 m long x 0.320 mm ID x 0.25 µm film thickness

(Agilent, Santa Clara, CA), and the second was an Rtx-200, 2 m long x 0.25 mm ID x 0.25 µm film thickness (Restek, Bellefonte, PA). Specific autosampler, gas chromatography, and mass spectrometry methods can be found in Appendix A.

3.4.6. Data analysis

Sample runs were first analyzed in ChromaTOF (LECO, St. Joseph, MI) to determine baseline, peak area, and peak identification. Briefly, settings included a baseline offset of 0.5, automatic smoothing, 1st dimension peak width of 24 seconds, 2nd dimension peak width of 0.10 seconds, and a match of 700 required to combine peaks with a minimum signal-to-noise (S/N) of 5 for all subpeaks. Peaks were required to have a S/N of 10 and have a minimum similarity score of 800 before assigning a name. Unique mass was used for area and height calculation.

To align the samples, MetPP (http://metaopen.sourceforge.net/metpp.html) was used.[19] Sample files and a derivatization reagent blank file were uploaded from ChromaTOF. Unknowns were retained during the peak alignment process. The derivatization reagent blank file for OCCs or the extraction blank file for OCSCs was used to subtract peaks attributable only to sample preparation reagents from the corresponding cells' sample files. On-the-fly alignment was used with quality control samples manually selected as the peak list for primary alignment. Peak alignment was performed using the default criteria. This was done for the OCC data only, OCSCs only, and the combined OCC and OCSC data set for both metabolic perturbation experiments. For the combined OCC and OCSC data sets, blank peaks were not deducted during alignment; instead they were aligned with the metabolite samples for later removal.

After alignment, further processing of the data was done based on the procedure laid out by Dunn, *et. al*.[20] Batch effects were removed from the intracellular data set using LOESS. To remove analytes that were not reproducibly detected, analytes for which more than half of the

values were missing in the QC samples or for which the QC samples had a coefficient of variance larger than 0.5 were removed from the data set. Then, missing values were manually corrected using small value correction only if all the values were missing in the biological replicate. Annotated analytes were then compared to the Kyoto Encyclopedia of Genes and Genomes (KEGG) or the Human Metabolome Database (HMDB); if they were listed in KEGG or HMDB they were identified as metabolites. The metabolites were then verified by a manual confirmation of similarity between the annotated peak spectrum and the library spectrum. Manual confirmation resulted in tetrahydrofuran and pyruvaldehyde peaks re-annotated from metabolite peaks to unknown peaks.

Finally, MetaboAnalyst (http://metaboanalyst.ca/) was used for statistical and enrichment analysis, applying both the statistical analysis and time series analysis modules.[21] For both analyses, remaining missing values were k-nearest neighbors (KNN) corrected. Data was filtered using the interquantile range method and then log-transformed using generalized logarithm transformation (base 2) and autoscaled.

For enrichment analysis, both metabolite set enrichment analysis (MSEA) and metabolite pathway enrichment analysis (MPEA) yielded similar results, so only MPEA results were considered further. The entire time series was uploaded as discrete data with compound names. Metabolites were properly matched to their HMDB codes before processing the data. Data processing followed the same steps as listed above for missing value imputation and data normalization. The *Homo sapiens* pathway library was used for analysis and an in-house metabolite reference library based on detectable metabolites for our system was uploaded. Global test was used for pathway enrichment analysis, with relative-betweeness centrality as the

pathway topology analysis. Pathways with an FDR < 0.05 were considered significantly enriched.

3.4.7. Removal of media and extraction effects

For the combined OCC and OCSC data sets only, differences potentially due to media effects and extraction methods were removed. To specifically identify media effects, MetaboAnalyst was first used to analyze the OCC media control samples. Any analytes found to have statistically significant differences (t-test, all time points, FDR < 0.05) between the OCCs grown in R10 and OCCs grown in stem cell media were then removed from the combined data set to eliminate metabolic changes due to media differences.

The different extraction methods for the OCCs and OCSCs resulted in systematic differences because of analytes extracted from the filter used for OCSCs. To identify differences due to extraction methods, the derivatization reagent blanks and filter extraction blanks were analyzed in MetaboAnalyst. Again, any analytes found to have statistically significant differences (t-test, FDR < 0.05) between the two blanks were removed from the combined OCC and OCSC data set.

3.5. References

1. Warburg, O. Origin of Cancer Cells. *Science* **123**, 309-314 (1956).
2. Warburg, O., Posener, K. & Negelein, E. On the metabolism of carcinoma cells. *Biochemische Zeitschrift* **152**, 309-344 (1924).
3. Hanahan, D. & Weinberg, R.A. Hallmarks of Cancer: The Next Generation. *Cell* **144**, 646-674 (2011).
4. Kroemer, G. & Pouyssegur, J. Tumor cell metabolism: Cancer's Achilles' heel. *Cancer Cell* **13**, 472-482 (2008).
5. Menendez, J.A. et al. Metformin is synthetically lethal with glucose withdrawal in cancer cells. *Cell Cycle* **11**, 2782-2792 (2012).
6. Vermeersch, K., Wang, L., Mezencev, R., McDonald, J.F. & Styczynski, M.P. OVCAR-3-derived ovarian cancer stem cells display distinct metabolic profiles. *PLoS ONE* **under review** (2014).
7. Li, C.P. et al. A phase II study of weekly docetaxel and cisplatin plus oral tegafur/uracil and leucovorin as first-line chemotherapy in patients with locally advanced or metastatic gastric cancer. *Br J Cancer* **103**, 1343-1348 (2010).

8. Shimasaki, T. et al. [Combination chemotherapy of docetaxel and UFT against hormone refractory prostate cancer]. *Hinyokika kiyo. Acta urologica Japonica* **57**, 163-166 (2011).
9. Tsuchiya, A. et al. Successful treatment of multiple lung metastases of hepatocellular carcinoma by combined chemotherapy with docetaxel, cisplatin and tegafur/uracil. *World journal of gastroenterology : WJG* **15**, 1779-1781 (2009).
10. Yang, K.C. et al. The unusual presentation of gastric adenocarcinoma as a testicular mass: a favorable response to docetaxel and Cisplatin plus oral tegafur/uracil and leucovorin. *Journal of the Chinese Medical Association : JCMA* **73**, 88-92 (2010).
11. Wang, L., Mezencev, R., Bowen, N.J., Matyunina, L.V. & McDonald, J.F. Isolation and characterization of stem-like cells from a human ovarian cancer cell line. *Mol Cell Biochem* **363**, 257-268 (2012).
12. Ferreira, A.K. et al. Anti-angiogenic and anti-metastatic activity of synthetic phosphoethanolamine. *PLoS One* **8**, e57937 (2013).
13. Ferreira, A.K. et al. Synthetic phosphoethanolamine induces cell cycle arrest and apoptosis in human breast cancer MCF-7 cells through the mitochondrial pathway. *Biomedicine & pharmacotherapy = Biomedecine & pharmacotherapie* **67**, 481-487 (2013).
14. Cabarcas, S.M., Mathews, L.A. & Farrar, W.L. The cancer stem cell niche--there goes the neighborhood? *Int J Cancer* **129**, 2315-2327 (2011).
15. Li, Z. & Rich, J.N. Hypoxia and hypoxia inducible factors in cancer stem cell maintenance. *Current topics in microbiology and immunology* **345**, 21-30 (2010).
16. Yvon, A.-M.C., Wadsworth, P. & Jordan, M.A. Taxol Suppresses Dynamics of Individual Microtubules in Living Human Tumor Cells. *Molecular Biology of the Cell* **10**, 947-959 (1999).
17. Lu, X., Bennet, B., Mu, E., Rabinowitz, J. & Kang, Y. Metabolomic Changes Accompanying Transformation and Acquisition of Metastatic Potential in a Syngeneic Mouse Mammary Tumor Model. *J. Biol. Chem.* **285**, 9317-9321 (2010).
18. Kind, T. et al. FiehnLib: Mass Spectral and Retention Index Libraries for Metabolomics Based on Quadrupole and Time-of-Flight Gas Chromatography/Mass Spectrometry. *Anal. Chem.* **81**, 10038-10048 (2009).
19. Wei, X. et al. MetPP: a computational platform for comprehensive two-dimensional gas chromatography time-of-flight mass spectrometry-based metabolomics. *Bioinformatics (Oxford, England)* **29**, 1786-1792 (2013).
20. Dunn, W.B. et al. Procedures for large-scale metabolic profiling of serum and plasma using gas chromatography and liquid chromatography coupled to mass spectrometry. *Nat Protoc* **6**, 1060-1083 (2011).
21. Xia, J.G., Mandal, R., Sinelnikov, I.V., Broadhurst, D. & Wishart, D.S. MetaboAnalyst 2.0-a comprehensive server for metabolomic data analysis. *Nucleic Acids Research* **40**, W127-W133 (2012).

Chapter 4 Metabolic changes during mesenchymal to epithelial transition

4.1. Introduction

The epithelial to mesenchymal transition (EMT) is an important process in embryonic development, allowing the epithelial phenotype cells to transition to a mesenchymal phenotype in order to populate all the developing tissues in the embryo.[1] Epithelial cells have a block-like shape and have tight cell-to-cell junctions, some of which are formed by cadherin transmembrane proteins such as E-cadherin. Mesenchymal cells have an elongated spindle shape and are more mobile than epithelial cells; they do not form cell-to-cell junctions. Recent cancer research has led many to believe that the EMT process is being utilized by tumors for metastasis.[2]

EMT is triggered in the primary tumor through interactions with the tumor microenvironment. Signaling from the stroma cells can induce tumor cells to produce transcription factors that trigger EMT.[2] After undergoing EMT, the new mesenchymal cells can migrate away from the tumor and throughout the body. Upon reaching a potential metastatic site, the cells undergo the reverse process, mesenchymal to epithelial transition (MET), and form a metastatic lesion. Forming a new metastatic lesion is not straightforward, as the cells have to adhere and grow in an unfamiliar and usually unwelcoming environment. Recent research into EMT provides a hypothesis of how cancer cells overcome this hurdle: EMT can give stem-like properties to the cancer cells.[3, 4] It has been shown that after undergoing EMT, cells obtain stem-like properties, such as stem cell markers, the ability to form spheres in culture, and chemoresistance.[5-7] This

evidence suggests that EMT allows for the metastatic event and gives the cancer cells the properties necessary to successfully form a metastatic lesion.

There has been no clinical evidence cancer cells undergoing the EMT-MET process for metastasis, but many groups have been able to model one or both of the transitions. EMT is usually induced in one of two ways: expression of transcription factors or through microRNA transfection. Research into microRNAs has shown that they are important regulators of EMT, since many target transcription factors that have been identified as playing a role in EMT.[8-12] Representative examples of these transcription factors include ZEB, Snail, Slug, Twist, which are responsible for regulating many different cellular pathways, but all commonly repress epithelial markers, such as E-cadherin, to facilitate EMT.[13-15]

The McDonald group was able to induce and sustain MET by transfecting HEY cells with a microRNA, miR-429.[16] Based on their results, a larger study was designed where transcriptomics, metabolomics, microRNA and protein measurements were all taken at identical time points during the process, tracking multiple omic-level changes in the cell. The experiment was designed to allow for an initial MET, followed by EMT. The cells were transfected initially with miR-429 to induce MET, and then with no other transfection to sustain the levels of miR-429, the cells subsequently underwent EMT during the latter part of the experiment. Presented here are the results of the metabolomics analysis of the experiment.

4.2. Results & Discussion

4.2.1. Mesenchymal to epithelial transition causes changes in phenotype and known mesenchymal and epithelial biomarkers

HEY cells were transfected with either miR-429 to induce MET or a control scrambled microRNA, specifically designed to avoid targeting any known microRNA binding sites. HEY

cells were initially transfected and then profiled over a period of 144 hours. After a period of 48 hours, clear morphological differences were noticed between miR-429 transfected and control cells, as shown in Figure 4.1. Control cells still had their original mesenchymal morphology, while miR-429 transfected cells had transitioned into an epithelial morphology. After a period of 144 hours, both miR-429 and control cells displayed their original mesenchymal morphology, as shown in Figure 4.1. During the experiment, known markers of MET were profiled and displayed changes correlating with a MET to EMT during the 144 hour period (data not shown). These phenotypic changes, along with morphological and supporting transcriptomic data, indicate that the HEY cells did undergo a MET and then a corresponding EMT.

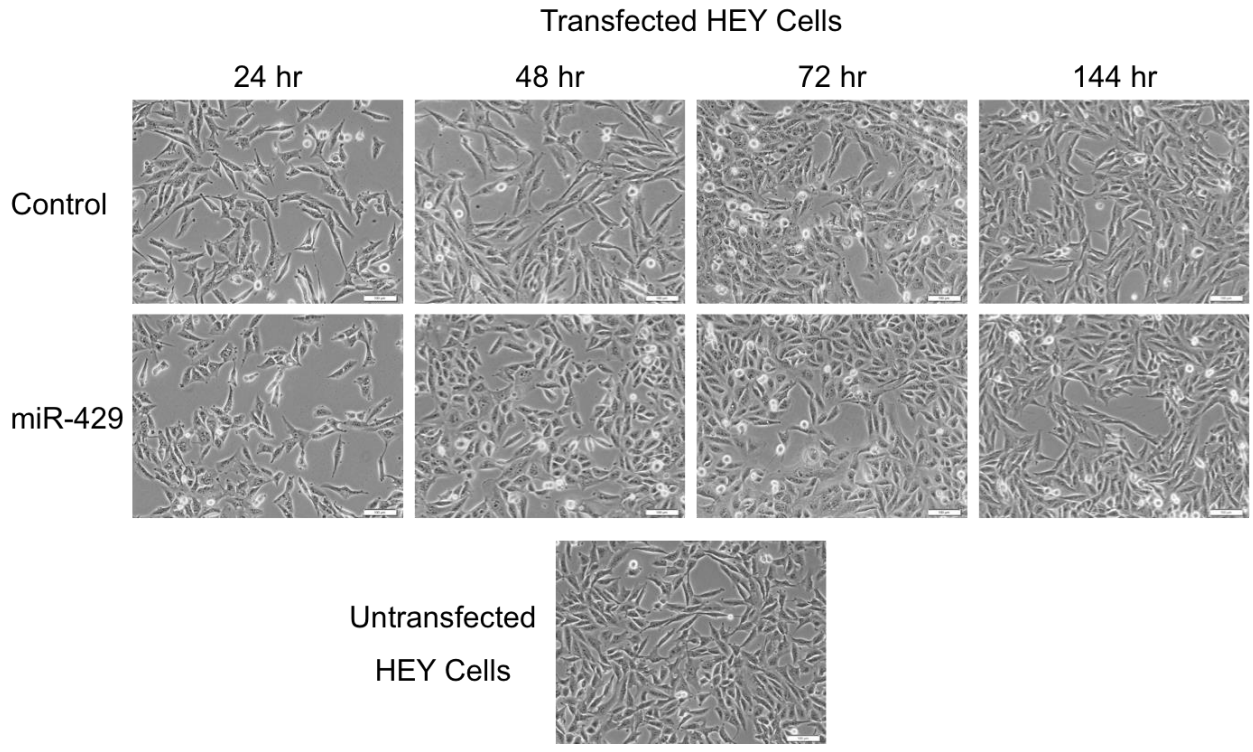

Figure 4.1: miR-429 transfected cells shift from a mesenchymal to epithelial back to mesenchymal morphology over the experimental time period. Untransfected HEY cells show the typical mesenchymal morphology with elongated spindles. Once transfected with miR-429, the HEY cells exhibit a shift towards an epithelial morphology, with the most cells exhibiting the morphology at 48 hours. After 48 hours, the cells show a clear shift back to mesenchymal morphology, with the change complete at 144 hours. Control transfected cells do not show a noticeable morphological change over the experimental time frame.

4.2.2. Metabolic profiling of MET

To capture both the immediate and late term effects of miR-429 transfection on the metabolome, a collection of early and late time points were taken. The early time points were expected to capture any changes that occurred due to the transfection and were taken at 0, 3, 5, and 7 hours. The late time points were designed to capture metabolic changes in response to MET and were taken at 24, 48, 72, and 144 hours. Both intracellular and extracellular samples were taken at each time point in biological triplicate for both the miR-429 and scrambled microRNA conditions. All the samples were then run on a two-dimensional gas chromatograph – mass spectrometer (GCxGC-MS). After initial analysis, it was discovered that two of the three intracellular 24 hour time point control samples were identified as outliers both during the alignment step as well as during initial principal components analysis. Therefore, the intracellular 24 hour time points were removed from subsequent analysis. As all the samples for this experiment were the same cell type, differences due to cells grown in different media were not an issue as they were in Chapter 2 and Chapter 3. Therefore, results gained from extracellular samples are valid.

4.2.2.1. Univariate analysis across all time points does not reveal consistent differences between control and miR-429 transfected cells

Overall, 253 intracellular and 252 extracellular analytes were detected and aligned across all the samples (see Methods for details on detection and alignment). These analytes included unknown and identified (annotated) analytes, as well as metabolites. (In this paper, analytes that are identified in the Human Metabolite Database (HMDB) or in the Kyoto Encyclopedia of Genes and Genomes (KEGG) database are referred to as metabolites.) After removal of unknown and annotated analytes not associated with HMDB or KEGG, there were 63 unique intracellular and

82 unique extracellular metabolites. Initial analysis of the control and miR-429 transfected cells showed that neither the intracellular nor extracellular samples exhibited large changes across all the time points. For the intracellular samples, there was only one analyte, heptacosane, that had a statistically significant difference (FDR-corrected p-value of 0.022) between control and miR-429 transfected cells across all the time points. For the extracellular samples, again there was only one metabolite, glucaric acid, that had a statistically significant difference (FDR-corrected p-value of 1.47×10^{-5}) between control and miR-429 transfected cells across all the time points.

This lack of difference between the control and miR-429 transfected cells was expected when all time points were included in the analysis since the HEY cells started out as a mesenchymal phenotype, then transitioned to an epithelial phenotype, and finally moved back to a mesenchymal phenotype. Therefore, if metabolism does change with MET, there should not be a consistent metabolic difference across the entire set of time points. Instead, a metabolic change is expected to be observable within a short time window wherein analysis should reveal a distinct difference between the control and miR-429 transfected cells.

4.2.2.2. PCA shows intracellular metabolic differences at 72 hours due to MET-EMT

Since a consistent metabolic change across all time points was not seen (or expected) in univariate analysis, the intracellular and extracellular data sets of annotated and unknown compounds were analyzed with principal component analysis (PCA). PCA allows for a graphical interpretation of the data and would therefore show cases were single time points exhibited differences between the control and miR-429 transfected cells. Again, analyzing the entire dataset across all time points, neither the intracellular nor extracellular data showed a difference between the control and miR-429 transfected conditions, as shown in Figure 4.2. Even though there was no difference between control and miR-429 transfected cells, distinct separation was

observed between early and late time points, as seen in Figure 4.3. This indicates that the time from the start to the finish of this experiment caused a larger variation in the metabolic data than did the transfection.

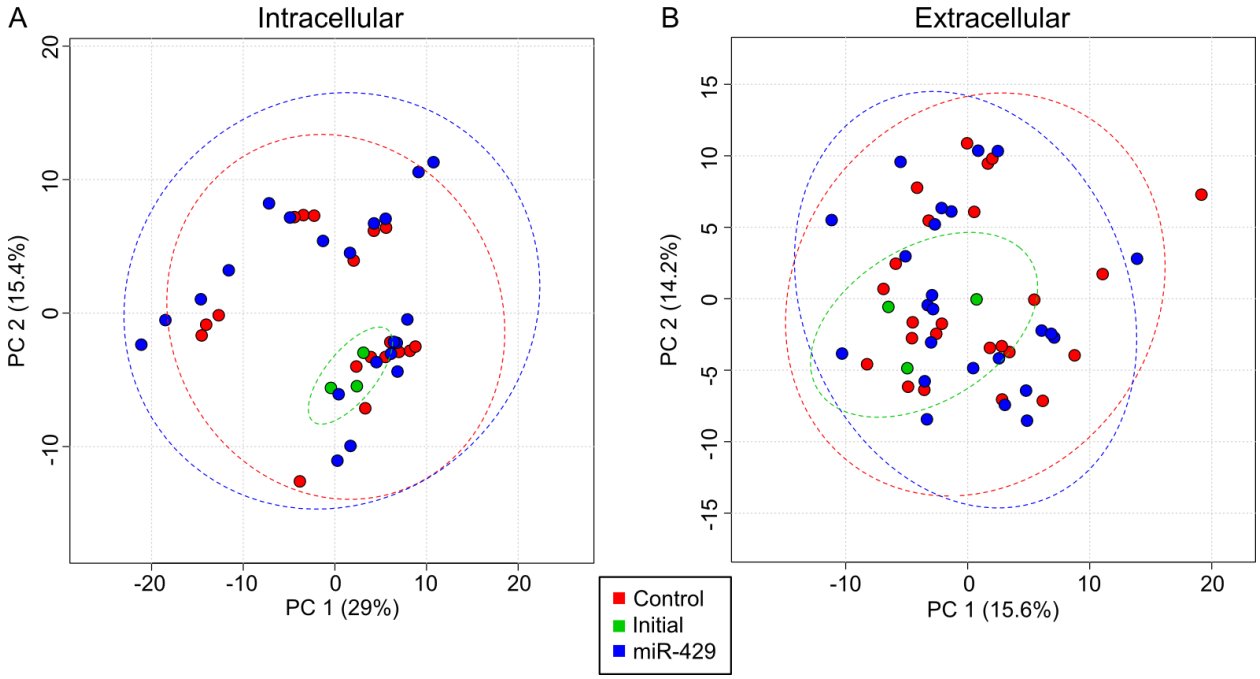

Figure 4.2: Principal components analysis shows no difference between control and miR-429 transfected samples. (A) PCA of intracellular samples shows no difference between control, initial, and miR-429 transfected cells. (B) PCA of extracellular samples shows no difference between control, initial, and miR-429 transfected samples.

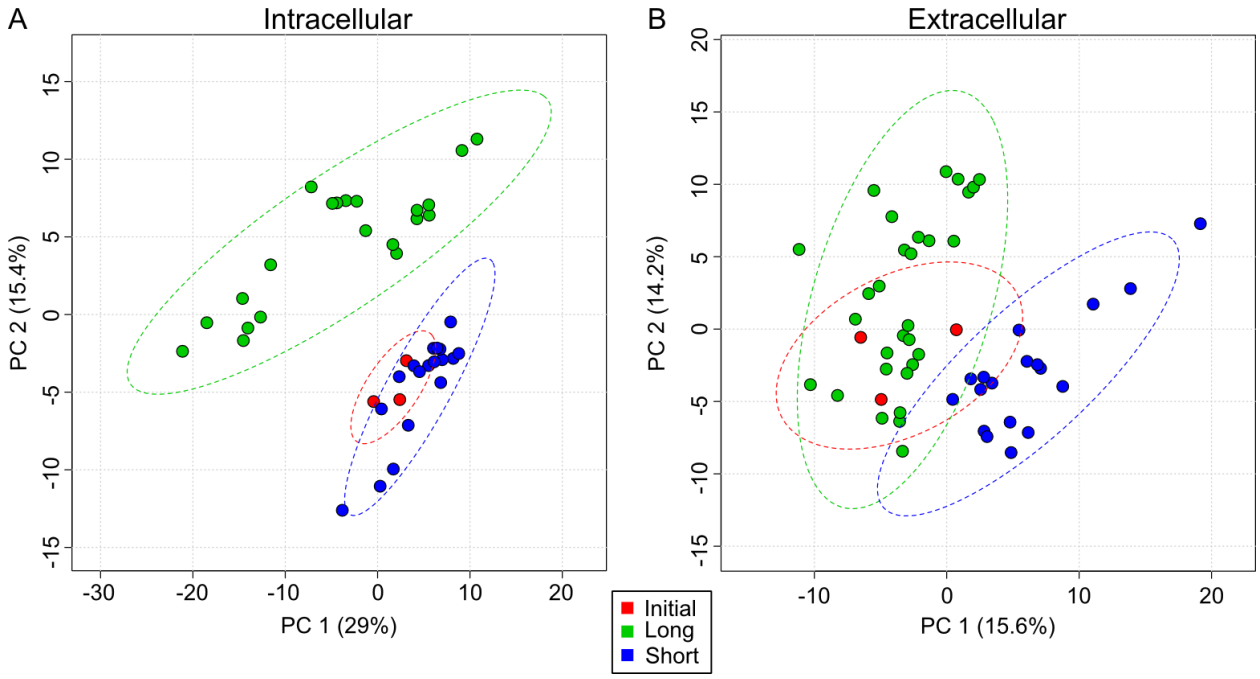

Figure 4.3: Principal components analysis shows clear difference between early and late time point samples. (A) Intracellular metabolomics data shows clear separation between late and early time point samples. (B) Late and early time points group together in the extracellular samples, but the distinction is not as clear as in the intracellular samples.

To further break down the datasets into individual time points and to help remove some of the time variation, the intracellular and extracellular matrices were split into early and late time points and PCA was performed on each group separately. For the earlier time points, Figure 4.4, neither the intracellular nor extracellular samples show separation between time points or control and miR-429 transfected cells. Therefore, it is likely that no substantial metabolic changes occur in either the intracellular or extracellular samples from the beginning of the experiment through seven hours.

The later time points, shown in Figure 4.5, exhibit clear separation by time point. In the intracellular samples (Figure 4.5A), separation was observed clearly by time point but this separation was also seen for the controls, suggesting the changes were not associated with MET. However, at 72 hours there is some separation seen between the control and miR-429 transfected

cells. The extracellular samples (Figure 4.5B) showed no separation by condition, but did suggest a trend of time point dependence on PC 1. Overall, most of the observed metabolic changes are likely due to changes in cellular growth, but small changes contributed to MET-EMT may occur intracellularly at 72 hours. The same results were seen using the annotated metabolite-only intracellular and extracellular data sets.

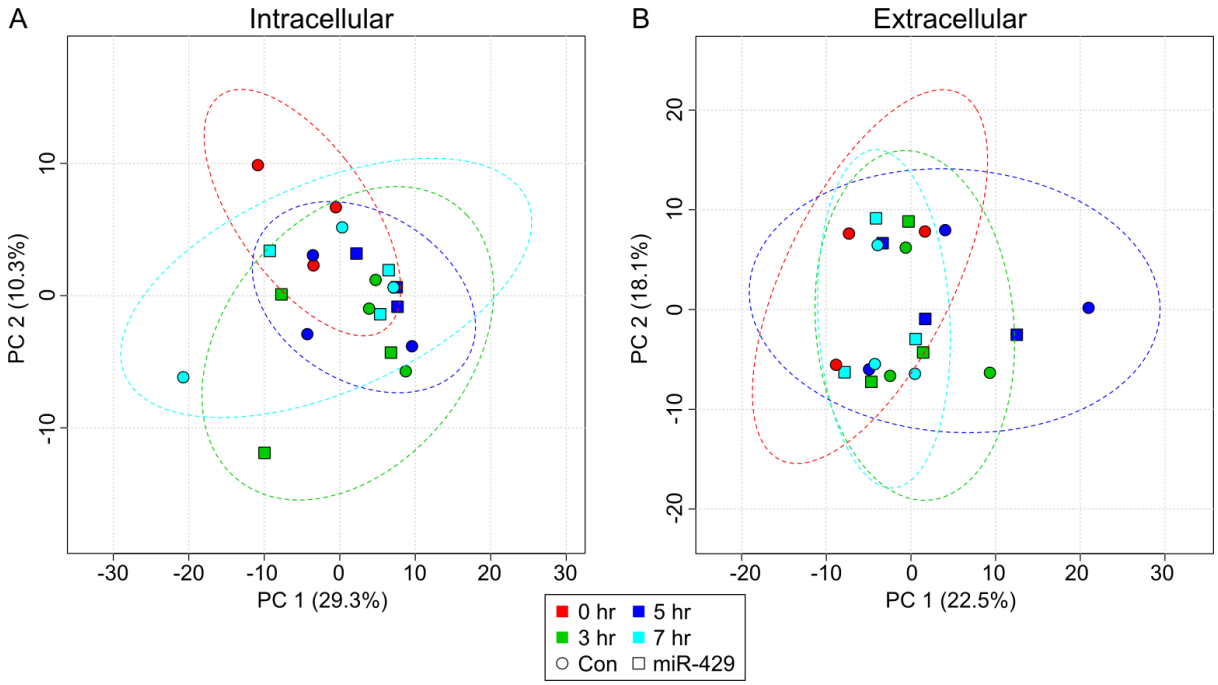

Figure 4.4: PCA shows no separation between time points for early time points only. Neither intracellular (A) nor extracellular (B) samples show only clear separation between time points or miR-429 transfected cells at the early time points.

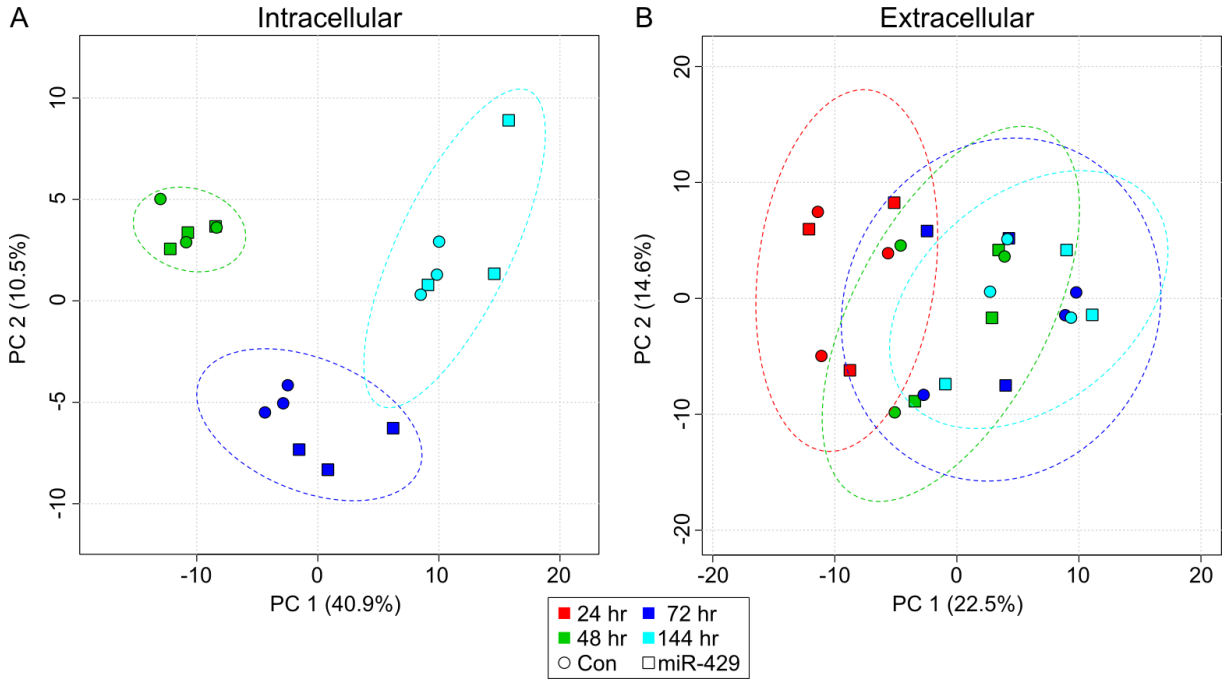

Figure 4.5: PCA shows some separation between time points for late time points only. Intracellular samples (A) show a clear separation between time points, but only separation between control and miR-429 transfected cells at 72 hours. Extracellular samples (B) show no difference between either time points or control and miR-429 transfected cells.

4.2.2.3. Time series analysis reveals a MET-EMT metabolic hysteresis effect

To further explore the MET-EMT differences seen intracellularly at 72 hours, two different analysis techniques were used to analyze the samples in a time-based manner. First, two-way ANOVA was used in MetaboAnalyst time series analysis, which takes greater advantage of the time series nature of the experiment. Two-way ANOVA uses a linear regression model to separate out effects based on group (miR-429 vs control), time, and interaction variables. Statistical values are assigned to the variables and are shown in Table 4.1 for intracellular and extracellular samples. Two-way ANOVA was performed on both the unknown and annotated compounds data set and the metabolite only data set. Most of the analytes with statistically significant values fall into the time variable, meaning that the analyte has a very similar time trend between control and miR-429 transfected cells. However, there are a few analytes for both the intracellular and extracellular samples that show statistically significant differences between

the control and miR-429 transfected cells. The metabolites that are statistically significantly different in the group category are listed in Table 4.1. The intracellular metabolites that differ between miR-429 and control transfected cells are all different classes, suggesting that miR-429 induced MET-EMT is not affecting a specific metabolism pathway, but instead slightly perturbs many different metabolites. The same holds true for the extracellular metabolites.

Table 4.1: Time series analysis results from two-way ANOVA. Number of analytes with a FDR corrected p value < 0.05 from time series analysis for intracellular and extracellular samples. The group term captures differences between control and miR-429 transfected cells; time term captures similarity between time series trends for each analyte; the interaction term captures the remaining effects.

	Intracellular		Extracellular	
	All Analytes	Metabolites	All Analytes	Metabolites
Group	26	7	21	9
Time	143	46	101	39
Interaction	41	10	29	9

Table 4.2: Metabolites identified as statistically significantly different for the group category using two-way ANOVA.

Metabolites	Group	Time	Interaction
Intracellular			
6-Phosphogluconic acid	1.05E-03	3.54E-19	5.45E-15
Pyroglutamic acid	1.05E-03	4.63E-15	1.41E-11
L-Malic acid	1.05E-03	9.49E-14	1.59E-12
L-Arginine	1.61E-03	4.45E-12	9.65E-07
2-Methylbenzoic acid	5.96E-03	4.65E-18	5.45E-15
Uridine 5'-monophosphate	0.0222	2.20E-15	3.28E-06
N-Decane	0.0427	0.2618	0.7521
Extracellular			
L-Serine	1.39E-04	3.06E-27	1.25E-26
Pentadecane	1.39E-04	1.30E-21	2.29E-21
Carbodiimide	4.94E-04	8.07E-19	3.41E-17
D-Psicose	5.26E-04	1.63E-19	2.71E-19
L-Lactic acid	3.78E-03	5.43E-19	2.84E-18
Pyridoxine	5.08E-03	9.20E-21	1.20E-17
Methanol	5.62E-03	9.76E-23	2.37E-13
Serotonin	9.39E-03	9.76E-23	1.96E-13
D-Glucaric acid	3.45E-02	0.0516	0.4198

Delving further, each time point was individually analyzed through t-test and fold change analysis to determine differences between control and miR-429 transfected cells. This was done for both the intracellular and extracellular samples. Unsurprisingly, no statistically significant differences were detected between the control and miR-429 transfected cells in any of the early time points (0, 3, 5, and 7 hours) either in the intracellular or extracellular samples. Interestingly though, when looking at the later time points, there are a small number of metabolites that are consistently different between control and miR-429 transfected cells at both 72 and 144 hours. Extracellularly, there are two metabolites that have consistently lower levels in miR-429 transfected cells. These metabolites are pyridoxine and glucarate. In the intracellular samples, there are two metabolites that have consistently lower levels in the miR-429 transfected cells as compared to the control transfected cells. These two metabolites are pyroglutamate and 6-phosphogluconate. Recently, 6-phosphogluconate has been shown to inhibit EMT extracellularly through competitive inhibitory interactions with the cytokine glucose phosphate isomerase/AMF in breast cancer cells.[17] No further studies were performed on intracellular levels of 6-phosphogluconate, though, but since the levels of 6-phosphogluconate dropped during EMT, it is possible that intracellular levels are kept lower to avoid any possible membrane transportation to extracellular regions. Overall, these metabolites show that the cells are not metabolically the same as they initially were, suggesting some degree of metabolic hysteresis occurs during MET-EMT.

4.3. Conclusions

Overall, there does not appear to be a system-wide metabolic perturbation caused by MET-EMT. Most large differences in metabolism were seen between time points, not between control and miR-429 transfected cells. This indicates that normal cellular growth and media depletion have a larger effect on cellular metabolism than the transfection of miR-429. Thus, a phenotypic change

large enough to detect morphologically did not affect the metabolome in a large way, perhaps contrary to expectation. This observation is particularly surprising and interesting in light of the other widespread changes observed during this phenotypic change in the protein, transcriptomic, and microRNA data. There do appear to be small changes during MET-EMT between control and miR-429 transfected cells though, suggesting a small hysteresis effect caused by the MET-EMT.

4.4. Methods

4.4.1. MicroRNA Transfection

The HEY cells were provided by Gordon Mills, Department of Molecular Therapeutics, University of Texas, MD Anderson Cancer Center. MicroRNA transfection of the HEY cells was based on the method developed in Chen, *et al*, 2011.[16] HEY cells were seeded in a six well plate with a surface area of 6.9 cm^2 at a density of $1x10^5$ cells per well ($1.45x10^4$ cells/cm^2) for the late time points and 3 x 10^5 cells per well ($4.35x10^4$ cells/cm^2) for the early time points. After 24 hours, the cells were transfected with 30 nM of miR-429 miRNA oligonucleotides (Ambion, Austin, TX) using Lipofectamine 2000 reagent (Invitrogen, Carlsbad, CA). The Ambion Pre-miRNA Precursor Negative Control was used as a control.

4.4.2. Time Point Collection

For the early time points, cells were harvested at 0, 3, 5, and 7 hours after microRNA transfection. For the late time points, cells were harvested at 24, 48, 72, and 144 hours. The 144 hours samples were subcultured at 72 hours, reseeded at the original density, and then allowed to grow for another 72 hours at which point they were harvested as detailed below.

4.4.3. Metabolite quenching and extraction

Plates were removed from the incubator and media from each well was removed and snap frozen in liquid nitrogen for the extracellular samples. Cells were then quickly washed with 1mL PBS at

37°C, which was aspirated off, and then 700µL of 80:20 methanol/water solution at -80°C was added immediately. The plate was then incubated at -80°C for 15 minutes. After incubation, remaining cellular debris were harvested using a cell scraper (BD Falcon, San Jose, CA) for intracellular analysis. The intracellular solution was then transferred to a microcentrifuge tube in a cold ethanol bath and centrifuged at 5,000 *g* for 5 minutes at -4°C. The supernatant was retained, and the pellet was subsequently re-extracted twice in 100µL of the cold 80:20 methanol/water solution, with all supernatants being pooled.[18] Both intracellular and extracellular samples were stored at -80°C until analysis.

4.4.4. Extracellular Sample Extraction

Immediately before two dimensional gas chromatography-mass spectrometry (GCxGC-MS) analysis, an acetonitrile precipitation was performed on the extracellular samples to remove protein.[19] Briefly, the extracellular samples were thawed on ice and 75µL was removed for GCxGC-MS analysis. 150µL of ice-cold acetonitrile was added to the sample, and the sample was vortexed for one minute. The sample was then centrifuged at 21,100 *g* for 7 minutes, and the supernatant removed for GCxGC-MS analysis.

4.4.5. GCxGC-MS Analysis

Before derivatization, both intracellular and extracellular samples were vacuum concentrated in a CentriVap at 40°C until completely dry. For the intracellular samples, a volume equated to $7.5x10^4$ cells for each sample was vacuum concentrated in order to achieve a concentration of $3x10^4$ cells/µL after derivatization. For the extracellular samples, the entire supernatant from the extracellular extraction was vacuum concentrated. The samples were derivatized using the protocol laid out by Fiehn, *et. al* as a basis.[20] Briefly, 2.5µL of 40mg/mL *O*-methylhydroxylamine hydrochloride (MP Biomedicals, LLC, Santa Ana, CA) in pyridine was added to the dried sample and shaken at 1400 rpm for 90 minutes at 30°C. 22.5µL of *N*-methyl-

N-(trimethylsilyl) trifluoroacetamide (MSTFA) + 1% trimethylchlorosilane (TMCS) (Thermo Scientific, Lafayette, CO) was then added to the samples which were then shaken at 1400 rpm for 30 minutes at 37°C. Samples were centrifuged at 21,100 *g* for 3 minutes and 15µL of the supernatant was added to an autosampler vial. Samples were spiked with 0.10µL of a retention time standard solution consisting of fatty acid methyl esters (FAMEs) and an internal standard of nonadecanoic acid methyl ester dissolved in dimethylformamide.

A LECO Pegasus 4D instrument with an Aglient 7683B autosampler, Agilent 7890A gas chromatograph and time-of-flight mass spectrometer (TOF-MS) was used to analyze the samples. The first column was an HP-5, 30m late x 0.320mm ID x 0.25µm film thickness (Agilent, Santa Clara, CA), and the second was an Rtx-200, 2m late x 0.25mm ID x 0.25µm film thickness (Restek, Bellefonte, PA). Specific autosampler, gas chromatography, and mass spectrometry methods can be found in Appendix A.

4.4.6. Data Analysis

Sample runs were first analyzed in ChromaTOF (LECO, St. Joseph, MI) to determine baseline, peak area, and peak identification. Briefly, settings included a baseline offset of 0.5, automatic smoothing, 1st dimension peak width of 21 seconds for intracellular and 12 seconds for extracellular, 2nd dimension peak width of 0.10 seconds, and a match of 700 required to combine peaks with a minimum signal-to-noise (S/N) of 5 for all subpeaks. Peaks were required to have a S/N of 10 and have a minimum similarity score of 800 before assigning a name. Unique mass was used for area and height calculation.

To align the samples, MetPP (http://metaopen.sourceforge.net/metpp.html) was used.[21] Sample files and a derivatization reagent blank file were uploaded from ChromaTOF. Unknowns were retained during the peak alignment process. The derivatization reagent blank file was used to

subtract peaks attributable only to derivatization reagents from the sample files. On-the-fly alignment was used with quality control samples manually selected as the peak list for primary alignment. Peak alignment was performed using the default criteria.

After alignment, further processing of the data was done using an in-house written MATLAB program. Quality control samples were used to remove analytes that were inconsistently measured. If more than half of the values for a given analyte were missing in the quality control samples or if the quality control samples had a coefficient of variance larger than 0.5 excluding missing values, the entire analyte was removed. Then, missing values were manually corrected using small value correction if all the values were missing in the biological replicate.

Finally, MetaboAnalyst (http://metaboanalyst.ca/) was used for statistical and enrichment analysis, applying both the statistical analysis and time series analysis modules.[22] Once the data was uploaded, remaining missing values were k-nearest neighbors (KNN) corrected. Data was filtered using the interquantile range method and then log-transformed using generalized logarithm transformation (base 2) and autoscaled. Analysis was performed using both unknown and annotated analytes together and annotated analytes only.

4.5. References

1. Thiery, J.P., Acloque, H., Huang, R.Y.J. & Nieto, M.A. Epithelial-Mesenchymal Transitions in Development and Disease. *Cell* **139**, 871-890 (2009).
2. Chaffer, C.L. & Weinberg, R.A. A perspective on cancer cell metastasis. *Science* **331**, 1559-1564 (2011).
3. Ouyang, G., Wang, Z., Fang, X., Liu, J. & Yang, C.J. Molecular signaling of the epithelial to mesenchymal transition in generating and maintaining cancer stem cells. *Cell. Mol. Life Sci.* **67**, 2605-2618 (2010).
4. Zavadil, J. A spotlight on regulatory networks connecting EMT and cancer stem cells. Comment on: Fuxe J, et al. Cell Cycle 2010; 9:2363-74. *Cell Cycle* **9**, 2927-2935 (2010).
5. Mani, S.A. et al. The Epithelial-Mesenchymal Transition Generates Cells with Properties of Stem Cells. *Cell* **133**, 704-715 (2008).

6. Ahmed, N., Abubaker, K., Findlay, J. & Quinn, M. Epithelial Mesenchymal Transition and Cancer Stem Cell-Like Phenotypes Facilitate Chemoresistance in Recurrent Ovarian Cancer. *Current Cancer Drug Targets* **10**, 268-278 (2010).
7. Morel, A.P. et al. Generation of breast cancer stem cells through epithelial-mesenchymal transition. *PLoS One* **3**, e2888 (2008).
8. Gregory, P.A., Bracken, C.P., Bert, A.G. & Goodall, G.J. MicroRNAs as regulators of epithelial-mesenchymal transition. *Cell Cycle* **7**, 3112-3118 (2008).
9. Korpal, M. & Kang, Y. The emerging role of miR-200 family of microRNAs in epithelial-mesenchymal transition and cancer metastasis. *RNA biology* **5**, 115-119 (2008).
10. Lamouille, S., Subramanyam, D., Blelloch, R. & Derynck, R. Regulation of epithelial-mesenchymal and mesenchymal-epithelial transitions by microRNAs. *Curr Opin Cell Biol* **25**, 200-207 (2013).
11. Gregory, P.A. et al. The miR-200 family and miR-205 regulate epithelial to mesenchymal transition by targeting ZEB1 and SIP1. *Nat Cell Biol* **10**, 593-601 (2008).
12. Zhang, J. et al. miR-30 inhibits TGF-beta1-induced epithelial-to-mesenchymal transition in hepatocyte by targeting Snail1. *Biochem Biophys Res Commun* **417**, 1100-1105 (2012).
13. Craene, B.D. & Berx, G. Regulatory networks defining EMT during cancer initiation and progression. *Nat Rev Cancer* **13**, 97-110 (2013).
14. Peinado, H., Olmeda, D. & Cano, A. Snail, Zeb and bHLH factors in tumour progression: an alliance against the epithelial phenotype? *Nat Rev Cancer* **7**, 415-428 (2007).
15. Yang, J. et al. Twist, a master regulator of morphogenesis, plays an essential role in tumor metastasis. *Cell* **117**, 927-939 (2004).
16. Chen, J., Wang, L.J., Matyunina, L.V., Hill, C.G. & McDonald, J.F. Overexpression of miR-429 induces mesenchymal-to-epithelial transition (MET) in metastatic ovarian cancer cells. *Gynecologic Oncology* **121**, 200-205 (2011).
17. Gallardo-Pérez, J.C., Rivero-Segura, N.A., Marín-Hernández, A., Moreno-Sánchez, R. & Rodríguez-Enríquez, S. GPI/AMF inhibition blocks the development of the metastatic phenotype of mature multi-cellular tumor spheroids. *Biochimica et Biophysica Acta (BBA) - Molecular Cell Research* **1843**, 1043-1053 (2014).
18. Lu, X., Bennet, B., Mu, E., Rabinowitz, J. & Kang, Y. Metabolomic Changes Accompanying Transformation and Acquisition of Metastatic Potential in a Syngeneic Mouse Mammary Tumor Model. *J. Biol. Chem.* **285**, 9317-9321 (2010).
19. Teja-Isavadharm, P. et al. A Simplified Liquid Chromatography-Mass Spectrometry Assay for Artesunate and Dihydroartemisinin, Its Metabolite, in Human Plasma. *Molecules* **15**, 8747-8768 (2010).
20. Kind, T. et al. FiehnLib: Mass Spectral and Retention Index Libraries for Metabolomics Based on Quadrupole and Time-of-Flight Gas Chromatography/Mass Spectrometry. *Anal. Chem.* **81**, 10038-10048 (2009).
21. Wei, X. et al. MetPP: a computational platform for comprehensive two-dimensional gas chromatography time-of-flight mass spectrometry-based metabolomics. *Bioinformatics (Oxford, England)* **29**, 1786-1792 (2013).
22. Xia, J.G., Mandal, R., Sinelnikov, I.V., Broadhurst, D. & Wishart, D.S. MetaboAnalyst 2.0-a comprehensive server for metabolomic data analysis. *Nucleic Acids Research* **40**, W127-W133 (2012).

Chapter 5 Conclusions and recommendations for future work

5.1. Conclusions

The work done in this thesis explored the differences in metabolism between ovarian cancer stem cells (OCSCs) and ovarian cancer cells (OCCs) through three separate avenues: (1) by defining the baseline metabolic differences between the two cell types, (2) by determining the differences between OCCs and OCSCs in their metabolic response to biologically based perturbations, and (3) by profiling the metabolic changes that occurred during the mesenchymal to epithelial transition (MET) and epithelial to mesenchymal transition (EMT). This is the first metabolomics study that characterizes the differences between an isogenic ovarian cancer cell line and ovarian cancer stem cell line. To date, there are only a handful of papers addressing cancer stem cell metabolism in any way and only one other paper studying metabolic differences on a systems-scale. Characterization of the metabolic differences between cancer cells and cancer stem cells provides us a greater understanding of how metabolic dynamics are altered and, once identified, may help us the ability to utilize these alterations for targeted treatment.

5.1.1. OVCAR-3-derived ovarian cancer stem cells display distinct metabolic profiles

Previous gene expression analysis of OCSCs and OCCs identified several metabolic pathways that were significantly enriched in differentially expressed genes. However, the relationship of enzyme expression to metabolic phenotype is complex and does not imply a direct one-to-one correlation. To determine if there were substantial metabolic changes corresponding with these transcriptional differences, two-dimensional gas chromatography coupled to mass spectrometry was used to measure the metabolite profiles of the OCCs and OCSCs. These two cell lines exhibited significant metabolic differences in intracellular metabolite measurements. Pathway

analysis of intracellular metabolomics data revealed close overlap with metabolic pathways identified from gene expression data, with four out of six pathways found to be enriched in gene-level analysis also enriched in metabolite-level analysis. One of the most significantly enriched pathways, arginine and proline metabolism, contained six metabolites that are each statistically significantly different between the two cells. Two of those metabolites, proline and putrescine, have been previously implicated in cancer, but the changes displayed between normal and cancer cells were discordant with the changes they displayed between the OCCs and OCSCs.

Lower levels of proline and putrescine in OSCSs may be explained in the context of current research in stem cell metabolism, where proline has been shown to cause differentiation and putrescine was found to have different levels in mESCs and induced pluripotent stem cells (iPSCs). These findings suggest that OCSCs may exist in a metabolic balance between potency and proliferation. This is noteworthy because OCSCs are thought to be transient (OCSCs may switch to OCCs and vice versa) and as the cancer cells become more stem-like, their metabolism must transition from supporting a highly proliferative phenotype to supporting a higher potency phenotype. Therefore, metabolism may play a larger role in retaining stemness than heretofore believed and further research into stem cell and cancer stem cell metabolism may reveal other metabolites that support stemness. Overall, metabolism in this OCSC line is distinct from that of more differentiated isogenic cancer cells, showing similarities to stem cell metabolism that suggest the potential importance of metabolism for the cancer stem cell phenotype.

5.1.2. Metabolic perturbations of OCCs and OCSCs

Chemotherapeutic, glucose deprivation, hypoxia, and ischemia perturbations were applied to OCCs and OCSCs grown *in vitro* to profile the heterogeneous metabolic profiles that would be expected in a tumor. Docetaxel was selected as the chemotherapeutic used for this experiment,

and it caused metabolic changes mostly within amino acid and carbohydrate metabolism in OCCs but did not affect OCSC metabolism. Docetaxel also increased the levels of uracil within the OCCs, which may be indicative of increased cellular dependence on uracil under docetaxel treatment. If this were the case, it would help to explain why treating tumors with docetaxel and a competitive inhibitor of uracil was shown to improve treatment results over treatment with docetaxel only.

Glucose deprivation, hypoxia, and ischemia all perturbed OCC and OCSC metabolism, but not equally. Hypoxia had a much larger effect on OCC metabolism, while glucose deprivation had a greater effect on OCSC metabolism. OCSCs may not respond to hypoxic conditions because they are normally found within a hypoxic niche in the tumor and therefore, their metabolism might be adapted to a hypoxic environment. The different responses to glucose deprivation suggests that OCSCs are much more dependent on glucose than OCCs, which may indicate that OCSCs utilize glucose differently than OCCs. Cancer cells have adapted different pathways for supplying their energy requirements, such as glutaminolysis, which can help negate glucose deprivation. These pathways may be lacking in OCSCs or OCSCs may use glucose for anabolic pathways that OCCs do not, which could explain the widespread alterations in OCSC metabolism during glucose deprivation. Ischemia perturbed metabolism in both of the cell types in many of the same pathways, suggesting that OCCs and OCSCs respond to this stress similarly. Both cells had metabolic pathways statistically significantly enriched under ischemia that did not appear in hypoxia for OCCs or in glucose deprivation for OCSCs, suggesting that ischemia is not simply an additive affect of hypoxia and glucose deprivation.

Even though OCCs and OCSCs responded differently to the three metabolic perturbations, there were a few metabolites that were altered in all of the conditions for both cell types. One of these

metabolites, phosphoethanolamine, showed a similar increasing trend in response to all the perturbations for both cell types, suggesting the phosphoethanolamine may just be responding to the stress the cells are under and not the specific perturbation. Recent research has also shown that phosphoethanolamine can induce apoptosis in cancer cells, suggesting some possible interaction between these stress and apoptotic pathways potentially metabolic in nature. Therefore, OCSCs and OCCs may be increasing phosphoethanolamine levels to induce apoptosis in response to the stress the cells are undergoing.

5.1.3. Metabolic changes during mesenchymal to epithelial transition

System-wide metabolic changes were not detected during MET-EMT in HEY cells. Instead, most of the metabolic differences were temporal, suggesting that normal cellular growth and media depletion have a larger effect on the cellular metabolism than miR-429 induced MET-EMT. A small number of metabolic differences were detected between control and miR-429 transfected cells while shifting back from epithelial to mesenchymal phenotype, which hints at a possible hysteresis effect caused by the MET-EMT. Overall, the lack of system-wide metabolite changes was contrary to expectation since miR-429 induced MET-EMT caused a phenotypic change large enough to detect morphologically and was observed in the protein, transcriptomic, and microRNA data collected alongside the metabolomics data. The differences noticed during MET-EMT in the other data may affect areas of metabolism (such as lipid metabolism) are not captured well by the techniques used in this study.

5.2. Relevance of thesis work

Altered metabolism has recently been identified as a hallmark of cancer. Many of the common oncogenes (such as HIF, PI3K, Myc, and p53) have been shown to alter metabolism, as well as mutations of key metabolic enzymes. Most of these discoveries have been made through studies of individual enzymes or pathways, but recently, metabolomics has begun to be used for

characterization of cancer metabolism, biomarker and diagnostic discovery, staging of cancer, and pharmacometabolomics. One area of cancer research that before this thesis had not been explored is characterization of the differences between cancer cell and cancer stem cell metabolism.

The work in this thesis used metabolomics to explore the metabolic differences between isogenic ovarian cancer and cancer stem cell lines. The baseline characterization and chemotherapeutic and environmental perturbations experiments had not been performed before with isogenic cancer cell and cancer stem cell lines. The experimental setup can be used for any isogenic cancer and cancer stem cell lines to expand cancer stem cell characterization into other cancer types. Besides the isogenic pair characterization, profiling the metabolic changes induced during mesenchymal-to-epithelial and epithelial-to-mesenchymal had never been reported before, even if no large-scale metabolic changes were detected. Moving forward, this same experimental design could be applied toward studying different areas of the metabolome during EMT and MET that were not captured here (such as lipids).

The novel findings of this thesis suggest a number of conclusions and future directions that would not have been possible without this work. First, it showed that there can be substantial metabolic differences between otherwise isogenic cells both in continuous culture propagation and in response to environmental challenges. Furthermore, some of the metabolic differences may result directly from the stemness of the cells, drawing the relationship between cancer stem cells and cancer cells closer to that of normal cells and stem cells (though this hypothesis still needs further validation as described in section 5.3.1). It was also found that OCSCs do not respond metabolically to docetaxel, suggesting that OCSCs are fully resistant to docetaxel. Also, OCSCs did not experience a metabolic shift while under hypoxic conditions, yet did during

glucose deprivation, suggesting that OCSCs have metabolically adapted to hypoxic conditions yet still depend on glucose for their altered metabolism despite their slow rate of proliferation.

Overall, the work in this thesis starts to fill in large gaps in the current knowledge of ovarian cancer stem cell metabolism and lays a foundation for continuing characterization of other cancer stem cell types. Importantly, the information and insight gleaned from this work can be used in the development of future therapeutics or treatment combinations to specifically target cancer stem cells, a putatively important cause of cancer recurrence and mortality, via metabolism.

5.3. Recommendations for future work

Moving forward, the next immediate steps for this project should involve validation experiments for further support of the hypothesis that differences in proline and putrescine levels between OCCs and OCSCs are directly related to the stemness of the cell. These experiments are described in section 5.3.1. After the validation experiments, the next experiments should involve expansion of the biologically based perturbations, especially for chemotherapeutics, as detailed in section 5.3.2. The metabolic response to different chemotherapeutics, such as treatments targeted toward the OCSCs, may reveal increased cellular dependence on certain pathways or metabolites, which could provide further targeted treatments to be supplied in conjunction with the chemotherapeutic. Finally, these experiments should be expanded to other cancer stem cell lines, as described in section 5.3.4, to determine if the results shown here are specific to the OCCs and OCSCs profiled or if they apply to cancer stem cells in general. Because cancer stem cell lines are not easily obtained, another option for expansion would be to mimic the tumor stroma *in vitro* with the OCCs and OCSCs and profile the metabolic responses of the cells in response to the biologically based perturbations already tested to determine the effect tumor

stroma interactions have on cellular metabolism. These experiments are described in greater detail in section 5.3.3.

5.3.1. Proline and putrescine validation experiments

During characterization of the baseline differences of OCSCs and OCCs, proline and putrescine were found to be key metabolites that might help explain the differences in metabolism between the two cells types in terms of the cell stemness. To support these findings, further validation studies should be performed to determine if the lower levels of proline and putrescine found in OCSCs do indeed help these cells retain their stem like state.

5.3.1.1. Gene knockdown

One such study would involve the knockdown, silencing, or inhibition of key enzymes used to metabolize proline and putrescine in OCCs to determine if these cells would then shift toward a more stem like state. For proline, proline oxidase (POX), which catalyzes the oxidation of proline to pyrroline-5-carboxylate (P5C), should be inhibited as it has been shown previously that the production of P5C from proline causes differentiation of mouse embryonic stem cells (mESCs).[1] POX was also found to be down-regulated in OCSCs as compared to OCCs during gene expression analysis. Therefore, inhibition of POX would drastically reduce the production of P5C, which might shift the OCCs towards a more stem-like state. For putrescine, no singular enzymatic reaction has been linked to the ability of putrescine to cause differentiation, so different enzymes that produce putrescine should be tested. N^1-acetylpolyamine oxidase (APAO), which catalyzes the breakdown of spermidine to putrescine in the polyamine catabolism pathway, would be one possible choice for knockdown as the polyamine catabolism pathway is known to be dysregulated in cancer. After inhibition or knockdown, expression of CD44 can be used to determine if the OCCs have become more stem-like, as OCSCs have been

shown to have higher expression of CD44 than OCCs.[2] Measurement of CD44 expression can be performed using flow cytometry. Phenotypic changes might also occur and indicate a shift toward OCSCs.

5.3.1.2. Metabolic flux analysis

Another experiment that can be performed to validate our findings regarding proline and putrescine would be to use metabolic flux analysis to profile the arginine and proline metabolism pathway. Profiling the flux for the OCCs and OCSCs will allow us to determine how the flow of metabolites through the arginine and proline metabolism pathway differs; for instance, if the metabolic flux is shunted off to avoid certain reactions (such as proline oxidation to P5C) for the OCSCs. The results from these experiments will not directly tie the levels of proline and putrescine to differentiation, but will further support that the arginine and proline metabolism pathway is utilized differently in the two cells.

5.3.2. Other biological perturbations

In this work, glucose deprivation, hypoxia, ischemia, and a chemotherapeutic treatment were applied as biologically-inspired perturbations to bring the *in vitro* environment closer to the *in vivo* tumor microenvironment and to determine the differences between OCCs and OCSCs in their response to these perturbations. Besides these four, other biologically-inspired perturbations can also be applied to this system to gain further insight into tumor metabolism. Lactic acid production is elevated in cancers cells due to the increased flux through glycolysis.[3] The lactic acid and CO_2 (generated by the PPP) produced by the cancer cells is enough to lower the extracellular pH from 7.4 (physiological pH) to below 6.5 in some tumor locations.[4] This acidic environment helps cancer cells to decrease sensitivity to hypoxia, stimulate metastasis, and increase drug resistance.[5, 6] Pilot experiments performed during this thesis work showed that

lowering media pH alone had no effect, but it would be interesting to combine a lowered media pH with hypoxia or a chemotherapeutic treatment to determine if the metabolism of the OCCs or OCSCs respond differently than when they subjected to hypoxia and chemotherapy only.

Another perturbation that might have effect on cancer cellular metabolism is estrogen. Estrogen, a steroid hormone, has been found to alter OCC proliferation. 17β-estradiol (E2) has been shown to promote cell proliferation in OVCAR-3 cells.[7] It has also been found that 4-hydroxy E2 (4-OHE2) can induce OVCAR-3 expression of HIF-1α.[8] To determine the metabolic response of the OCCs and OCSCs, estrogen would be supplied to the cells at varying physiological levels. As estrogen induces the expression of HIF-1α, OCCs and OCSCs might exhibit metabolic profiles similar to those from the hypoxia studies.

As stated in Chapter 3, ovarian cancer is commonly treated with a platinum compound and a taxane compound. Docetaxel, a taxane, was chosen as the initial chemotherapeutic treatment for the metabolic perturbation experiment due to the fact that it interrupts cellular division and thus would likely have an effect on cellular metabolism. Other chemotherapeutics should be explored in order to determine the metabolic responses to different chemotherapies, especially those with different method of actions. For example, cisplatin, a platinum compound and one of the most frequently used first line treatments against ovarian cancer, reacts with DNA to form DNA adducts that trigger signal transduction pathways which can evidently lead to apoptosis.[9] Since docetaxel and cisplatin have differing methods of action, it is expected that the cellular metabolism response would differ as well. Another interesting chemotherapeutic option would be to use one that is targeted toward cancer stem cells. Since chemotherapeutics targeted toward cancer stems are only just now being developed, this is an option that could only be explored in future.

5.3.3. Profile metabolism of OCICs and OCCs in response to stroma

The environment surrounding the tumor (its microenvironment) lends important stimulatory biological signaling to the tumor. Through these interactions, the tumor is able to expand and resist interferences from the body (e.g., the immune system) or outside sources (e.g., chemotherapy). Stroma lends greater drug resistance to the tumor cells they surround; therefore, tumor-stroma interaction pathways are emerging as possible therapeutic targets.[10] Because of the drug resistance that the stroma interactions give to the tumor, high-throughput screening methods are being developed to identify chemotherapeutics with increased activity against stroma cells.[11] In order to better understand how these interactions may impact metabolism, the tumor microenvironment can be simulated *in vitro* to determine how tumor-stroma interactions affect the OCCs' and OCSCs' response to environmental perturbations.

The results of this study would identify whether interactions between the stroma and CCs cause metabolic changes that help to sustain the tumor under applied stress. Metabolic pathways that undergo regulation from the tumor-stroma signaling could be identified by comparison to the data from the OCCs or OCSCs only. With this information, potential inhibitors or activators of the metabolic pathways involved in the tumor-stroma interactions could be identified and used as therapeutics to make the tumor more sensitive to other treatments.

5.3.4. Explore metabolism differences using different cell lines for ovarian cancer and expand into other cancers

Besides the isogenic system used for the studies in this work, there exist a few other isolated cancer stem cells in ovarian cancer and other cancers.[12-15] Extending this same study into other cancer stem cells would help to determine if the results found here are specific to this cell system, to ovarian cancer, or to cancer stem cells in general. The drawback to this extension is that these other isolated cancer stem cells are difficult to obtain. They are not available through

traditional means (such as ATCC) and would only be obtainable through direct contact with the group that isolated the cancer stem cells. Hopefully, as the research into cancer stem cells continues, these cells will be more easily obtainable which would allow the continuation of this research.

5.4. References

1. Casalino, L. et al. Control of embryonic stem cell metastability by L-proline catabolism. *Journal of Molecular Cell Biology* **3**, 108-122 (2011).
2. Wang, L., Mezencev, R., Bowen, N.J., Matyunina, L.V. & McDonald, J.F. Isolation and characterization of stem-like cells from a human ovarian cancer cell line. *Mol Cell Biochem* **363**, 257-268 (2012).
3. Warburg, O. Origin of Cancer Cells. *Science* **123**, 309-314 (1956).
4. Fukamachi, T. et al. Tumor specific low pH environments enhance the cytotoxicity of lovastatin and cantharidin. *Cancer Lett* **297**, 182-189 (2010).
5. Gillies, R.J., Robey, I. & Gatenby, R.A. Causes and consequences of increased glucose metabolism of cancers. *Journal of nuclear medicine : official publication, Society of Nuclear Medicine* **49 Suppl 2**, 24S-42S (2008).
6. Kato, Y. et al. Acidic extracellular microenvironment and cancer. *Cancer Cell Int* **13**, 89 (2013).
7. Wang, Y. et al. Regulatory effect of E2, IL-6 and IL-8 on the growth of epithelial ovarian cancer cells. *Cell. Mol. Immunol.* **2**, 365-372 (2005).
8. Gao, N., Nester, R.A. & Sarkar, M.A. 4-Hydroxy estradiol but not 2-hydroxy estradiol induces expression of hypoxia-inducible factor 1α and vascular endothelial growth factor A through phosphatidylinositol 3-kinase/Akt/FRAP pathway in OVCAR-3 and A2780-CP70 human ovarian carcinoma cells. *Toxicol. Appl. Pharmacol.* **196**, 124-135 (2004).
9. Siddik, Z.H. Cisplatin: mode of cytotoxic action and molecular basis of resistance. *Oncogene* **22**, 7265-7279 (2003).
10. Agarwal, A. et al. Identification of a Metalloprotease-Chemokine Signaling System in the Ovarian Cancer Microenvironment: Implications for Antiangiogenic Therapy. *Cancer Res.* **70**, 5880-5890 (2010).
11. McMillin, D.W. et al. Tumor cell-specific bioluminescence platform to identify stroma-induced changes to anticancer drug activity. *Nat. Med. (N. Y., NY, U. S.)* **16**, 483-489 (2010).
12. Garvalov, B.K. & Acker, T. Cancer stem cells: a new framework for the design of tumor therapies. *Journal of Molecular Medicine-Jmm* **89**, 95-107 (2011).
13. Bapat, S.A., Mali, A.M., Koppikar, C.B. & Kurrey, N.K. Stem and Progenitor-Like Cells Contribute to the Aggressive Behavior of Human Epithelial Ovarian Cancer. *Cancer Res.* **65**, 3025-3029 (2005).
14. Curley, M.D. et al. CD133 Expression Defines a Tumor Initiating Cell Population in Primary Human Ovarian Cancer. *Stem Cells* **27**, 2875-2883 (2009).
15. Bapat, S.A. Human ovarian cancer stem cells. *Reproduction* **140**, 33-41 (2010).

APPENDIX A

AS Method

An Agilent 7683 autosampler was used. Three pre-washes with pyridine were performed before each injection. The sample was then pumped into the syringe 4 times. The syringe size was 10µL with a sample volume of 1µL injected into the inlet. Three post-washes with pyridine were performed after injection.

GC Method

An Agilent 7890 gas chromatograph adapted to GCxGC analysis was used. The first column was an HP-5, 30m long x 0.320mm ID x 0.25µm film thickness (Agilent, Santa Clara, CA), and the second was an Rtx-200, 2m long x 0.25mm ID x 0.25µm film thickness (Restek, Bellefonte, PA). The excluded masses in auto mass defect mode option was chosen. Helium was used as the carrier gas with a corrected constant flowrate of 1.00mL/min. An inlet septum purge flow of 3mL/min was chosen. The inlet was operated in splitless mode with a purge flow of 100mL/min set to start 30 seconds after injection, yielding a total flow of 101mL/min. Gas saver mode was used, with a flow of 20mL/min set to start a minute after injection.

Table A1: Main Oven Temperature Program for Intracellular and Extracellular Samples

Rate (°C/min)	Target Temp (°C)	Duration (min)
Initial	70	1
10	315	2

The main oven temperature program can be found in Table A1. The secondary oven temperature offset was 5°C and the modulator temperature offset was 20°C from the main oven. An equilibration time of 60 seconds was set for the ovens. The modulation timing is listed in Table A2. The transfer line was set to 320°C for the entire run.

Table A2: Modulation Timing

#	Start (s)	End (s)	Modulation Period (s)	Hot Pulse Time (s)	Cold Pulse Time (s)
Intracellular Samples					
1	Start	575	5.00	1.00	1.50
2	575	797	6.00	1.50	1.50
3	797	End	4.00	1.50	0.50
Extracellular Samples					
1	Start	492	4.00	0.50	1.50
2	492	747	5.00	1.00	1.50
3	747	1099	4.00	1.00	1.00
4	1099	End	4.00	1.50	0.50

MS Method

A LECO Pegasus IV D time of flight mass spectrum (TOF-MS) was used. The total MS method time was based on the GC method time. The acquisition delay was set to 240 seconds, with the filaments being turned off until then. The collection mass range was from 50 to 500u. The acquisition rate was set to 200 spectra/second. The detector voltage was set to 100V above the optimized voltage with the electron energy set to -70V. The mass defect mode was set to manual with the mass defect 0mu/ 100u. The ion source temperature was 220°C and the run had to wait for the ion source temperatures to reach the set point before starting acquisition.